

PLASTIC SHRINKAGE PROPERTIES OF BALER TWINE FIBRE REINFORCED CONCRETE

**A Thesis Submitted to the College of
Graduate Studies and Research
in Partial Fulfillment of the Requirements
for the Degree of Master's of Science
in the Department of Civil and Geological Engineering
University of Saskatchewan
Saskatoon**

By
Ying Chen

© Copyright Ying Chen, May 2008. All rights reserved.

COPYRIGHT

In presenting the thesis in partial fulfillment of the requirements for a postgraduate degree from the University of Saskatchewan, I agree that the libraries of this University may make it freely available for inspection. I further agree that permission for copying of this thesis in any manner, in whole or in part, for scholarly purposes may be granted by the professor who supervised my thesis work or, in his absence, by the Head of the Department or the Dean of the College in which my thesis work was done. It is understood that any copying or publication or use of this thesis or parts thereof for financial gain shall not be allowed without my written permission. It is also understood that due recognition shall be given to me and to the University of Saskatchewan in any scholarly use which may be made of any material in my thesis.

Requests for permission to copy or to make other use of material in this thesis in whole or part shall be addressed to:

Head of the Department of Civil and Geological Engineering

University of Saskatchewan

Saskatoon, Saskatchewan, S7N 5A9, Canada

ABSTRACT

The large amount of used polypropylene baler twine generated from the agricultural community may provide a low-cost, environmentally friendly source of fibre reinforcement that can be used to improve the properties of concrete. However, the performance of such fibres for the application has not yet been explored. The effectiveness of using small amounts of chopped baler twine to control the restrained plastic shrinkage cracking of portland cement mortar was investigated in this study. To determine the influence of baler twine fibre type, length and volume fraction on their performance, two types of baler twine (one composed of strands with circular cross section, the other composed of flat band shape strands) in two lengths (19 mm and 38 mm) and three volume fractions (0.05%, 0.1%, and 0.3%) were evaluated. To compare the performance of baler twine fibre with that of other commercially available synthetic fibres, fibrillated polypropylene fibres at equal lengths and volume fractions was investigated.

The restrained plastic shrinkage tests were carried out by subjecting the fibre-reinforced mortar specimens, cast on rough substrate bases, to a wind speed of 2.6 m/s, and relative humidity less than 3% at 35 °C for 22 hours. To evaluate the effectiveness of the fibres, the crack numbers were recorded, and the maximum crack width and total crack area on the surface of each specimen were measured using an image analysis technique. Unrestrained plastic shrinkage tests were also conducted in which fibre-reinforced mortar specimens without the substrate bases were tested under the same environmental conditions.

Test results indicate that both types of baler twine are capable of controlling restrained plastic shrinkage cracking to some extent, but are not as effective as fibrillated polypropylene. The baler twine composed of band shape strands performed better than the one composed of strands with circular cross section. Compared with plain specimens, the total crack area was reduced by 95.3, 77.5 and 38.7% when 0.3% volume fraction of 38 mm fibrillated polypropylene, band shape baler twine and

circular baler twine fibres, respectively, were added. Similar reductions in maximum crack width were observed. Fibre length did not significantly influence cracking behaviour. Free plastic shrinkage was significantly reduced only when long fibre lengths (38 mm) and high volume fractions (0.3%) were used.

ACKNOWLEDGEMENTS

I would like to sincerely thank my supervisor, Dr. Leon D. Wegner for his patient guidance and continuous assistance throughout this study. I also want to thank Dr. Bruce Sparling, Dr. Moh Boulfiza, and Dr. Doug Milne for their advice and for taking time out of their busy schedules to be my research committee members.

The help from the laboratory technicians in the Structures and Materials Laboratory, Mr. Dale Pavier and Mr. Brennan Pokoyoway, is deeply appreciated. I also would like to extend my gratitude to those staff in the university and friends who helped me during the course of this investigation.

At last, I would like to express my deepest and sincerest gratitude to my family, especially my parents and my husband for their support and encouragement throughout my life.

TABLE OF CONTENT

COPYRIGHT	i
ABSTRACT	ii
ACKNOWLEDGEMENTS	iv
TABLE OF CONTENT	v
LIST OF TABLES	vii
LIST OF FIGURES	viii
LIST OF NOMENCLATURE	xi
CHAPTER 1 INTRODUCTION	1
1.1. Background	1
1.2. Objectives	2
1.3. Scope	3
1.4. Methodology	3
1.5. Dissertation Organization	4
CHAPTER 2 LITERATURE REVIEW	5
2.1. Introduction	5
2.2. Plastic Shrinkage Cracking Mechanism	5
2.2.1. Plastic shrinkage	5
2.2.2. Plastic settlement	6
2.3. Factors that Affect Plastic Shrinkage Cracking	6
2.3.1. Influence of fibres	6
2.3.2. Influence of environmental conditions	10
2.3.3. Influence of other factors	10
2.4. Experimental Methods for Plastic Shrinkage	12
2.4.1. Restrained plastic shrinkage tests	12
2.4.2. Unrestrained plastic shrinkage tests	16
CHAPTER 3 EXPERIMENTAL PROGRAM	17
3.1. Introduction	17
3.2. Materials	17
3.2.1. Concrete ingredients	17

3.2.2.	Fibres	18
3.2.3.	Mixture proportions.....	22
3.3.	Test Procedures for Restrained Plastic Shrinkage	24
3.3.1.	Specimen preparation	24
3.3.2.	Specimen testing.....	27
3.3.3.	Crack measurement	29
3.4.	Test Procedures for Unrestrained Plastic Shrinkage	31
3.5.	Environmental Conditions	32
3.5.1.	Environmental Chamber.....	32
3.5.2.	Temperature and relative humidity.....	33
3.5.3.	Wind speed	36
3.5.4.	Evaporation rate.....	43
CHAPTER 4	TEST RESULTS AND DISCUSSION	46
4.1.	Introduction	46
4.2.	Restrained Plastic Shrinkage Test Results	46
4.3.	Unrestrained Plastic Shrinkage Test Results	57
4.4.	Discussion and Analysis	62
4.4.1.	Role of reduced shrinkage tendency in the reduction of restrained shrinkage cracking	62
4.4.2.	Performance of different fibre types.....	68
4.4.3.	Analysis of the influence of fibre surface area.....	69
4.4.4.	Improving the effectiveness of baler twine fibres	72
CHAPTER 5	CONCLUSIONS AND RECOMMENDATIONS	74
5.1.	Summary and Conclusions	74
5.2.	Suggestions for Future Work	76
REFERENCES	77
APPENDIX A	— Comparison of Different Settings for Crack Measurement	82
APPENDIX B	— Environmental Conditions	83
APPENDIX C	— Restrained Shrinkage Test Results	94
APPENDIX D	— Unrestrained Shrinkage Test Results	111

LIST OF TABLES

Table 3.1. Properties of coarse and fine aggregates (Wang 2003).....	18
Table 3.2. Fibre properties.....	21
Table 3.3. List of specimens and the number of specimens used for each combination.	23
Table 3.4. Mix proportions by mass.	24
Table 3.5. Sample record of temperature and relative humidity (RH) during a test.	36
Table 3.6. Wind speed at different points and depths in Tunnel A (m/s).....	41
Table 3.7. Wind speed at different points and depths in Tunnel B (m/s).....	42
Table 3.8. Evaporation rate at different locations in each tunnel (kg/m ² /h).....	44
Table 4.1. Restrained plastic shrinkage test results.	50
Table 4.2. Unrestrained plastic shrinkage strains recorded 22 hours after casting.....	60
Table 4.3. The actual and expected reductions in total crack area for all specimens due to a reduced shrinkage tendency.	64
Table 4.4. Weight of 20 pieces of 38 mm fibre and the resulting linear density of different fibre types.....	70
Table 4.5. The average number of pieces that different fibre types divided into.	71
Table 4.6. Specific surface area (mm ² /mm ³) of different fibre types and volume fractions.	72

LIST OF FIGURES

Figure 2.1. Schematic of capillary meniscus development between solid particles. (a) Surface water starts to evaporate. (b) Water meniscus forms between the solid particles at or near the surface of concrete due to water evaporation..	6
Figure 2.2. Plastic cracking caused by differential settlement above rebar, large aggregates and changes in concrete section thickness.	7
Figure 2.3. Evaporation rate estimation (ACI 305R 1999).	11
Figure 2.4. Details of ring specimen used by Groth (2000).	13
Figure 2.5. Side view of slab specimen used by Najm and Balaguru (2002).	14
Figure 2.6. Side view of slab specimen used by Qi et al. (2003).	14
Figure 2.7. Side view of end restrained beam test used by Banthia et al. (1993).	14
Figure 2.8. Side view of shrinkage test specimen used by Banthia et al. (2000).	15
Figure 2.9. Side view of shrinkage test specimen used by Naaman et al. (2005).	15
Figure 2.10. Side view of shrinkage test specimen used by Boghossian and Wegner (2003).	16
Figure 3.1. Fibre types used in the experiment. (FPP: fibrillated polypropylene, WBT: white baler twine, RBT: red baler twine)	19
Figure 3.2. White baler twine strands.	20
Figure 3.3. Red baler twine strand.	20
Figure 3.4. Fibrillated polypropylene fibre.	21
Figure 3.5. Baler twine cutting operation.	22
Figure 3.6. The mould for casting substrate bases.	25
Figure 3.7. Reinforcing bars positioned in the mould.	25
Figure 3.8. The substrate base.	26
Figure 3.9. Casting of overlays over the substrate bases.	27
Figure 3.10. Locations of the first batch specimens in the two wind tunnels.	28
Figure 3.11. Locations of the second batch specimens in the two wind tunnels.	28
Figure 3.12. Image analysis procedure.	29
Figure 3.13. Specimens for unrestrained shrinkage tests.	32
Figure 3.14. The indented thumbtacks on the specimens for the unrestrained shrinkage	

test.....	33
Figure 3.15. Schematic diagram of the environmental chamber - plan view.	34
Figure 3.16. Interior of the environmental chamber.	35
Figure 3.17. The heater system in the environmental chamber.	35
Figure 3.18. Side view of wind tunnel.	37
Figure 3.19. Top view of wind tunnel.	37
Figure 3.20. The insert in a wind tunnel, with specimens in place.	38
Figure 3.21. The pressure transducer for measuring wind speed.	38
Figure 3.22. Layout of wind speed measurement points.	39
Figure 3.23. Measured wind speed in tunnel A.	40
Figure 3.24. Measured wind speed in tunnel B.	40
Figure 3.25. Locations of evaporation rate measurement specimens.	44
Figure 3.26. Evaporation rate at different locations in each tunnel (kg/m ² /h).	45
Figure 4.1. Typical plastic shrinkage cracking of specimens with fibrillated polypropylene fibres (scanned image).	47
Figure 4.2. Typical plastic shrinkage cracking of specimens with red baler twine fibres (scanned image).	48
Figure 4.3. Typical plastic shrinkage cracking of specimens with white baler twine fibres (scanned image).	49
Figure 4.4. Total crack area for all restrained plastic shrinkage specimens. Asterisks indicate cases that did not differ significantly from plain control specimens at the 95% level of confidence.	52
Figure 4.5. Maximum crack widths for all restrained plastic shrinkage specimens. Asterisks indicate cases that did not differ significantly from plain control specimens at the 95% level of confidence.	52
Figure 4.6. Average number of cracks observed for all restrained plastic shrinkage specimens. Asterisks indicate cases that did not differ significantly from plain control specimens at the 95% level of confidence.	53
Figure 4.7. Total crack area of specimens with all fibre types plotted against volume fraction.	55

Figure 4.8. Maximum crack width of specimens with all fibre types plotted against volume fraction.....	55
Figure 4.9. Comparison of maximum crack widths for specimens with the best fibre lengths.....	58
Figure 4.10. Comparison of total crack areas for specimens with the best fibre lengths.	58
Figure 4.11. Typical development of free shrinkage over time for 38 mm white baler twine.	59
Figure 4.12. Measured unrestrained plastic shrinkage strains 22 hours after casting. Asterisks indicate cases that did not differ significantly from plain control specimens at the 95% level of confidence.....	61
Figure 4.13. Unrestrained plastic shrinkage strains of all fibre types measured at 22 hours, plotted against volume fraction.	61
Figure 4.14. Schematic of restrained specimen, showing the contribution of various factors to the expected crack area.....	63
Figure 4.15. The contribution of various factors to the expected crack area for specimens reinforced with fibrillated polypropylene fibres.....	66
Figure 4.16. The contribution of various factors to the expected crack area for specimens reinforced with red baler twine fibres.....	67
Figure 4.17. The contribution of various factors to the expected crack area for specimens reinforced with white baler twine fibres.	67
Figure 4.18. Effect of specific surface area of fibres on total crack area for 38 mm long fibres.	73

LIST OF NOMENCLATURE

FPP	Fibrillated Polypropylene
RBT	Red Baler Twine
WBT	White Baler Twine
rms	Root-Mean-Square
RH	Relative humidity
i_u	the ratio of rms to mean
C.O.V.	Coefficient of Variation
S.D.	Standard Deviation
ASTM	American Society for Testing and Materials
FRC	Fibre Reinforced Concrete
S	Standard Deviation
n	Number of Samples
ν	Total Degrees of Freedom
S_c	Pooled Standard Deviation
S_d	Standard Error of the Difference Between Two Means
t	Difference Between Means Divided by Standard Error of Sample Means
t_{crit}	T-test Critical Value
T	Time
L	Length Between Indentations on the Thumb Tacks
ΔL (mm)	Length Change Between Indentations on the Thumb Tacks
dpi	Dots Per Inch

CHAPTER 1 INTRODUCTION

1.1. Background

Plastic shrinkage cracking of concrete is still a major problem in concrete members with large surface areas, such as slabs on grade, bridge decks and concrete pavements. Plastic shrinkage occurs in all fresh cement-based materials within the first few hours after they have been placed (Tolêdo Filho and Sanjuán 1999), especially during hot, windy and arid weather which can cause a fast rate of surface water evaporation. When the rate of evaporation exceeds the rate of bleed water rising to the surface, the concrete mixture will begin to shrink (Wang et al. 2001). If the shrinkage is restrained, tensile stress develops and can cause cracks.

Plastic shrinkage cracks become critical weak points for concrete members because aggressive substances can more easily penetrate into the internal portion of the concrete along the cracks, which leads to the acceleration of concrete deterioration. Consequently, the performance, serviceability, durability, and aesthetic qualities of concrete structures are reduced. Controlling plastic shrinkage cracking in concrete is essential for developing more durable and longer-lasting structures at a minimum life-cycle cost (Bayasi and McIntyre 2002).

To prevent plastic shrinkage cracking, the most widely accepted method is the use of randomly distributed fibres in volume fractions below 0.5% (Bayasi and McIntyre 2002). The fibres provide bridging forces across cracks and thus prevent the cracks from growing. In addition, the large pores that are introduced at the fibre-matrix interfaces are believed to provide bleeding channels which supply water to replenish the water lost from the surface. As a result, the capillary stress between the solid particles,

and hence the free plastic shrinkage potential, is reduced (Qi 2003).

It is well known that polypropylene fibres have gained acceptance for use as concrete reinforcement. However, the potential of used polypropylene materials, such as used polypropylene baler twine, has not received much attention.

Every year, thousands of tonnes of baler twine are used to bale hay and straw by farmers and ranchers in Canada. For example, each year, Alberta's agricultural sector alone generates close to 3500 tonnes of waste polypropylene baler twine (Randall Conrad & Assoc. Ltd. 2000). The used baler twine is normally discarded and either burned or transported to landfills after its first use, which leads to a severe waste of resources. If the used baler twine can be collected, chopped and packaged inexpensively, it may provide an alternative low cost fibre for the concrete industry. However, the effect of using chopped baler twine as concrete reinforcement must first be investigated.

A previous study found that baler twine fibres are capable of increasing flexural toughness to concrete, although slightly higher dosages are required to achieve the same performance as found with fibrillated polypropylene fibres (Hameed 2002). The research described in this thesis investigated another important potential use for baler twine fibres, the effect of baler twine fibres on plastic shrinkage of cement mortars.

1.2. Objectives

The main objective of the research described in this thesis is to determine whether low volume fraction baler twine fibres are useful for controlling the restrained and unrestrained plastic shrinkage of mortar. Specific sub-objectives include the following:

- to determine to what extent the addition of polypropylene baler twine, cut to short lengths, is able to reduce the size and total area of cracks caused by restrained plastic shrinkage;

- to determine the influence of baler twine fibre addition on the propensity for free plastic shrinkage;
- to compare the performance of baler twine fibre with that of a commercially available synthetic fibre at equal lengths and volume fractions; and
- to determine the influence of baler twine fibre length and volume fraction on their performance.

1.3. Scope

The scope of this project is limited to investigating the influence of the following factors on the plastic shrinkage properties of cement mortar:

- Fibre type: two types of baler twine (one composed of strands with circular cross section, the other composed of flat band shape strands), and fibrillated polypropylene were considered;
- Fibre length: 19 mm and 38 mm nominal lengths were investigated; and
- Fibre volume fraction: 0.05%, 0.1% and 0.3% were studied.

Fibre lengths of 19 mm and 38 mm were chosen because they are typical fibre lengths of commercially available synthetic fibres. The volume fractions investigated are typical of the amount of fibrillated polypropylene fibres commonly used.

The influence of these factors on the restrained plastic shrinkage properties of fibre reinforced cement mortar was investigated by measuring the total crack area and maximum crack width on specimen surfaces.

The unrestrained plastic shrinkage tests were carried out to determine whether the reduction in restrained plastic shrinkage cracking could be partially attributed to the overall reduction in free plastic shrinkage.

1.4. Methodology

In this research, all mixtures were prepared using traditional concrete materials and mixing methods. For the restrained plastic shrinkage tests, substrate bases were cast before casting overlays and underwent a standard 28 day curing procedure. Then, the fresh fibre-reinforced overlay mortars were cast over the roughened substrate bases and transferred to the environmental chamber with hot, dry and windy conditions. Crack numbers were recorded 22 hours later. At the same time, maximum crack width and total crack area were measured using an image analysis method. For unrestrained plastic shrinkage tests, all mortar specimens were cast into moulds directly, without the substrate bases. Then the specimens were transferred into the environmental chamber with the same environmental conditions as the restrained shrinkage tests. Two indented thumb tacks were embedded on each specimen's top surface after demoulding. The distance between the thumb tacks was measured using a digital caliper every 30 minutes for 5 hours, with a final measurement made 22 hours later.

1.5. Dissertation Organization

This thesis is organized into five chapters. Details of each chapter are described as follows.

Chapter 1 gives an introduction to the research.

Chapter 2 provides a literature review of the plastic shrinkage mechanisms, factors affecting plastic shrinkage cracking and typical test methods for measuring plastic shrinkage.

Chapter 3 describes the experimental methods, including materials, concrete mix design, specimen preparation, environmental chamber setup and test procedures.

Chapter 4 provides test results, as well as an analysis and discussion of the results. Both Chapter 3 and Chapter 4 contain two phases: restrained plastic shrinkage testing and unrestrained plastic shrinkage testing.

Chapter 5 presents conclusions of this research and recommendations for future work.

CHAPTER 2 LITERATURE REVIEW

2.1. Introduction

In this chapter, a summary of previous studies on plastic shrinkage cracking is provided. The mechanisms for plastic shrinkage cracking are first reviewed. Then, the factors that affect the plastic shrinkage cracking are summarized. In this part, the influence of fibres on the plastic shrinkage cracking of concrete is emphasized. Finally, the experimental methods for plastic shrinkage testing are introduced.

2.2. Plastic Shrinkage Cracking Mechanism

2.2.1. Plastic shrinkage

Plastic shrinkage is caused by the volume change that occurs in all fresh cement-based materials within the first few hours after placement when the mixture is still plastic and has not yet achieved any significant strength (Toledo Filho et al. 2005). This volume change is mainly caused by the pressure that develops in the capillary pores of concrete when the evaporation rate of concrete surface water exceeds the rate at which bleeding water rises to the surface. During evaporation, water is lost from near the surface of a concrete element and forms curved liquid surfaces between the surfaces of solid particles within the concrete, introducing surface menisci. Negative capillary pressure forms within the concrete as a result of the surface tension within the menisci, which, in turn, reduces the distance between the concrete solid particles, as shown in Fig. 2.1. As a result, the concrete starts to shrink. If this shrinkage is restrained in any way, tensile stress develops, and plastic shrinkage cracking may occur (Wang et al. 2001).

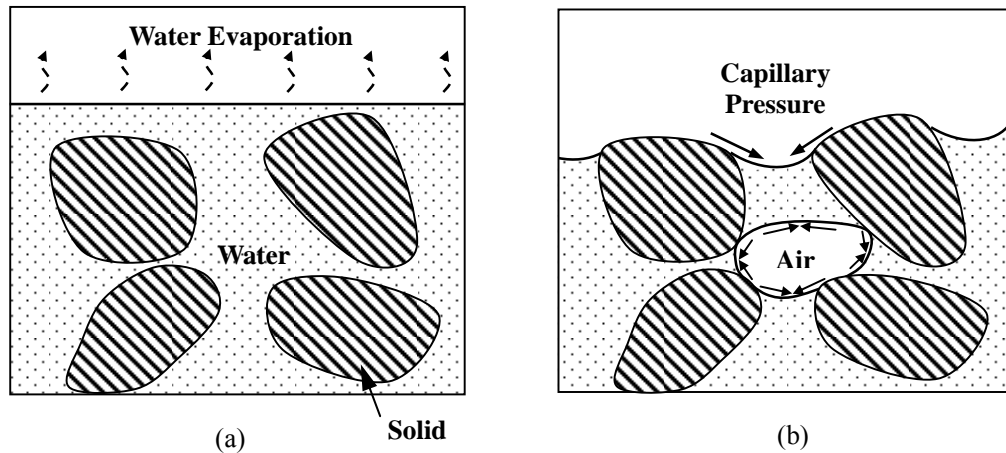


Figure 2.1. Schematic of capillary meniscus development between solid particles. (a) Surface water starts to evaporate. (b) Water meniscus forms between the solid particles at or near the surface of concrete due to water evaporation.

2.2.2. Plastic settlement

Plastic shrinkage cracking can also be caused by plastic settlement. As concrete is placed, the solid particles start to settle and water among the particles of the freshly mixed concrete rises or bleeds to the surface. When the solid particles are obstructed by rigid objects in concrete such as large aggregates and rebar, differential settlement occurs and tension stresses are induced above the obstructions, which will cause plastic cracking. The plastic cracking can be also found at changes in section depth which causes differential settlement. Figure 2.2 illustrates the formation of plastic cracking above the large aggregate particles, rebar and section thickness changes (Weyers et al. 1982).

2.3. Factors that Affect Plastic Shrinkage Cracking

2.3.1. Influence of fibres

To date, a large amount of research has been carried out to investigate the influence of randomly distributed fibres on plastic shrinkage cracking of concrete. It has been suggested that fibre reinforcement is one of the most effective methods to reduce plastic shrinkage cracking (Banthia and Yan 2000). Among the different fibres used for controlling plastic shrinkage cracking, the most promising are synthetic fibres, such as

polypropylene fibres. Wang et al. (2001) studied five different types of fibres (PVA, steel, fibrillated polypropylene, polypropylene microfibre, and cellulose). They found that when 0.1% volume fraction of fibres were added, the total plastic shrinkage crack area was reduced by 30 to 40%. The average crack widths were reduced by 20%. Polypropylene microfibrils and steel fibres were more effective when compared with the other three types of fibres for reducing the total crack area. Najm and Balaguru (2002) investigated the effect of polymeric fibres on plastic shrinkage cracking of mortar specimens. They reported that polymeric fibres were more effective than steel fibres in controlling plastic shrinkage cracking. The polymeric fibres provided the same crack reduction as steel fibres at half the steel fibre volume fraction. Banthia et al. (1996) found that steel fibres not only reduced the maximum crack widths but also caused multiple cracking in the composite up to a fibre volume fraction of 0.5%. Only minimal cracking occurred at a 0.1% volume fraction even under a severe environment (temperature = 38°C, and relative humidity = 5%). Polyolefin fibres were found to be very effective in reducing the extent of shrinkage cracking and in reducing the crack widths (Banthia and Yan 2000). Sanjuán and Moragues (1997) and Ma et al. (2005) found that the addition of polypropylene fibres in cement mortar can reduce the plastic shrinkage cracking effectively.

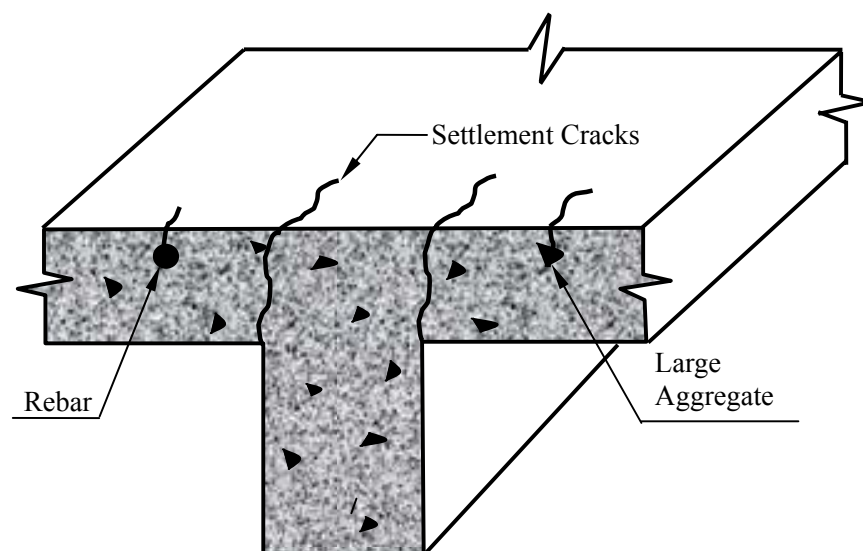


Figure 2.2. Plastic cracking caused by differential settlement above rebar, large aggregates and changes in concrete section thickness.

Different fibre parameters, such as volume fraction, diameter, length and geometry have different influences on plastic shrinkage cracking. Naaman et al. (2005) reported that higher volume fractions of fibres will lead to better control of plastic shrinkage cracking. This trend has also been found by Wang et al. (2001), Banthia et al. (1996), Qi (2003), Boghossian and Wegner (2003), Sanjuán and Moragues (1997), and Banthia and Gupta (2006).

Fibre diameter was also found to be one of the most influential parameters in controlling plastic shrinkage cracking of concrete. Naaman et al. (2005) reported that, for a given fibre volume fraction, a decrease in fibre diameter led to a significant improvement in control of plastic shrinkage cracking. The same result has also been observed by Qi (2003) and Banthia and Gupta (2006).

Boghossian and Wegner (2003), Naaman et al. (2005) and Wongtanakitcharoen (2005) found that the fibre length or aspect ratio (the ratio of fibre length to diameter) only had a slight influence on how well plastic shrinkage cracking could be controlled. However, tests carried out by Banthia and Yan (2000) and Najm and Balaguru (2002) found that fibres with a higher aspect ratio were generally more effective at controlling cracking.

The geometry of fibres is also an important parameter in mitigating plastic shrinkage cracking. Banthia and Gupta (2006) found that fibrillated fibres were more effective in controlling shrinkage cracking than their monofilament counterparts. However, according to the test carried out by Naaman et al. (2005), fibrillated polypropylene fibres were found to be less effective than monofilament polypropylene fibres in controlling plastic shrinkage cracking; however, this difference almost vanished when the volume fraction of fibre was increased to 0.4%. Qian et al. (2005) found that fibres with polygonal cross sections performed better than those with circular cross sections in reducing the plastic shrinkage cracking.

Recently, more and more studies have begun to focus on the effectiveness of natural fibres in controlling plastic shrinkage cracking. It was found that flax fibres

were as effective as other commercially available fibres in reducing plastic shrinkage cracking, decreasing the total crack area and maximum crack width by 99% relative to plain mortar at 0.3% volume fraction (Boghossian and Wegner 2003). Toledo-Filho and Sanjuán (1999) found that the addition of 25 mm long sisal fibres, at 0.2% by volume, were as effective as polypropylene fibres in controlling plastic shrinkage cracking. Toledo-Filho et al. (2005) reported that free plastic shrinkage was significantly reduced by the inclusion of 0.2% volume fraction of 25 mm short sisal fibres in cement mortar. Furthermore, the addition of 0.2% volume fraction of 25 mm sisal and coconut fibres was found to delay the initial cracking caused by restrained plastic shrinkage and to effectively control crack development at early ages of concrete.

The influence of fibres on free plastic shrinkage is also a primary factor used to evaluate the effectiveness of fibres in reducing plastic shrinkage cracking, even though a reduction in free shrinkage does not necessarily indicate the overall reduction in crack tendency (Toledo-Filho and Sanjuán 1999). According to the tests carried out by Boghossian and Wegner (2003), among the fibre types investigated (flax, monofilament polypropylene, fibrillated polypropylene and glass fibre), only glass fibres had a significant influence on the free plastic shrinkage. In 1999, Toledo-Filho and Sanjuán found that low-volume sisal and polypropylene fibres were very effective in reducing free plastic shrinkage. Wongtanakitcharoen (2005) reported that an average reduction of free shrinkage strain of 34% and 30% could be achieved by adding polypropylene, PVA, or carbon fibres to fresh concrete at 0.4% and 0.1% volume fraction, respectively. The fibre elastic modulus, fibre aspect ratio, and fibre bond with the matrix did not have a significant effect on free plastic shrinkage strain.

It is well accepted that adding fibres to concrete is an effective way to reduce plastic shrinkage cracking. However, the precise mechanism by which fibres reduce plastic shrinkage cracking is still not clear. Wang et al. (2001), Qi (2003) and Wongtanakitcharoen (2005) concluded that fibres introduced a group of large pores at the fibre-matrix interfaces. These large pores provided bleeding channels along the fibres in the mixture, which supplied water to replenish the water lost from the surface. As a result,

the capillary stress between the solid particles, and hence the plastic shrinkage cracking potential, was reduced. Besides this conclusion, Qi (2003) believed that fibre reinforced mixtures exhibited less plastic settlement than plain mixture, resulting in a reduction in plastic cracking. In tests carried out by Soroushian et al. (1995), they found that concrete with polypropylene fibres bled less and set faster than plain concrete; therefore, the time of exposure to plastic shrinkage and the quantity of harmful capillaries formed by bleeding were reduced. Boghossian and Wegner (2003) believed that the ability of fibres to reduce cracking must be attributed primarily to its ability to improve the tensile capacity of the fresh mortars and prevent the cracks from growing.

2.3.2. Influence of environmental conditions

Plastic shrinkage cracking generally occurs in fresh concrete when the evaporation rate is high. High evaporation rates are caused by high temperatures, high wind speeds and low relative humidity. A graphical method to estimate evaporation rate is described in ACI 305R (1999) and reproduced in Fig. 2.3. If the evaporation rate approaches 1 kg/m²/h, the chance of plastic shrinkage cracking occurring is high (ACI 305R 1999). Waris (1996) also found that the evaporation rate, as well as crack length and crack area on concrete specimens, increased with increasing wind velocity and ambient temperature and decreasing relative humidity. However, the effect of relative humidity on the evaporation rate was not significant when the wind speed was high.

2.3.3. Influence of other factors

Plastic shrinkage can be also affected by the mix proportions. Sanjuán and Moragues (1997) reported that plastic shrinkage decreased when the cement/sand or water/cement ratios were reduced. The combined influence of both parameters was larger than that of the water/cement ratio alone. Tests carried out by Wang et al. (2001) found that specimens with a high water/cement ratio had a high water loss and cracked later than specimens with a low water/cement ratio.

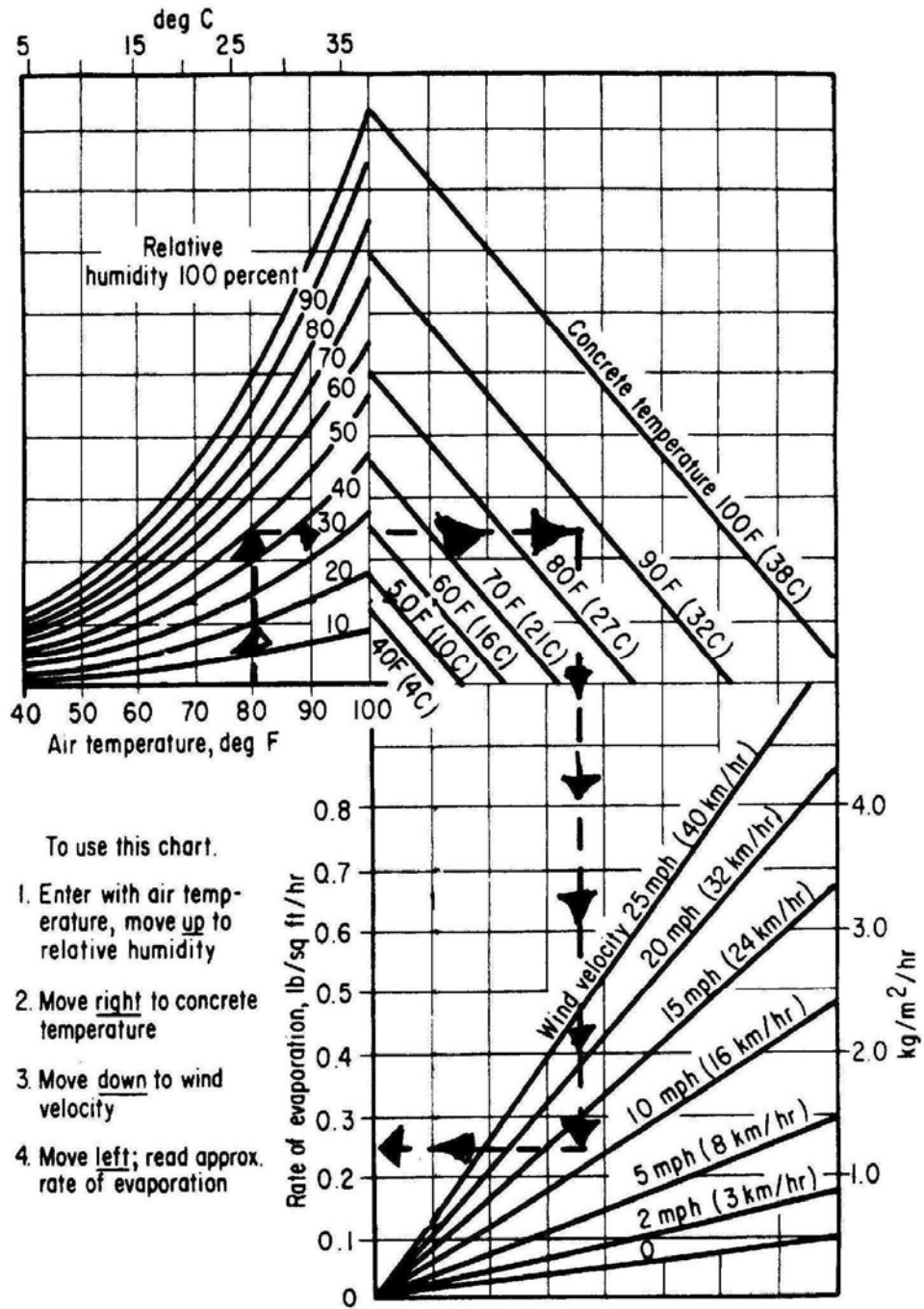


Figure 2.3. Evaporation rate estimation (ACI 305R 1999).

Some pozzolanic materials and chemical admixtures in concrete can also affect plastic shrinkage. It was found by Bayasi and McIntyre (2002) that the crack area and maximum crack width consistently increased with increasing silica fume volume fraction. Al-Amoudi et al. (2004) reported that an increase of plastic shrinkage strain was found with an increasing dosage of silica fume and that all specimens with silica fume had higher plastic shrinkage strains than plain specimens. Wang et al. (2001) conducted a study to examine the influence of fly ash and fibres on plastic shrinkage cracking in concrete materials. They found that different types of fly ash influenced plastic shrinkage in different ways. Pastes with 30 and 50% Regular Class F fly ash developed smaller total crack areas than plain paste. However, the paste with ultra-fine Class C fly ash had a higher crack area than the plain paste. The opposite effects produced by silica fume and regular fly ash are believed to be caused by their different particle size. The paste with silica fume, which has smaller particle sizes, has a denser texture, smaller bleeding rate and more plastic shrinkage than the paste with fly ash. The effect of superplasticizer on plastic shrinkage of concrete was investigated by Al-Amoudi et al. (2006). They reported that superplasticizer had a positive effect of reducing plastic shrinkage cracking.

2.4. Experimental Methods for Plastic Shrinkage

2.4.1. Restrained plastic shrinkage tests

To date, there are no standard test methods to measure plastic shrinkage cracking. Specimens with different shapes, sizes and restraint conditions have been used to evaluate plastic shrinkage cracking. Classified by different specimen shape, there are three main test methods: tests with ring-type specimens, tests with slab-type specimens, and tests with linear beam specimens.

Ring specimens have been used by a number of researchers to investigate plastic shrinkage cracking over the past several decades. In this test, the specimen is cast between two rigid rings as shown in Fig. 2.4. The outer ring is placed concentrically with the inner ring to provide the required thickness of the specimen. It

is removed before the specimen is subjected to drying. The inner ring provides the restraint while the specimen is subjected to drying. After the outer ring is removed, the top and bottom surfaces of the concrete ring are sealed in order to allow drying in one direction only (Carlson and Reading 1988, Swamy and Stravides 1979, Balaguru and Bhatt 2000, Groth 2000).

In 1985, Kraai proposed the slab test method to evaluate the cracking potential due to drying shrinkage of concrete. From then on, slab specimens of different sizes and methods of restraint have been widely used by many other researchers (Shaeles and Hover 1988, Cohen et al. 1990, Balaguru, 1994, Soroushian et al. 1995). For example Najm and Balaguru (2002) used slab specimens to study the plastic shrinkage properties of mortar reinforced with large-diameter polymeric fibres. The specimen was cast in a 600×900×19 mm mould which was composed of a plywood base and plexiglas edges, as shown in Fig. 2.5. A tile board was glued on top of the plywood to obtain a smooth non-absorbing surface, and a thin polyethylene sheet was placed on top of the tile board to allow the concrete slab to shrink freely. The restraint was provided by a strip of wire mesh which was nailed to the base along the perimeter of the slab. In a later study (Qi et al. 2003), a 508×254 mm slab specimen that incorporated sheet metal stress risers, as shown in Fig. 2.6, was used to assess early age cracking. In this type of specimen, cracking is expected to occur above the stress riser, extending across the width of the specimen. This test procedure was modified from Berke and Dalliare (1994).

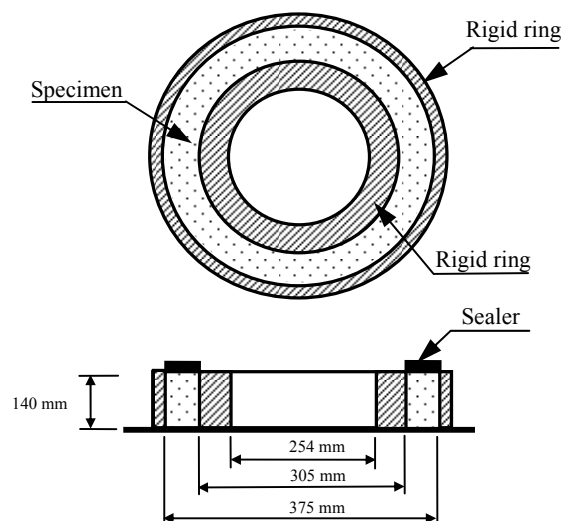


Figure 2.4. Details of ring specimen used by Groth (2000).

A beam specimen with end restraints was used by Banthia et al. (1993) to study the restrained shrinkage cracking in fibre-reinforced cementitious composites. A $40 \times 40 \times 500$ mm prismatic specimen was restrained by two triple-bar anchors attached to a rigid frame, as shown in Fig. 2.7.

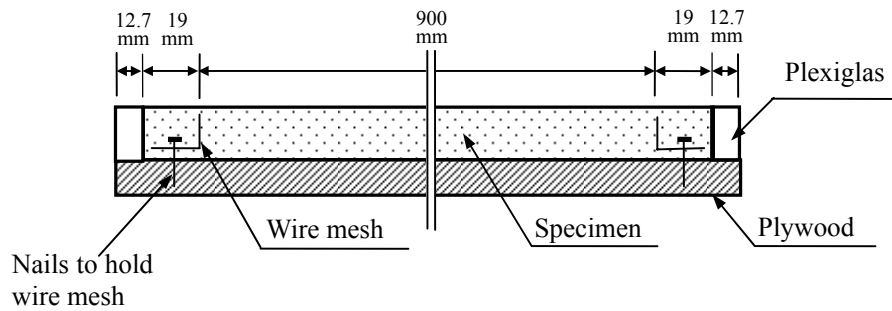


Figure 2.5. Side view of slab specimen used by Najm and Balaguru (2002).

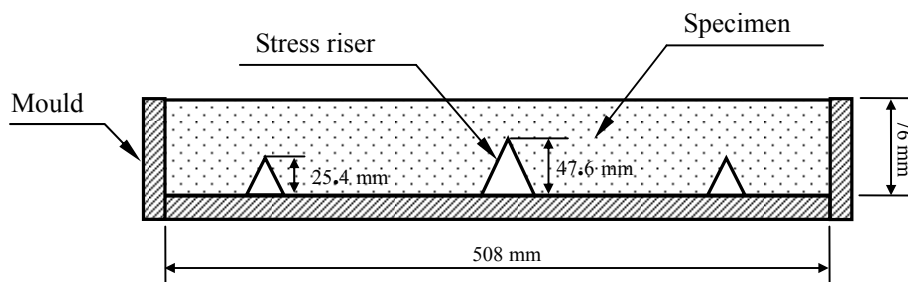


Figure 2.6. Side view of slab specimen used by Qi et al. (2003).

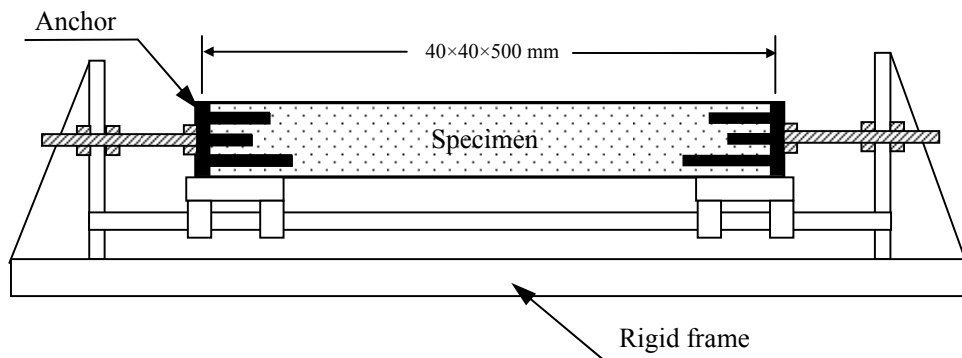


Figure 2.7. Side view of end restrained beam test used by Banthia et al. (1993).

All the test methods mentioned above are idealized approximations of real conditions, and do not consider the bond between a concrete topping and substructure that influences the crack behaviour (Banthia et al. 1993). In order to more accurately simulate the actual restraint conditions, Banthia et al. (1996) proposed a new method to evaluate the cracking potential of cement-based materials. In this test, substrate bases with 20 mm aggregates protruding above the surface were prepared. Next, fresh overlays were cast on the hardened bases. The rough surfaces of the bases provided restraining forces to the overlays while the whole assembly was subjected to a drying environment. Figure 2.8 shows the test set-up. Modifications to Banthia's test method have been used by many other researchers. For example, concrete substrates with notched surfaces, as illustrated in Fig. 2.9, were used to apply restraint to concrete overlays in the tests carried out by Naaman et al. (2005). In 2003, Boghossian and Wegner studied the plastic shrinkage properties of flax fibre reinforced concrete by casting mortar specimens directly on substrate bases. These bases had a regular pattern of hemispherical bumps protruding 1 cm above the surface, as shown in Fig. 2.10. These hemispherical bumps provided more or less uniform restraint to the overlays. This method had previously been used by Banthia's group at the University of British Columbia, but was apparently not published until later (Banthia and Gupta 2006).

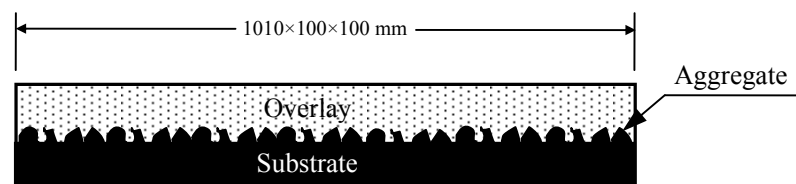


Figure 2.8. Side view of shrinkage test specimen used by Banthia et al. (2000).

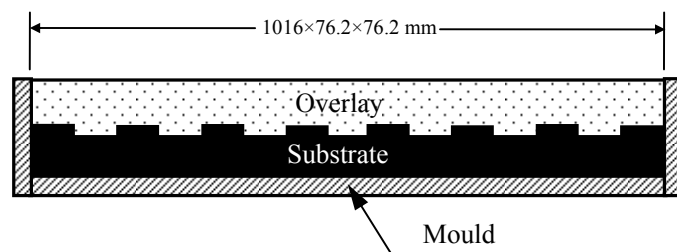


Figure 2.9. Side view of shrinkage test specimen used by Naaman et al. (2005).

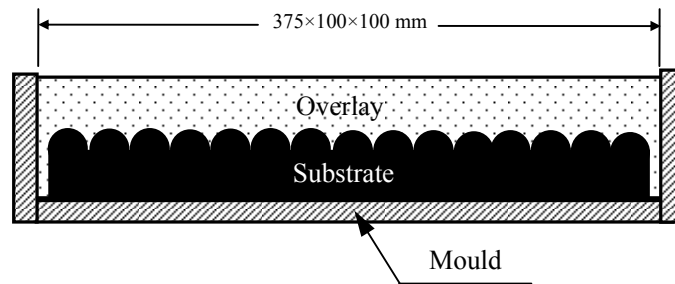


Figure 2.10. Side view of shrinkage test specimen used by Boghossian and Wegner (2003).

Because of the various test methods, test results differ considerably, and there is no consensus regarding how to properly interpret the data. A standardized test method is urgently needed to enable researchers to effectively investigate plastic shrinkage cracking (Banthia et al. 1996, Qi 2003).

2.4.2. Unrestrained plastic shrinkage tests

A standard test method for measuring the length change of hardened mortar or concrete specimens was introduced in ASTM C157. However, it is still a challenge to measure the early-age shrinkage of concrete, while it is still in a plastic state, and no standardized method exists to evaluate unrestrained plastic shrinkage (Holt 2004). Toledo Filho and Sanjuán (1999) and Toledo Filho et al. (2005) used dial gauge extensometers located on the upper surface of fresh specimens to measure the horizontal deformation. In tests carried out by Al-Amoudi et al. (2004), Al-Amoudi et al. (2006) and Holt (2004), the horizontal shrinkage was measured by linear variable differential transducers connected to a data acquisition system. Tia et al. (2005) embedded a strain gauge in the centre of fresh concrete specimens to record the length change. In the tests carried out by Boghossian and Wegner (2003), two small indented brass plates were embedded on the surface of each specimen, separated longitudinally by a distance of about 200 mm. The distance between plate indentations was measured using a digital caliper every 30 minutes for 6 hours.

CHAPTER 3 EXPERIMENTAL PROGRAM

3.1. Introduction

This chapter gives a detailed description of the materials and experimental methods used in this study. The materials and mixture proportions are described in detail in the first section. The second section includes the detailed testing procedure and environmental conditions. The experimental program was divided into two experiments:

- **Restrained plastic shrinkage test:** In this test, fresh fibre-reinforced overlay mortars were cast over roughened concrete substrate bases and subjected to hot, dry and windy conditions in an environmental chamber to promote cracking. Crack numbers, widths and lengths were measured 22 hours after the specimens were transferred to the environmental chamber.
- **Unrestrained plastic shrinkage test:** In this test, all fresh mortar specimens were cast directly into moulds, without the substrate bases. Then the specimens were transferred into the environmental chamber with the same environmental conditions as those of the restrained shrinkage test. The free shrinkage strains were measured every 30 minutes for 5 hours, with a final measurement made 22 hours later.

3.2. Materials

3.2.1. Concrete ingredients

Crushed stone (nominal maximum size 12.5 mm) and river sand, both found in the Saskatoon area, were used as coarse and fine aggregate, respectively. The specific gravity and gradation of aggregates were measured by Wang (2003) according to ASTM

Standards C29 (1997) and C136 (2001). Table 3.1 provides the results. Both fine and coarse aggregates met the grading requirements of ASTM Standard C33-03 (2003). A Type 10 cement with 8% silica fume, supplied by Lafarge Canada Inc. (Saskatoon, SK), was used in all mixes.

Water from the Saskatoon municipal water supply was used to prepare all specimens in this test. Superplasticizer (DARAC[®] 100, W.R. GRACE, Ajax, ON) was used to increase the workability of concrete for substrate bases. The dosage recommended by the manufacturer was 0.325 to 1.25 L per 100 kg of cement.

Table 3.1. Properties of coarse and fine aggregates (Wang 2003).

Aggregates	Specific Gravity (10 ³ kg/m ³)	Standard Sieve Size (mm)	Percent Passing (%)
Coarse	2.6	19	100.0
		12.5	96.5
		9.5	66.7
		4.75	15.4
		2.36	9.8
		1.18	7.6
Fine	2.3	9.5	100.0
		4.75	95.9
		2.36	88.5
		1.18	77.4
		0.6	48.8
		0.3	17.3
		0.15	3.3

3.2.2. Fibres

Three types of fibres were investigated in this study. They are referred to as white baler twine (Plastic twine P-0700, Barry & Boulerice Inc. Dallard-Des-Ormeaux, QC), red baler twine (Field King Super Round 280, Interprovincial Cooperative Limited, Winnipeg, MB) and fibrillated polypropylene fibres (Forta[®] ECONONET[™], FORTA

Corporation, Grove City, PA). Figure 3.1 shows a picture of these fibres. These three types of fibres are all made from polypropylene. However, the fibre forms are quite different from each other. The white baler twine was composed of flat band-shaped strands which are twisted together (see Fig 3.2). The red baler twine was composed of strands with circular cross sections. These strands are not only twisted together but also glued together at certain intervals along their length as shown in Fig. 3.3. The fibrillated polypropylene fibres are composed of film sheets which are collated or held together by cross linking fine fibres along their length as shown in Fig. 3.4 (Brown et al. 2002). Two fibre lengths (19 mm and 38 mm) and three volume fractions (0.05%, 0.1%, and 0.3%) were investigated for each type of fibre. Some of the physical and mechanical properties of these fibres are summarized in Table 3.2.

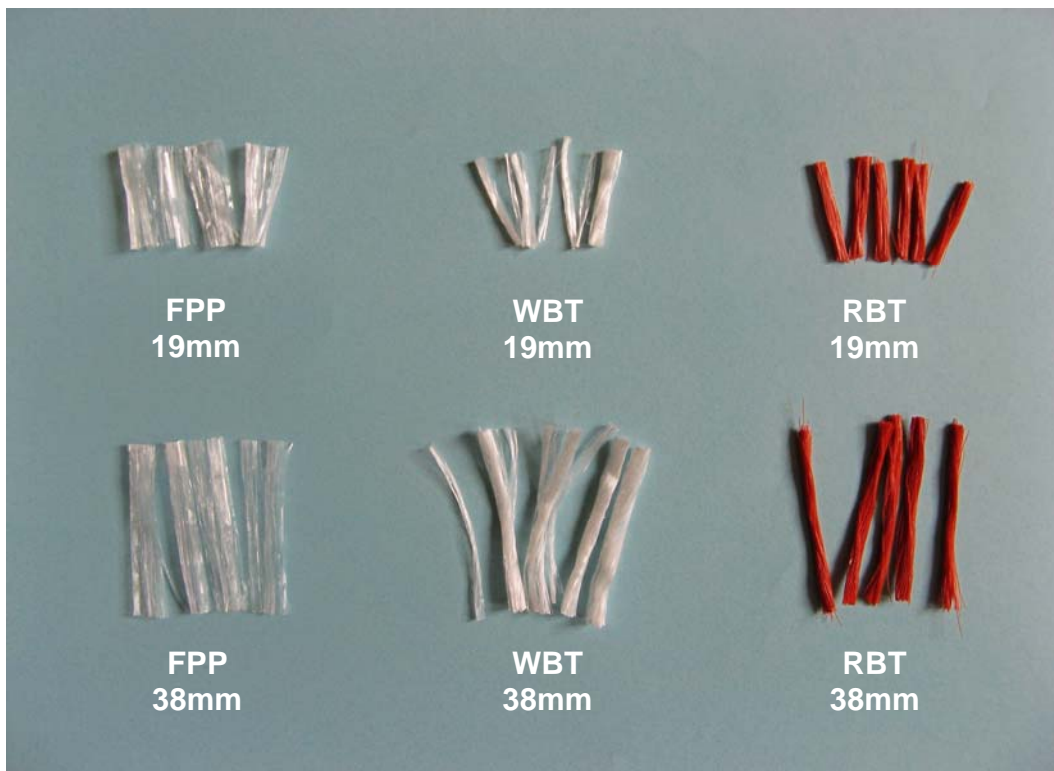


Figure 3.1. Fibre types used in the experiment. (FPP: fibrillated polypropylene, WBT: white baler twine, RBT: red baler twine)



Figure 3.2. White baler twine strands.

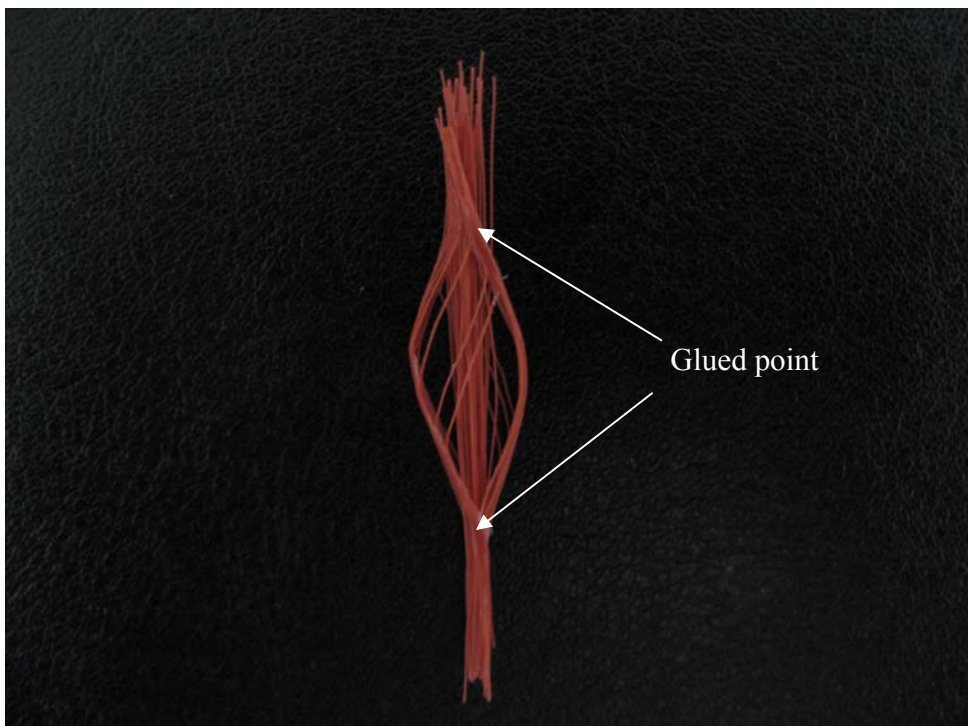


Figure 3.3. Red baler twine strand.

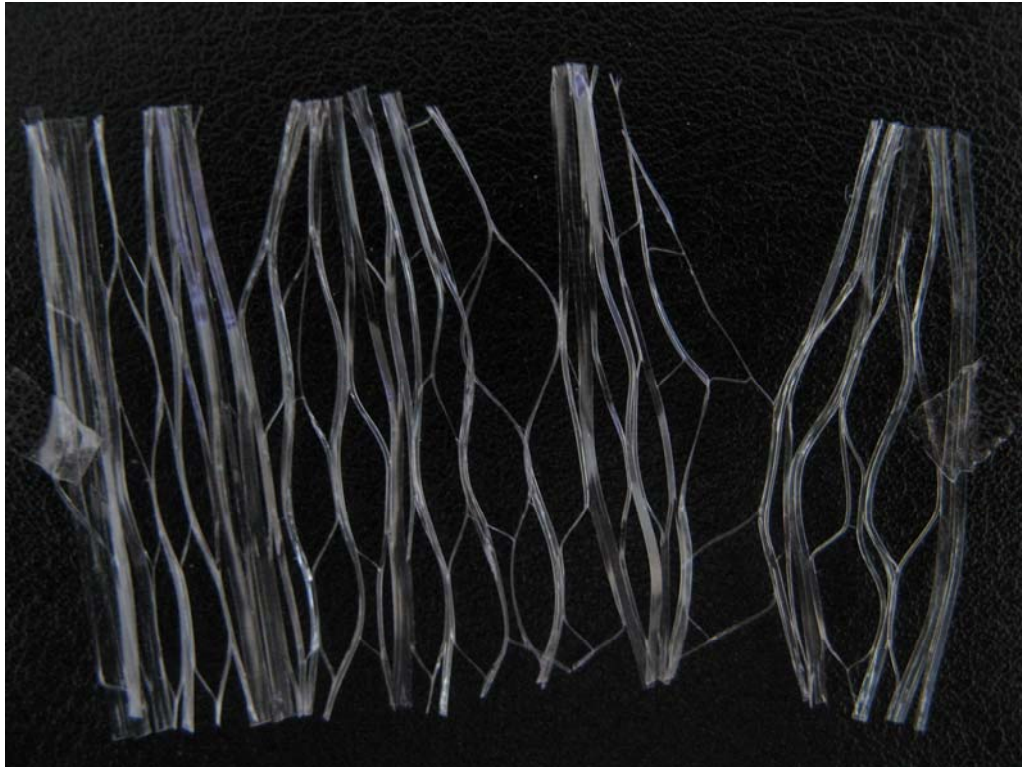


Figure 3.4. Fibrillated polypropylene fibre.

Table 3.2. Fibre properties.

Fibre type	Strand shape	Specific gravity (g/cc)	Tensile strength (MPa)	Length (mm)	Diameter (μm)
Red Baler Twine (RBT)	Circular	0.91	415*	19, 38	170
White Baler Twine (WBT)	Flat	0.91	N/A	19, 38	N/A [‡]
Fibrillated Polypropylene (FPP)	Flat	0.91	620-758 [†]	19, 38	N/A [‡]

* Estimated from manufacturer reported properties

[†] As reported by manufacture

[‡] Individual fibres cannot be identified

The unused polypropylene baler twine was taken directly from a new roll and was chopped into lengths of 19 mm and 38 mm using the method proposed by Hameed (2002), as shown in Fig. 3.5. Baler twine was wrapped on a V-notched hollow shaft in a single layer with the assistance of a motor driven drill-press chuck (J. Walter Co. Ltd.). The perimeter of the shaft was equal to the desired length of the fibre. The shaft was laid on a flat surface with the V-notch on top. The shaft was then pressed against the surface to avoid slackness in the wrapped twine and the twine was cut by passing a blade through the V-notch.



Figure 3.5. Baler twine cutting operation.

3.2.3. Mixture proportions

The specimens for the restrained plastic shrinkage tests consisted of two different parts: substrate bases and overlays. Plain concrete with a water to cement ratio of 0.28 was used to prepare the substrate bases. To enhance the strength of the substrate bases, Type 10 cement with 8% silica fume was used and superplasticizer was added to obtain an adequate level of workability.

In order to increase the potential for cracking and enhance the ability to compare the performance of different fibre types, two means were adopted. First, mortar rather than concrete, with a water to cement ratio of 0.46 was used to make overlays. Second, Type 10 cement with 8% silica fume was used in the mortar. As discussed in Chapter 2, silica fume has been shown to increase the propensity for plastic shrinkage cracking. Nineteen different kinds of overlay mortars were cast on top of the hardened substrate bases, each one having a different combination of fibre type, length, and volume fraction as shown in Table 3.3. Table 3.4 provides the mixture proportions for substrate bases and overlays. These mix proportions are identical to those used by Boghossian (2004) and are similar to those used at the University of British Columbia for restrained plastic shrinkage studies (Banthia and Yan 2000).

Table 3.3. List of specimens and the number of specimens used for each combination.

Specimen	Fibre length (mm)	Fibre volume fraction (%)	Number of specimens
Plain			24
Specimens with fibrillated polypropylene	19	0.05	4
	19	0.1	4
	19	0.3	4
	38	0.05	4
	38	0.1	4
Specimens with red baler twine	38	0.3	4
	19	0.05	4
	19	0.1	4
	19	0.3	4
	38	0.05	4
Specimens with white baler twine	38	0.1	4
	38	0.3	4
	19	0.05	4
	19	0.1	4
	19	0.3	4

Table 3.4. Mix proportions by mass.

Ingredient	Overlay Mortars	Substrate Bases
Type 10 cement (8% silica fume)	1.00	1.00
Water	0.46	0.28
Sand	0.95	1.36
Coarse aggregate	—	1.36
Superplasticizer	—	3mL/kg
Fibres	varied	—

Specimens for the unrestrained plastic shrinkage tests were prepared by directly casting the fresh mortar in the mould, without the substrate bases. The mortar mix proportions were identical to those of the overlay mortars used in the restrained plastic shrinkage tests.

3.3. Test Procedures for Restrained Plastic Shrinkage

3.3.1. Specimen preparation

The specimens used for restrained plastic shrinkage testing were identical to those used by Boghossian (2004), which were modelled after work conducted by Banthia at the University of British Columbia. The specimens were prepared in two steps. First, the mixture for the substrate bases was prepared according to ASTM C 192 (2002). A rotary mixer (Monarch Industries, Type C9-CE, Winnipeg, MB) with a capacity of approximately 0.15 m³ was used for all substrate mixes. The substrate bases were cast into 95 x 325 x 40 mm deep oiled PVC moulds. The bottom surface of the moulds had a regular pattern of hemispherical holes which were 1 cm in radius, as shown in Fig. 3.6. To enhance the linear stiffness and the restraint to the overlay, two 15 mm diameter steel bars were placed longitudinally into each base (See Fig. 3.7). The bases were demoulded 24 hours after casting and immersed in lime-saturated water at 25°C for at least 28 days to achieve sufficient strength. The bases were subsequently removed from the water and air-dried at a temperature of approximately 22°C for one day before testing. The bases cast from these moulds had a regular pattern of

hemispherical bumps protruding 1 cm above the surface, as shown in Fig. 3.8. These bumps supplied more or less uniform restraint conditions for the overlays, which were identical for all specimens.

Secondly, 19 different kinds of overlay mortars were cast. Except for the plain specimens, each one had a different combination of fibre type, length, and volume fraction, as shown in Table 3.3. Four specimens for each combination were cast and tested. All the specimens were mixed in 12 batches. Each batch consisted of two plain control specimens and six fibre reinforced specimens having the same fibre type and length. Two specimens were cast for each of the three volume fractions tested. In this way, the differences between batches were minimized. In total, 96 specimens, including plain control specimens, were cast.



Figure 3.6. The mould for casting substrate bases.



Figure 3.7. Reinforcing bars positioned in the mould.



Figure 3.8. The substrate base.

All mortars used in this test were mixed in a pan mixer (Brook Motor Ltd, Type Z.T.3, Toronto, ON). The mixing procedure for each batch was consistently timed. After placing the appropriate amount of mixing water in the pan, cement and sand were added and allowed to mix for one minute. The mixer was then stopped, and the mortar was allowed to rest for two minutes. During this time the mixer was scraped to ensure that no mortar was adhering to the side or bottom of the pan. After the mortar was mixed for a final two minutes, plain specimens were cast. After that, enough fibres to produce a volume fraction of 0.05% were added to the running mixer gradually over a period of three minutes to ensure the even distribution of fibres; the mixer was then stopped for two minutes and scraped. Two specimens were cast after mixing two more minutes. The specimens with the other two volume fractions were prepared by adding additional fibres to the same batch. This was done after the first two specimens at 0.05% volume fraction had been cast, and then again after a second two specimens with 0.1% volume fraction had been cast. This procedure minimized the differences in mortar properties among the specimens with different fibre volume fractions.

Before casting the specimens, all moulds were oiled. The hardened substrate bases were positioned in the centre of moulds, which were 100 mm x 375 mm in plan and 100 mm in depth. The overlay mortars were then cast over the substrate bases as shown in Fig. 3.9. The resulting mortar overlays were 60 mm thick and slightly larger in plan than the bases, which can prevent curling-up of the overlays at the ends. The specimens were vibrated on a vibrating table until the surface of concrete became smooth and no

large air bubbles broke through the top surface. After vibrating, the surfaces were lightly trowelled by a smooth steel trowel.

3.3.2. Specimen testing

After finishing the specimens' surfaces, they were transferred to two wind tunnels located in a 3 m x 3 m environmental chamber where they were subjected to conditions to promote cracking. Details of the wind tunnels and environmental chamber, including a description of test conditions, are provided in Section 3.5. Since each wind tunnel could accommodate four specimens, two different batches were required to produce and test all 12 specimens with a certain fibre type and fibre length at all different fibre volume fractions along with the four additional plain control specimens. For each batch, the locations of identical specimens in the wind tunnels were varied as shown in Fig. 3.10 and Fig. 3.11. In this way, the influence of slight differences in environmental conditions among the different locations and between the two tunnels, as described in Section 3.5, was minimized. About one hour after the samples were moved into the environmental chamber, moulds were removed carefully using quick release levers to avoid disturbing the fresh mortar. The crack numbers, maximum crack width and total crack area were measured 22 hours after casting, as described in the following section.



Figure 3.9. Casting of overlays over the substrate bases.

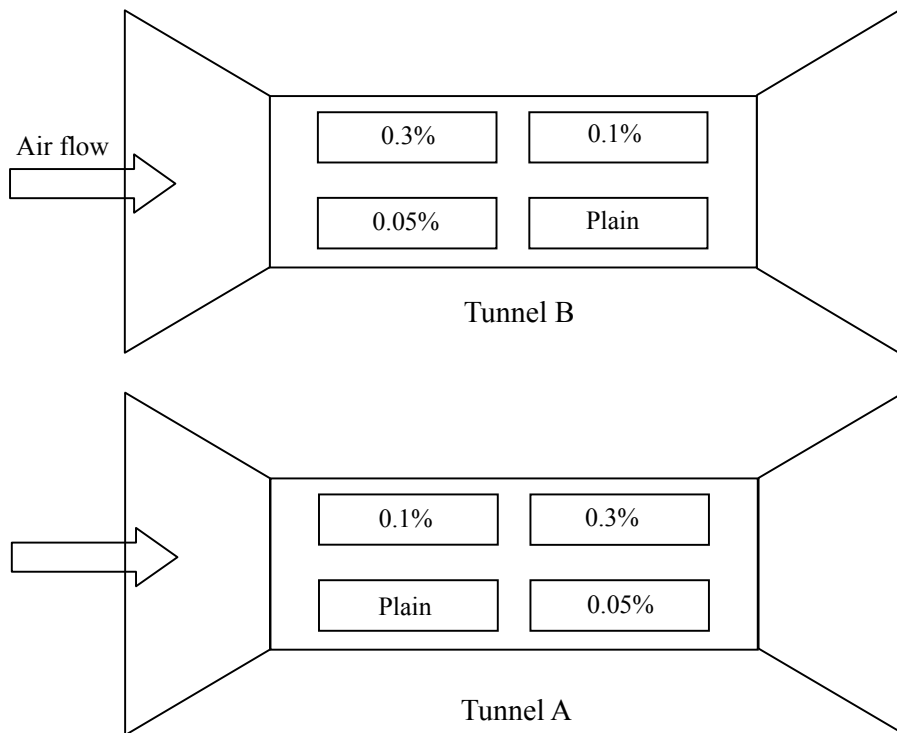


Figure 3.10. Locations of the first batch specimens in the two wind tunnels.

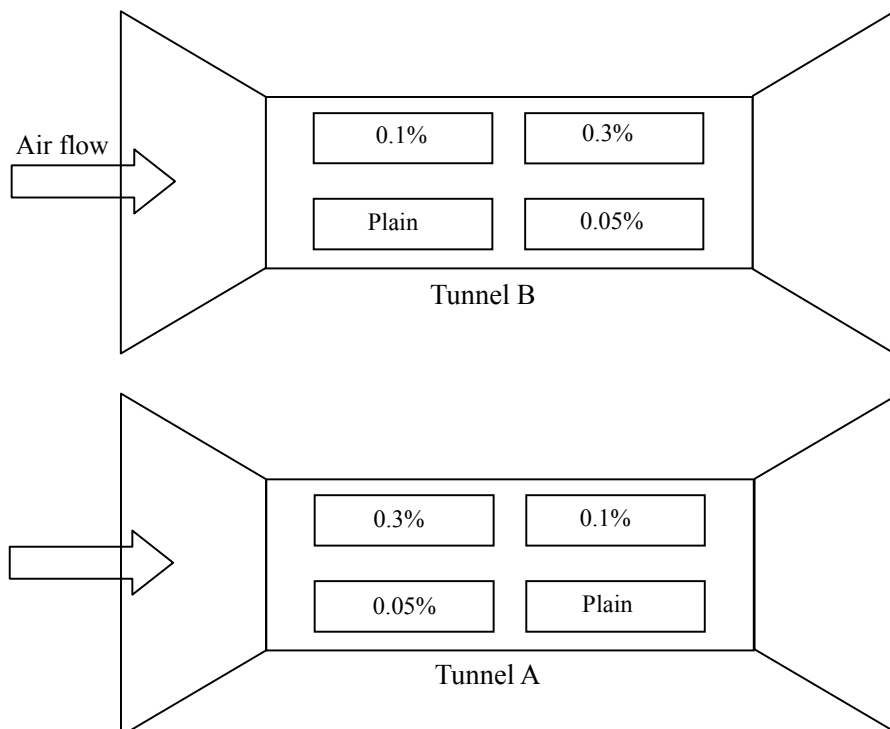


Figure 3.11. Locations of the second batch specimens in the two wind tunnels.

3.3.3. Crack measurement

An image analysis method similar to the one used by Qi et al. (2003) was used to measure maximum crack width and total crack area for this study. It consisted of three steps: image acquisition, image processing and crack measurement. A detailed description of each step is provided in the following paragraphs, with a summary of the process illustrated in Fig. 3.12.

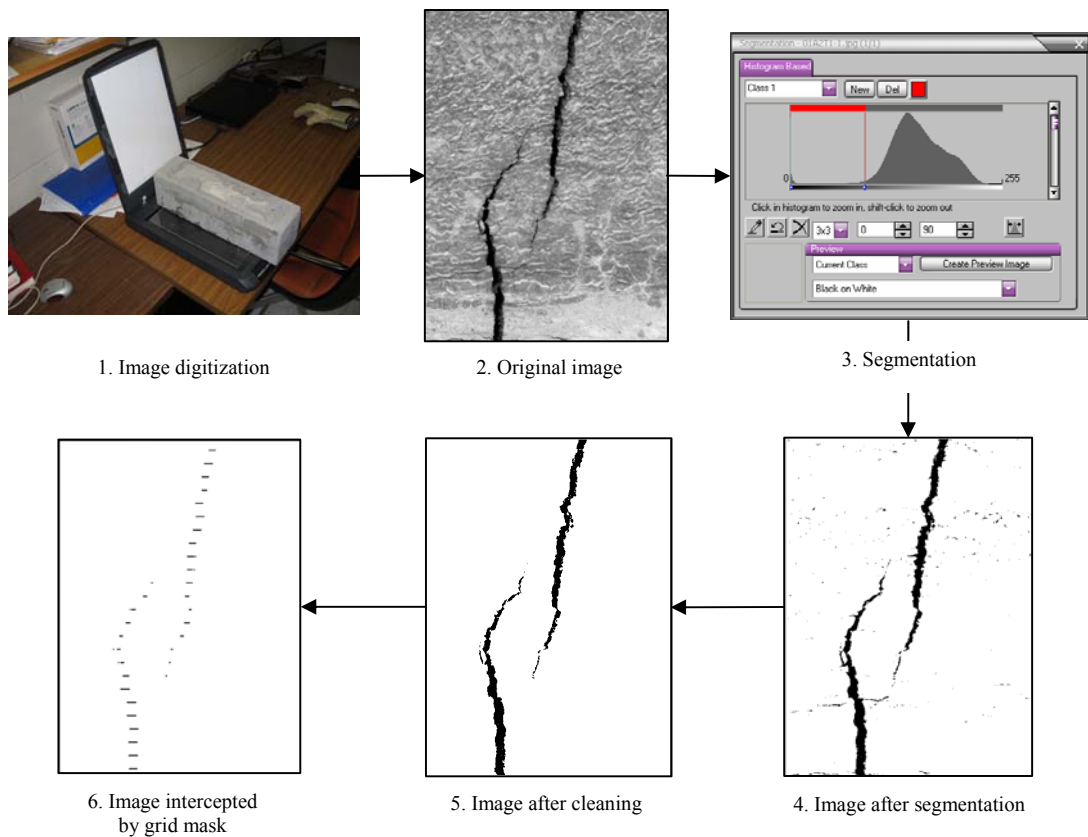


Figure 3.12. Image analysis procedure.

To acquire the image, the surface of a specimen was digitized using a high resolution flatbed scanner (Epson Perfection 3490 Photo) as shown in Fig. 3.12-1. To protect the scanner from scratches, a thin Plexiglas sheet was placed over the scanner's glass plate prior to placing the specimen on it. A scanning resolution of 1200 dpi and 8 bit grey scale were selected when the samples were scanned. With these settings, crack

widths smaller than 0.0212 mm were not detectable. These settings were chosen on the basis of a comparison of the influence of different settings on the resulting measurements. Details of this comparison are provided in Appendix A. These original digitized gray level images were saved for further image processing.

The image analysis software package Image-Pro Plus (Media Cybernetics, Inc. Bethesda, MD) was used in this study to process and analyze the image. First, areas on the surface that contained cracks (Fig. 3.12-2) were extracted from the rest of the image by selecting the area of interest and resizing it in a new window. Next, pixels having intensities within a range from 0 and 90 were isolated from the remainder of the image using the “segmentation” command in order to isolate the crack contours from the mortar background, as shown in Fig. 3.12-3. In this way, all pixels containing intensities within this range were set to black, while those outside of this range were set to white, as shown in Fig. 3.12-4. Because of small differences in the colour of each specimen’s surface, the threshold intensity value was adjusted slightly based on a visual observation of the crack boundary.

As seen in Fig. 3.12-4, the resulting binary image contained some areas outside of the crack that were also set to black. This was because there were some small craters, creases and other imperfections on the specimen’s surface. The pixel intensities of those imperfections were within the same segmented range as cracks. In order to remove these areas, the next step was to clean the image. To do this, the original image and the image after segmentation were opened simultaneously in the window. Then, using the original image as a reference, these black areas on the background of the segmented image were deleted. As a result, only the crack was black and everything else was white, as shown in Fig. 3.12-5.

The cleaned image was used for performing measurement operations. The total crack area was measured automatically using the “count/size” command. It should be noted that there were still some small areas belonging to the crack which were set to white at this stage. This was because the intensity value of some fibres and small aggregates that were close to the crack surface were outside of the segmented range. In

order to count those areas as part of the crack area, the “fill holes” option was selected to treat all pixels encompassed in the perimeter as part of the crack, regardless of their intensity value.

To measure the maximum crack width, a “grid mask” — i.e. a grid of perpendicular lines — was created. The vertical interval between the horizontal lines was set at 0.5 mm, while the horizontal interval between vertical lines was set larger than the width of the image in order not to come into play. The cleaned crack image was subtracted from the grid mask in order to represent the crack as a series of line segments oriented more or less perpendicular to the crack, as shown in Fig. 3.12-6. The intercepted length of these grid lines corresponded to the crack width and was measured automatically. In this way, the crack width was measured every 0.5 mm along the length of the crack. From the statistical results of line lengths, the maximum crack width was selected.

3.4. Test Procedures for Unrestrained Plastic Shrinkage

The mix proportions and mixing procedure used to prepare unrestrained plastic shrinkage specimens were identical to those described for the overlay mortars in the restrained shrinkage tests. Also similar to the restrained shrinkage tests, nineteen different combinations, with four specimens for each combination, totalling 96 samples, were tested.

However, in contrast to the restrained shrinkage specimens, all mortar specimens were cast in the 100 mm x 375 mm x 100 mm deep moulds directly, without the substrate bases. In order to minimize restraint, oiled polyethylene sheets were placed into the moulds before the specimens were cast, as shown in Fig. 3.13. After vibrating and trowelling, the fresh specimens were moved immediately to the environmental chamber. The environmental conditions and the locations of the specimens from a single batch with different fibre volume fractions in the wind tunnels were identical to those described for the restrained shrinkage tests (see Figs. 3.10 and 3.11). Approximately one hour after transfer to the environmental chamber, the specimens were demoulded

carefully. After demoulding, two thumb tacks were embedded on the longitudinal axis of each specimen's top surface, separated longitudinally by a distance of approximately 200 mm, as shown in Fig. 3.14. Each thumb tack had an indentation at the centre. A digital caliper with a precision of 0.01 mm was used to measure the distance between the indentations on the thumb tacks initially and every 30 minutes thereafter for five hours, with a final measurement made 22 hours after casting.



Figure 3.13. Specimens for unrestrained shrinkage tests.

3.5. Environmental Conditions

3.5.1. Environmental Chamber

A 3 m × 3 m insulated environmental chamber built of wood framing and OSB (oriented strand board) sheathing was used to provide hot, windy and dry conditions for the specimens. The setup of the chamber is shown in Fig. 3.15. It housed two wind tunnels (see Fig. 3.16), each of which accommodated four specimens. Access to the specimens was allowed by removing a Plexiglas lid on each wind tunnel. Some trial and error was required to achieve the desired environmental conditions and evaporation rate. A description of this process is provided in Appendix B.



Figure 3.14. The indented thumbtacks on the specimens for the unrestrained shrinkage test.

The air outside the chamber was cooled by an air conditioner. In summer and spring, three dehumidifiers (Model: DDR503H, Danby Products Ltd., Guelph, ON) were used to dehumidify the air when the air was not dry enough to give an expected evaporation rate. The cool dry air was drawn into the chamber with the assistance of a box fan which was installed at the inlet to the chamber. Three 4800 W heaters (Dimplex North America DCH-4831, Cambridge, ON), which are shown in Fig. 3.17, were available to heat the cool dry air when it flowed into the chamber. However, only one of these heaters was required to achieve suitable conditions in the chamber. The hot air was then drawn through the wind tunnels by an exhaust fan which was mounted on the roof of the Engineering Building and was capable of drawing air at a rate of 42 m³ /min. The outlets of the wind tunnels were connected directly to the building's exhaust ventilation system, which also drew air through a fume hood located in a separate room of the laboratory.

3.5.2. Temperature and relative humidity

A humidity sensor (HX94-SS RH PROBE, Omega Technologies Company,

Laval, PQ) with an accuracy of $\pm 0.6^{\circ}\text{C}$ for temperature and $\pm 2\%$ for relative humidity was clipped on a stand which was placed in front of one of the wind tunnels. It was connected to a computer which not only kept a record of these parameters, but also controlled the power supply to the operating heater during the test. A sample record of measured temperature and relative humidity over a 24 hour period is shown in Table 3.5. As can be seen, the temperature and relative humidity in the chamber were held constant at $35.2 \pm 2.2^{\circ}\text{C}$ and less than 3%, respectively.

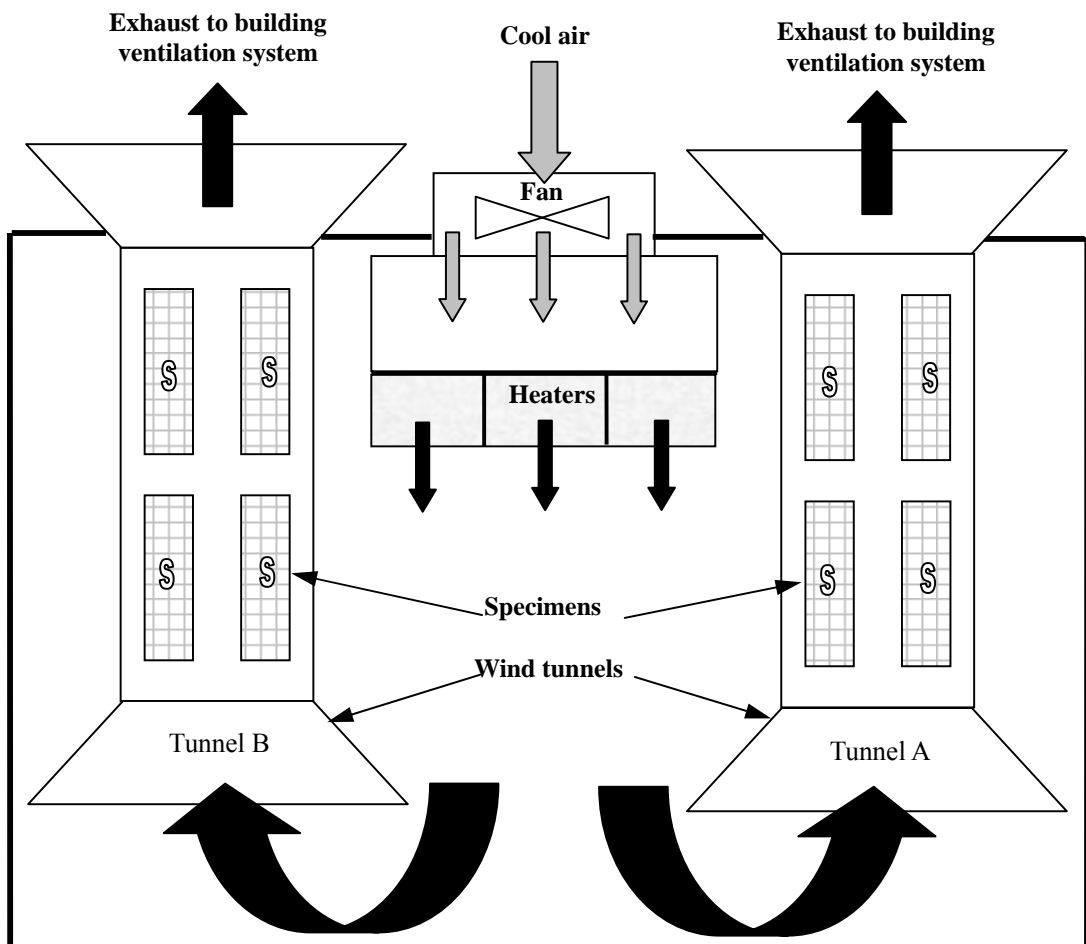


Figure 3.15. Schematic diagram of the environmental chamber - plan view.



Figure 3.16. Interior of the environmental chamber.



Figure 3.17. The heater system in the environmental chamber.

Table 3.5. Sample record of temperature and relative humidity (RH) during a test.

Time	Temperature (°C)	RH (%)	Time	Temperature (°C)	RH (%)
4:00:12 PM	34.3	1.4	5:00:22 AM	34.7	1.3
5:00:20 PM	36.0	1.0	6:00:23 AM	36.2	0.2
6:00:20 PM	35.2	0.7	7:00:23 AM	34.5	0.9
7:00:20 PM	34.9	1.4	8:00:23 AM	35.9	0.7
8:00:20 PM	36.1	0.2	9:00:23 AM	35.5	0.2
9:00:20 PM	34.4	1.0	10:00:24 AM	34.7	1.4
10:00:21 PM	36.2	0.7	11:00:24 AM	36.3	0.1
11:00:21 PM	35.3	0.2	12:00:24 PM	34.7	0.9
12:00:21 AM	34.4	1.4	1:00:24 PM	33.4	1.5
1:00:22 AM	36.3	0.1	2:00:24 PM	35.7	0.5
2:00:22 AM	34.6	0.7	3:00:24 PM	34.8	0.2
3:00:22 AM	36.1	0.5	4:00:25 PM	34.9	0.7
4:00:22 AM	35.4	0.2	5:00:25 PM	35.7	0.2
			Average	35.2	0.7
			C.O.V%	2.18%	67.68%

3.5.3. Wind speed

A plexiglas insert was placed in each tunnel after the specimens were in place. Four rectangular openings in the insert fit over the specimens so that only the top surfaces of the specimens were exposed to the wind. This provided a uniform rectangular cross section through which air flowed, resulting in more uniform wind speeds over all specimens. Figures 3.18 and 3.19 show side and top views, respectively, of the wind tunnel. Figure 3.20 shows a photograph of the insert with specimens in place.

Prior to conducting the tests, the wind speed in both wind tunnels across the surface of specimens was measured using a pressure transducer (DP15, Validyne Engineering, Validyne Engineering, Northridge, CA). It was connected to a demodulator (CD12, Validyne Engineering, Northridge, CA) and a computer equipped with a data acquisition card system (PCI-6024E, National Instruments Corporation, Austin, TX). The pressure transducer was equipped with a probe that was inserted into the wind tunnels through small holes which had been drilled through the Plexiglas lid, as shown in Fig. 3.21. The holes were plugged by cork stoppers when not used for measuring the wind speed.

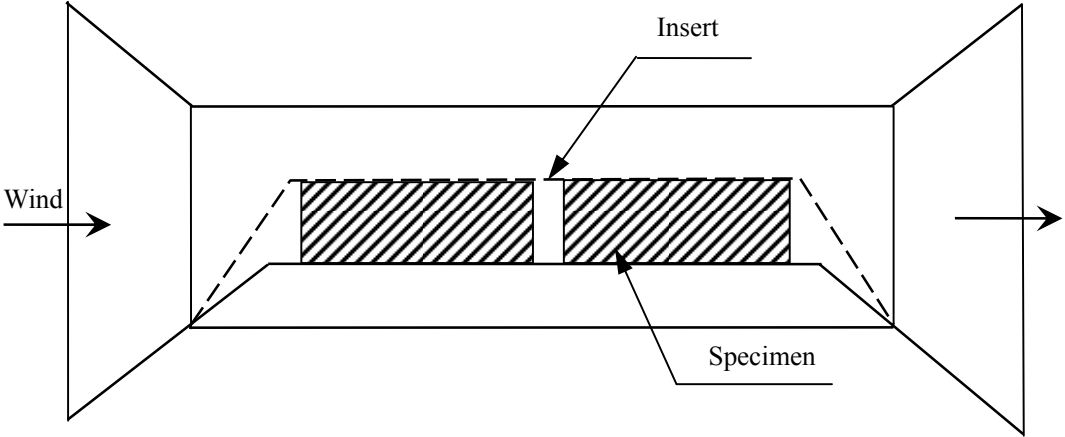


Figure 3.18. Side view of wind tunnel.

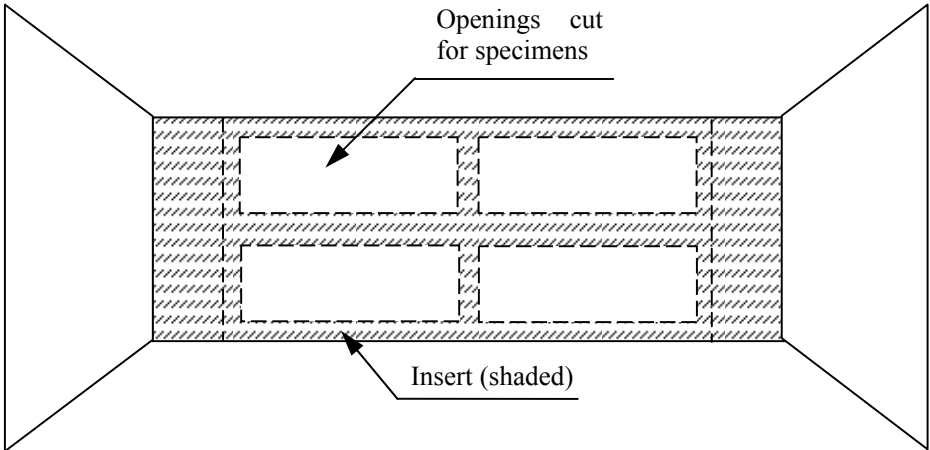


Figure 3.19. Top view of wind tunnel.



Figure 3.20. The insert in a wind tunnel, with specimens in place.

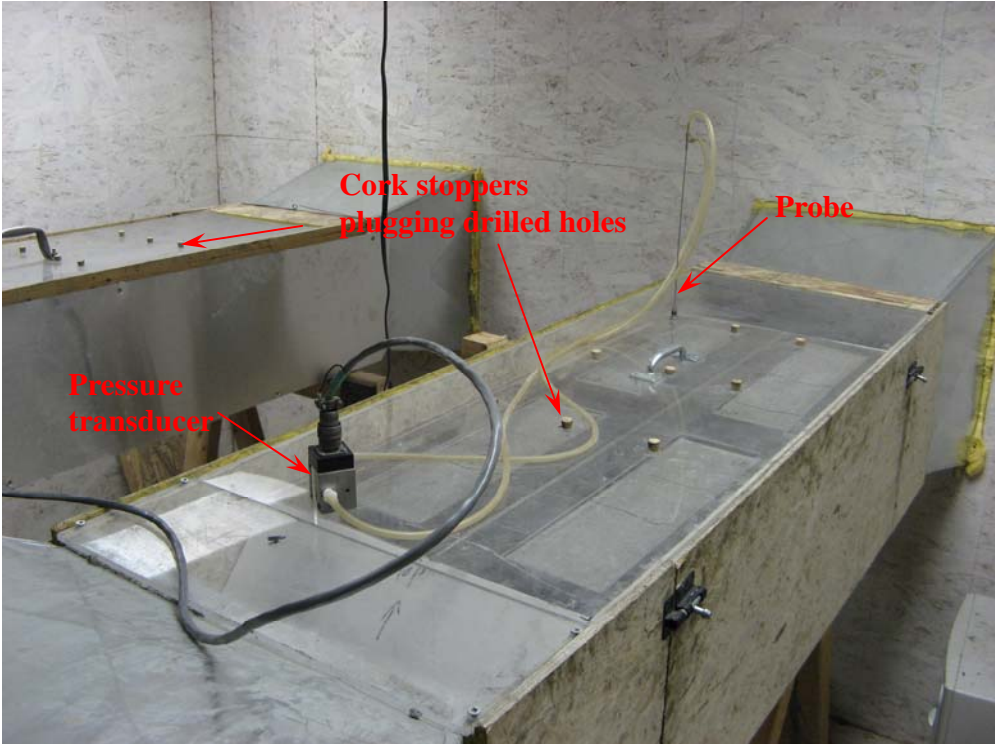


Figure 3.21. The pressure transducer for measuring wind speed.

Wind speeds were measured at the nine different plan locations shown in Fig. 3.22 in each wind tunnel. At each location, wind speeds were measured at three different depths: top (right under the lid), middle (in the middle of the space between insert and lid) and bottom (just above the top surface of the specimen). In this study, the wind speed at the bottom was considered more crucial when compared to the wind speed at the top and middle locations.

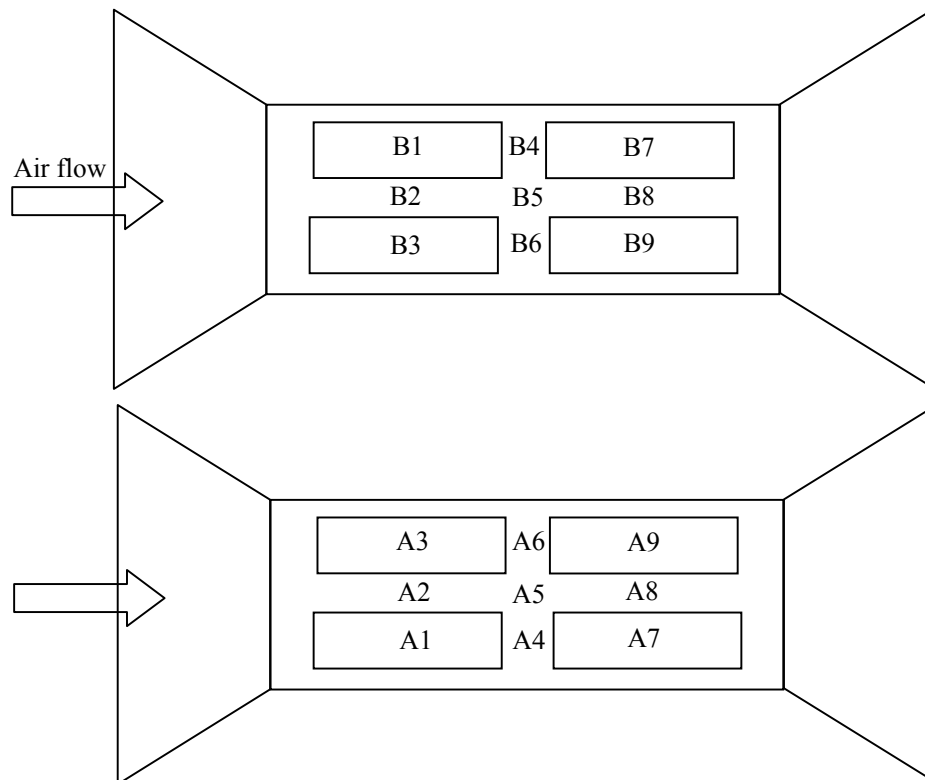


Figure 3.22. Layout of wind speed measurement points.

The wind speeds were recorded every 0.1 seconds for 10 minutes at each location. Table 3.6 and 3.7 provide the mean wind speeds at all 54 measurement points, as well as the root-mean-square of wind speed records (equivalent to the standard deviation) to provide an indication of the level of turbulence in the air flow. Observed mean wind speeds were relatively uniform within each tunnel, with standard errors of the mean being less than three percent of the mean. Wind speeds were also

approximately the same in both tunnels. In addition, relatively low levels of turbulence were observed, with turbulence intensities, i_u (the ratio of rms to mean), ranging from approximately 0.03 to 0.07 just above the specimens. Graphical presentations of these conditions are provided in Figs. 3.23 and 3.24, with error bars corresponding to rms values. The time histories of wind speeds at different points and depths of each tunnel are included in Appendix B.

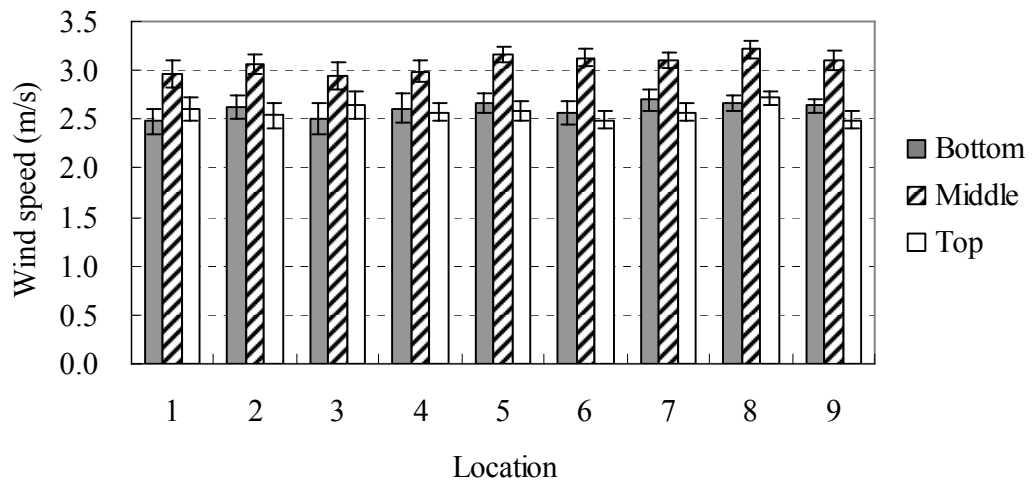


Figure 3.23. Measured wind speed in tunnel A.

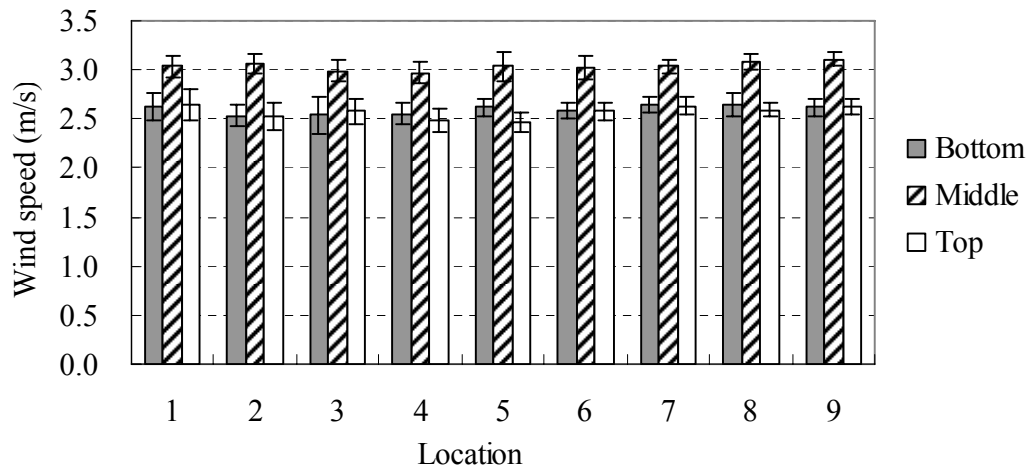


Figure 3.24. Measured wind speed in tunnel B.

Table 3.6. Wind speed at different points and depths in Tunnel A (m/s).

Tunnel A Bottom										
Location	1	2	3	4	5	6	7	8	9	Wind speed statistics
Mean	2.481	2.620	2.500	2.611	2.669	2.563	2.698	2.661	2.635	2.604 (mean of means)
rms	0.131	0.122	0.159	0.144	0.102	0.117	0.104	0.081	0.075	0.075 (standard error of means)
i_u	0.053	0.046	0.064	0.055	0.038	0.046	0.038	0.030	0.029	2.89% (C.O.V. of means)
Tunnel A Middle										
Location	1	2	3	4	5	6	7	8	9	Wind speed statistics
Mean	2.963	3.057	2.939	2.992	3.161	3.129	3.106	3.215	3.100	3.074 (mean of means)
rms	0.139	0.099	0.135	0.108	0.076	0.085	0.075	0.085	0.101	0.093 (standard error of means)
i_u	0.047	0.032	0.046	0.036	0.024	0.027	0.024	0.027	0.032	3.04% (C.O.V. of means)
Tunnel A Top										
Location	1	2	3	4	5	6	7	8	9	Wind speed statistics
Mean	2.600	2.539	2.642	2.574	2.580	2.495	2.572	2.720	2.487	2.579 (mean of means)
rms	0.124	0.125	0.138	0.085	0.095	0.096	0.090	0.070	0.090	0.072 (standard error of means)
i_u	0.048	0.049	0.052	0.033	0.037	0.039	0.035	0.026	0.036	2.80% (C.O.V. of means)

Table 3.7. Wind speed at different points and depths in Tunnel B (m/s).

Tunnel B Bottom										
Location	1	2	3	4	5	6	7	8	9	Wind speed statistics
Mean	2.630	2.535	2.538	2.551	2.618	2.583	2.651	2.645	2.616	2.596 (mean of means)
rms	0.143	0.106	0.182	0.112	0.094	0.082	0.084	0.116	0.081	0.046 (standard error of means)
i_u	0.054	0.042	0.072	0.044	0.036	0.032	0.032	0.044	0.031	1.76% (C.O.V. of means)
Tunnel B Middle										
Location	1	2	3	4	5	6	7	8	9	Wind speed statistics
Mean	3.040	3.068	2.985	2.970	3.040	3.027	3.034	3.084	3.112	3.040 (mean of means)
rms	0.108	0.100	0.107	0.111	0.149	0.119	0.078	0.079	0.068	0.045 (standard error of means)
i_u	0.036	0.033	0.036	0.037	0.049	0.039	0.026	0.025	0.022	1.47% (C.O.V. of means)
Tunnel B Top										
Location	1	2	3	4	5	6	7	8	9	Wind speed statistics
Mean	2.651	2.525	2.579	2.481	2.464	2.581	2.632	2.594	2.632	2.571 (mean of means)
rms	0.158	0.143	0.133	0.121	0.101	0.093	0.089	0.073	0.077	0.067 (standard error of means)
i_u	0.060	0.057	0.052	0.049	0.041	0.036	0.034	0.028	0.029	2.61% (C.O.V. of means)

3.5.4. Evaporation rate

Fresh mortar specimens without fibres were cast to measure the evaporation rate. The size and mix proportions for the specimens were the same as those of the plain specimens used in the unrestrained shrinkage tests (see Table 3.4). In order to prevent water from leaking out of the moulds, polyethylene sheets were placed into the moulds before the specimens were cast. The specimens were weighed to the nearest 1g (PJ15, Mettler Toledo, Mississauga, ON) and transferred to the environmental chamber immediately after casting. The environmental conditions were identical to those used for the restrained shrinkage tests. The locations of evaporation rate measurement specimens are shown in Fig. 3.25. The mass lost from each specimen over a period of two hours was measured. The evaporation rate in $\text{kg/m}^2/\text{h}$ was then calculated from the weight of water lost. This measurement was repeated six times in each tunnel.

The results are shown in Table 3.8 and Fig. 3.26. It can be observed that the average evaporation rate was $0.805 \text{ kg/m}^2/\text{h}$ in Tunnel A and $0.783 \text{ kg/m}^2/\text{h}$ in Tunnel B, a difference of less than 3%. At each location, the evaporation rate was quite uniform, with coefficients of variation ranging from 2.6% to 5.5%. It can be also seen that the evaporation rates at the front of the wind tunnels (mean of means = $0.829 \text{ kg/m}^2/\text{h}$, standard error of means = $0.019 \text{ kg/m}^2/\text{h}$) were higher than those at the back of the wind tunnels (mean of means = $0.760 \text{ kg/m}^2/\text{h}$, standard error of means = $0.015 \text{ kg/m}^2/\text{h}$). This is believed to be because the air carried the moisture which had evaporated from the specimens at the front over the specimens at the back. While the differences between the evaporation rates at different locations were statistically significant, the maximum difference was only 13.4%, which is believed to be relatively small. In addition, the movement of replicate specimens among different locations, as described in Section 3.3.2, served to average out and minimize the differences in restrained plastic shrinkage cracking and unrestrained shrinkage that may have resulted from the small differences in environmental conditions. T-test calculations were carried out to assess whether the means of the evaporation rates at different points of each tunnel were statistically different from each other. The calculated results are summarized in Appendix B.

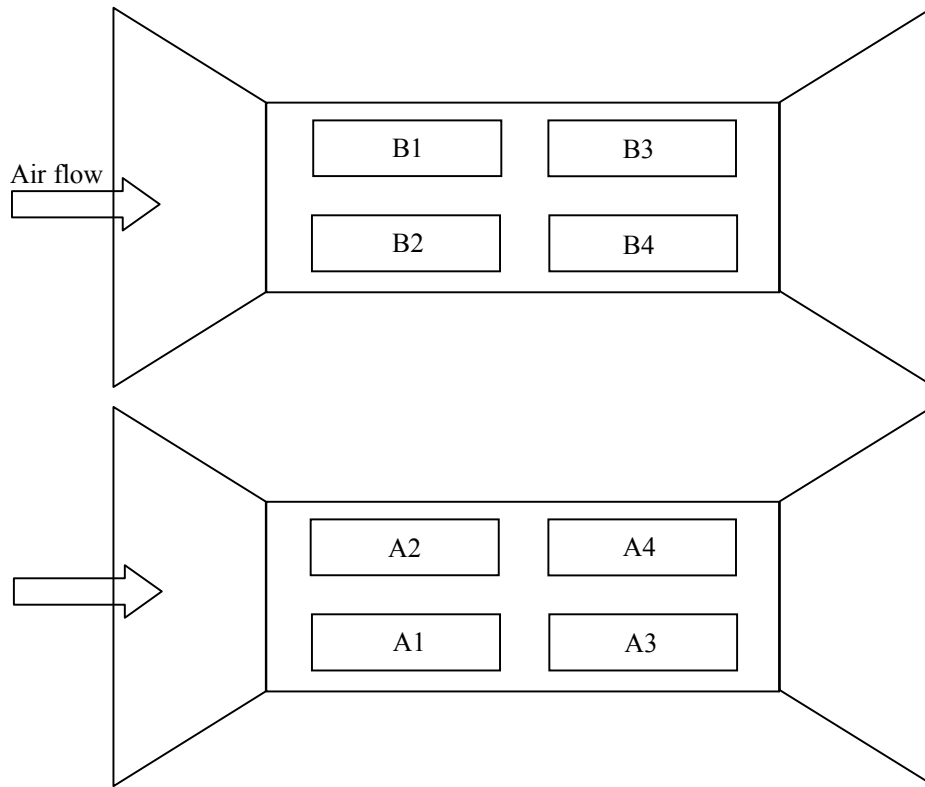


Figure 3.25. Locations of evaporation rate measurement specimens.

Table 3.8. Evaporation rate at different locations in each tunnel (kg/m²/h).

Location*	A1	A2	A3	A4	B1	B2	B3	B4
test1	0.787	0.880	0.867	0.787	0.867	0.867	0.760	0.720
test2	0.787	0.800	0.747	0.773	0.787	0.747	0.707	0.733
test3	0.880	0.893	0.773	0.760	0.893	0.800	0.747	0.760
test4	0.867	0.853	0.747	0.800	0.813	0.760	0.760	0.747
test5	0.813	0.827	0.773	0.720	0.827	0.813	0.747	0.773
test6	0.853	0.813	0.747	0.773	0.840	0.827	0.773	0.733
mean	0.831	0.844	0.776	0.769	0.838	0.802	0.749	0.744
S.D.	0.041	0.037	0.047	0.028	0.038	0.044	0.023	0.020
C.O.V.	4.9%	4.4%	6.0%	3.6%	4.5%	5.5%	3.1%	2.6%

* The letter in the location code indicates the wind tunnel, while the number indicates the specimen location (see Fig. 3.25).

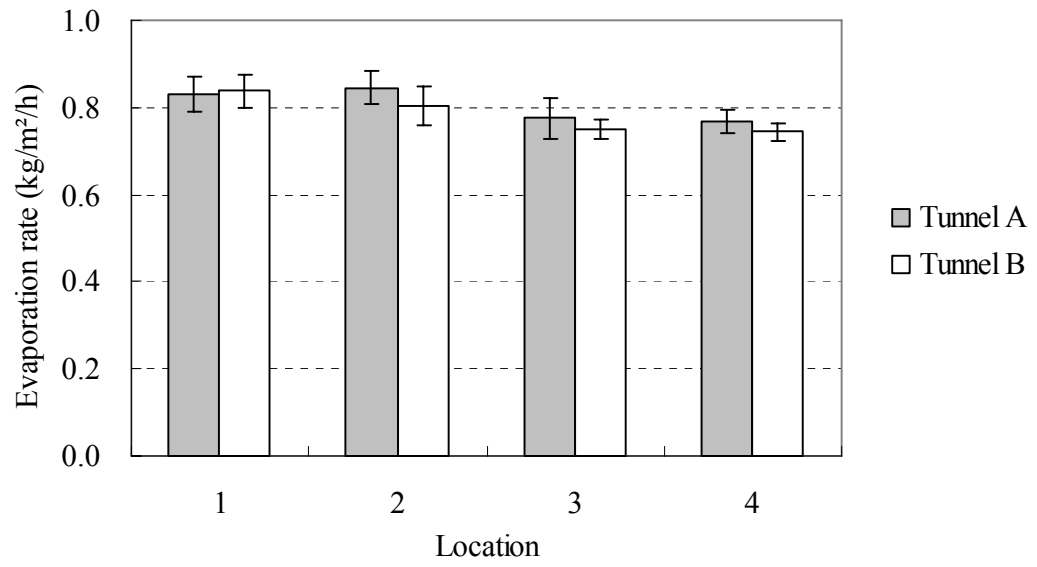


Figure 3.26. Evaporation rate at different locations in each tunnel (kg/m²/h).

CHAPTER 4 TEST RESULTS AND DISCUSSION

4.1. Introduction

The detailed test results are presented in this chapter. The influence of the different fibre types, lengths and volume fractions on the restrained and free plastic shrinkage properties is summarized. The possible causes of the different performance of various fibre types and to what extent the addition of baler twine was able to reduce the plastic shrinkage cracking are discussed at the end of this chapter.

4.2. Restrained Plastic Shrinkage Test Results

Figures 4.1 to 4.3 show the scanned images of the surfaces of typical plastic shrinkage cracking specimens with the different fibre types, fibre lengths and volume fractions. It can be observed that the plastic shrinkage cracks formed generally parallel to the width of the specimen. For the plain specimens and the specimens with low fibre content (0.05%), one or two straight cracks extended continuously across the entire width of the specimen and grew to a relatively wide size. These few dominant cracks accounted for the majority of the total crack area. For the specimens with high fibre volume fractions, especially those with 0.3% fibres, multiple, relatively fine, tortuous and disconnected cracks were observed. The photographs show in a qualitative manner the beneficial effect of adding fibres at increasing volume fractions. It is also apparent that high volume fractions of the fibrillated polypropylene fibres were the most effective at reducing plastic shrinkage cracking.

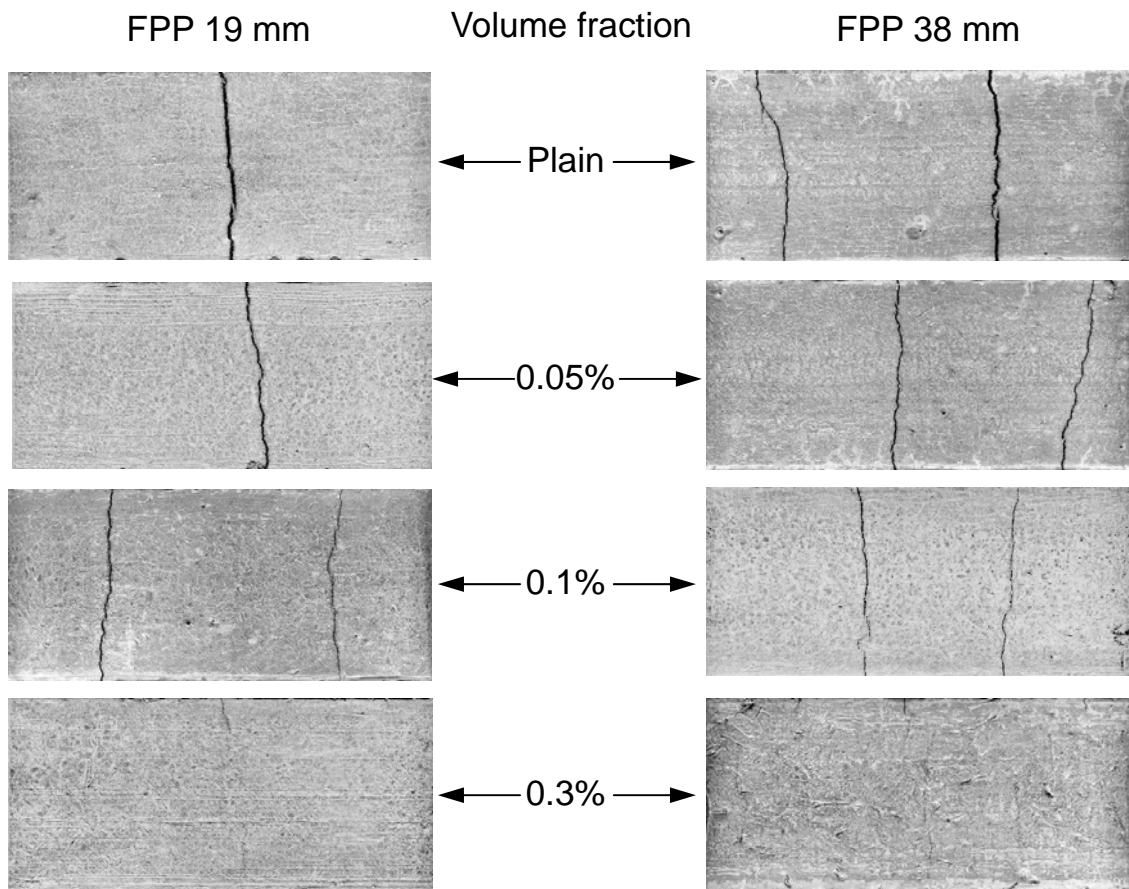


Figure 4.1. Typical plastic shrinkage cracking of specimens with fibrillated polypropylene fibres (scanned images).

The quantitative results of the restrained plastic shrinkage tests are summarized in Table 4.1. The number of cracks, maximum crack width and total crack area reported in Table 4.1 are the averages obtained from four specimens for the fibre reinforced mixtures and 24 specimens for plain control mixtures. A crack which was disconnected from any other cracks was counted as an individual crack. The summation of the individual cracks on each specimen's surface was defined as the number of cracks. The decreases in the crack widths and areas are given as a percent of corresponding values on the plain specimens. All detailed restrained plastic shrinkage test results for different combinations of fibre type, length, and volume fraction are summarized in Appendix C. Also included in this appendix are summaries of T-tests that were carried out to assess whether the means of two groups were statistically different from each other.

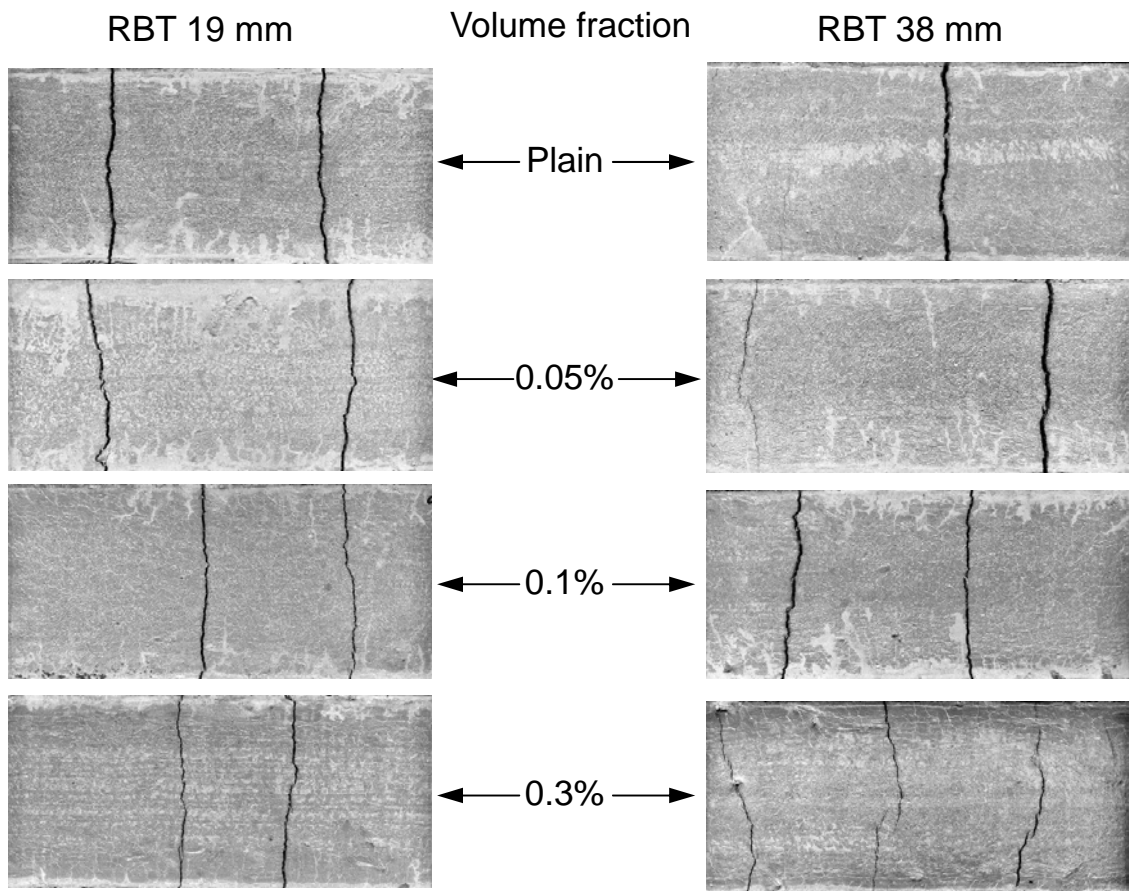


Figure 4.2. Typical plastic shrinkage cracking of specimens with red baler twine fibres (scanned images).

The influence of adding fibres of all types, lengths and volume fractions on plastic shrinkage cracking in terms of the total crack area, maximum crack width and crack numbers is illustrated in Figs. 4.4 to 4.6. In these figures, cases marked with an asterisk indicate that the average data observed for a given set of specimens did not differ significantly from those of the plain control specimens at the 95% level of confidence. The error bars shown in these figures correspond to the standard deviation on either side of the mean. It can be observed that different fibre parameters such as the length, volume fraction and fibre type had different influences on the plastic shrinkage cracking.

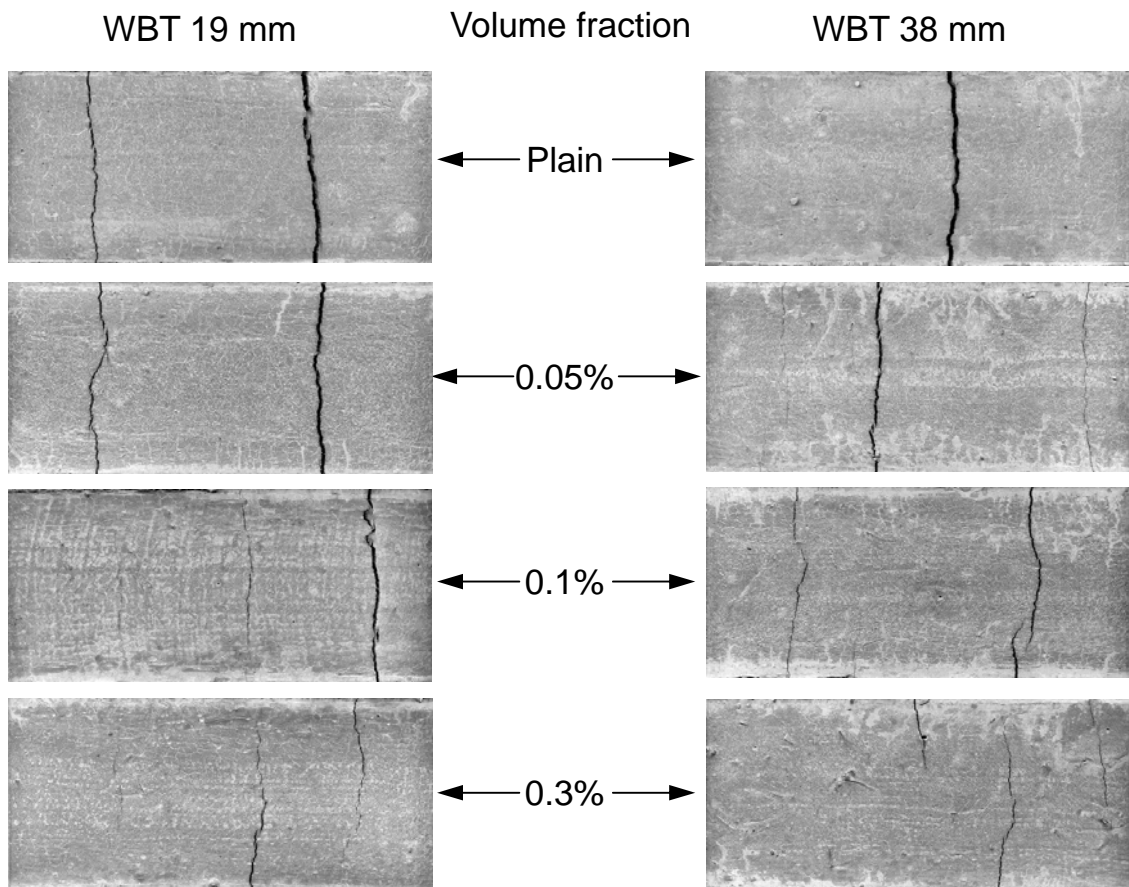


Figure 4.3. Typical plastic shrinkage cracking of specimens with white baler twine fibres (scanned image).

As a first observation, it is clear that the fibrillated polypropylene fibre was the most effective in controlling plastic shrinkage cracking compared with the other two types of fibres. Both total crack areas and maximum crack widths were significantly reduced by the addition of fibrillated fibres at all three volume fractions. When 38 mm fibrillated polypropylene fibre at a volume fraction of 0.3% was added, the maximum crack width and total crack area relative to plain specimens were reduced to the greatest extent, by 87.0% and 95.3%, respectively. The maximum crack width was limited to less than 0.34 mm.

Table 4.1. Restrained plastic shrinkage test results.

Fibre Type	Fibre Length (mm)	Volume Fraction (%)	Number of Specimens	Number of Cracks	C.O.V. (%)	Max. Crack Width (mm)	C.O.V. (%)
Plain	—	—	24	5.1	52.5	2.64	16.7
Fibrillated Polypropylene	19	0.05	4	4.3	67.6	1.66	22.3
		0.10	4	10.0	29.4	1.25	5.3
		0.30	4	8.5	11.8	0.38	20.2
	38	0.05	4	9.5	42.5	1.58	12.4
		0.10	4	15.3	27.5	1.17	23.3
		0.30	4	17.0	29.2	0.34	16.1
Red Baler Twine	19	0.05	4	8.0	32.3	2.16	10.1
		0.10	4	5.5	56.5	2.02	25.3
		0.30	4	15.5	35.5	1.90	19.9
	38	0.05	4	7.5	38.5	2.47	15.8
		0.10	4	10.0	28.3	2.19	12.4
		0.30	4	22.5	23.4	1.45	36.1
White Baler Twine	19	0.05	4	6.3	35.5	2.28	14.2
		0.10	4	10.3	37.7	1.76	24.7
		0.30	4	24.5	28.4	0.94	10.7
	38	0.05	4	13.3	40.1	1.85	18.5
		0.10	4	9.8	39.6	1.82	19.9
		0.30	4	21.8	21.4	0.67	24.3

Table 4.1. (Cont'd) Restrained plastic shrinkage test results.

Fibre Type	Fibre Length (mm)	Volume Fraction (%)	Total Crack Area (mm ²)	C.O.V. (%)	Decrease in Max Crack Width (%)	Decrease in Total Crack Area (%)
Plain	—	—	254.2	18.9	—	—
Fibrillated Polypropylene	19	0.05	151.0	19.0	36.9	40.6
		0.10	128.1	21.5	52.7	49.6
		0.30	14.8	43.0	85.4	94.2
	38	0.05	149.7	6.2	40.2	41.1
		0.10	114.8	40.8	55.6	54.8
		0.30	11.9	48.5	87.0	95.3
Red Baler Twine	19	0.05	253.7	11.5	18.0	0.2
		0.10	226.9	9.1	23.4	10.7
		0.30	185.2	6.3	28.1	27.2
	38	0.05	265.8	7.2	6.4	-4.6
		0.10	241.7	14.8	16.8	4.9
		0.30	157.4	27.9	45.0	38.1
White Baler Twine	19	0.05	255.0	10.8	13.6	-0.3
		0.10	208.6	15.7	33.2	17.9
		0.30	100.7	19.1	64.2	60.4
	38	0.05	195.8	14.0	29.7	23.0
		0.10	184.3	18.0	31.0	27.5
		0.30	58.3	28.1	74.8	77.1

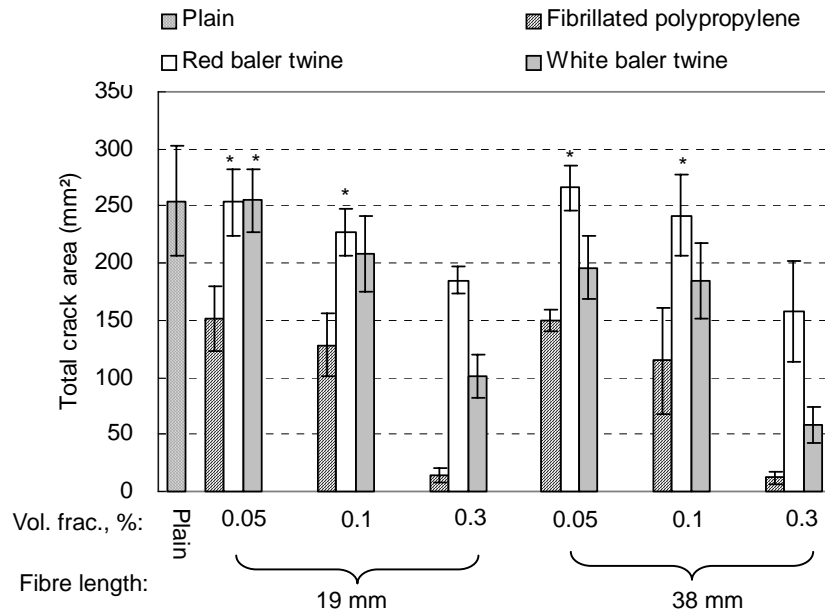


Figure 4.4. Total crack area for all restrained plastic shrinkage specimens. Asterisks indicate cases that did not differ significantly from plain control specimens at the 95% level of confidence.

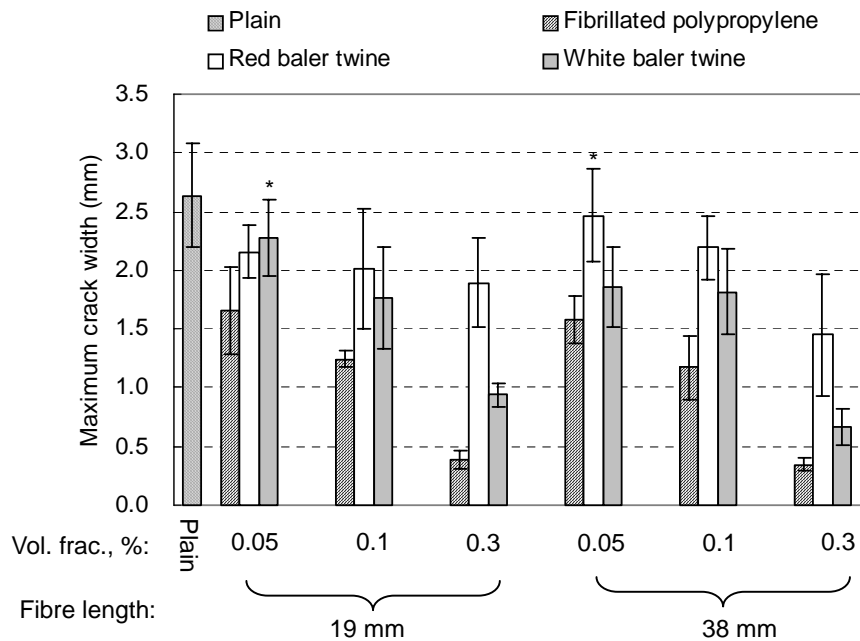


Figure 4.5. Maximum crack widths for all restrained plastic shrinkage specimens. Asterisks indicate cases that did not differ significantly from plain control specimens at the 95% level of confidence.

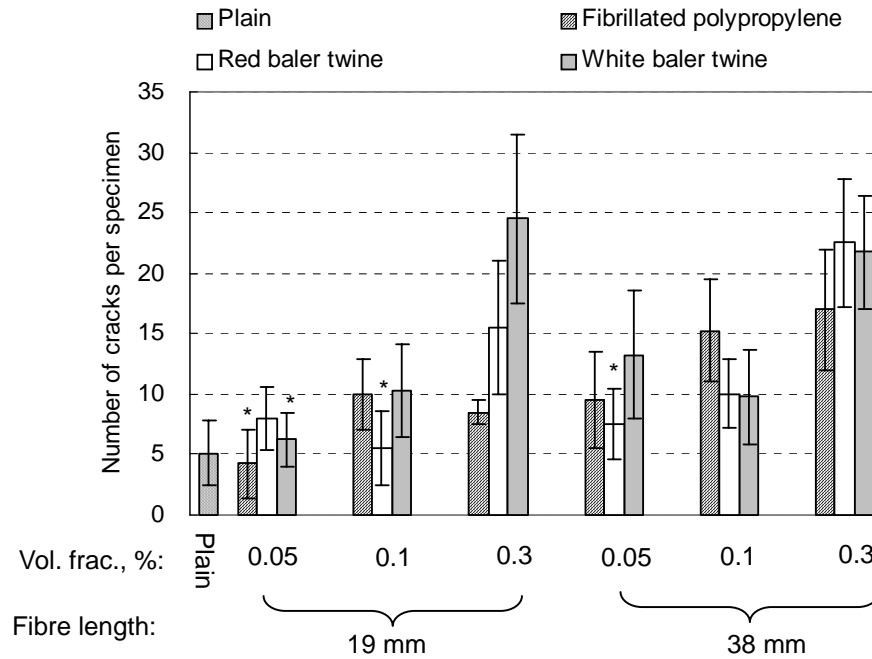


Figure 4.6. Average number of cracks observed for all restrained plastic shrinkage specimens. Asterisks indicate cases that did not differ significantly from plain control specimens at the 95% level of confidence.

The performance of white baler twine fibre was slightly inferior to the fibrillated polypropylene fibre. The maximum reduction in maximum crack width and total crack area reached 74.8% and 77.1%, respectively. The maximum crack width was limited to no more than 0.67 mm when 0.3% white baler twine fibre cut to 38 mm was used. At lower volume fractions, the reductions were more modest, and the addition of 0.05% fibres at 19 mm had a negligible effect.

The effect of red baler twine in controlling the plastic shrinkage cracking was the least among the three fibre types studied. The best it could do was to reduce the maximum crack width by 45.0% to 1.45 mm, and reduce the total crack area by 38.1% when the volume fraction was 0.3% and fibre length was 38 mm. The reduction of total crack area by the addition of less than 0.3% fibres was negligible; in addition, the reduction of maximum crack width was less than 30% except at the highest length and volume fraction.

Figures 4.7 and 4.8 illustrate the influence of fibre volume fraction on total

crack area and maximum crack width, respectively. Fibre volume fraction can be seen to be a very influential factor in controlling plastic shrinkage cracking. The figures clearly show that there is a general decrease in total crack area with increasing volume fraction of fibre reinforcement, regardless of fibre type, although the fibrillated polypropylene fibres are clearly superior to the other two. This reduction is most noticeable when the volume fraction increases from 0.1% to 0.3%. At the 0.05% volume fraction, fibrillated polypropylene fibres reduced the total crack area by 41% compared with the plain control specimens. When 0.05% baler twine fibres were used, only the white 38 mm baler twine fibre reduced the total crack area, with a reduction of 30%. For other baler twine fibres at that volume fraction, the changes in total crack area compared with the plain control specimens were not statistically significant. When the volume fraction of fibres increased to 0.1%, the total crack area decreased by 50% to 55% and 18% to 28% for specimens reinforced with fibrillated polypropylene and white baler twine fibres, respectively. Red baler twine still did not reduce the total crack area significantly. When 0.3% fibres were added, the total crack area decreased by 94 % to 95%, 60% to 70% and 27% to 38% for fibrillated polypropylene, white baler twine and red baler twine fibres, respectively. The reduction in total crack area for all fibre types and lengths was statistically significant at the 0.3% volume fraction.

From Fig 4.7, it also can be seen that the slopes of total crack area against volume fraction for all fibre types are similar, although the lines are offset from each other. This demonstrates that for different fibre types, the reductions of total crack area caused by a certain volume increment are similar. For example, the total crack area of specimens with 38 mm fibrillated polypropylene and 19 mm white baler twine decreased by 103 mm² and 108 mm², respectively, when the volume fraction increased from 0.1% to 0.3%. The reductions caused by the same volume increment are very close for the different fibre types.

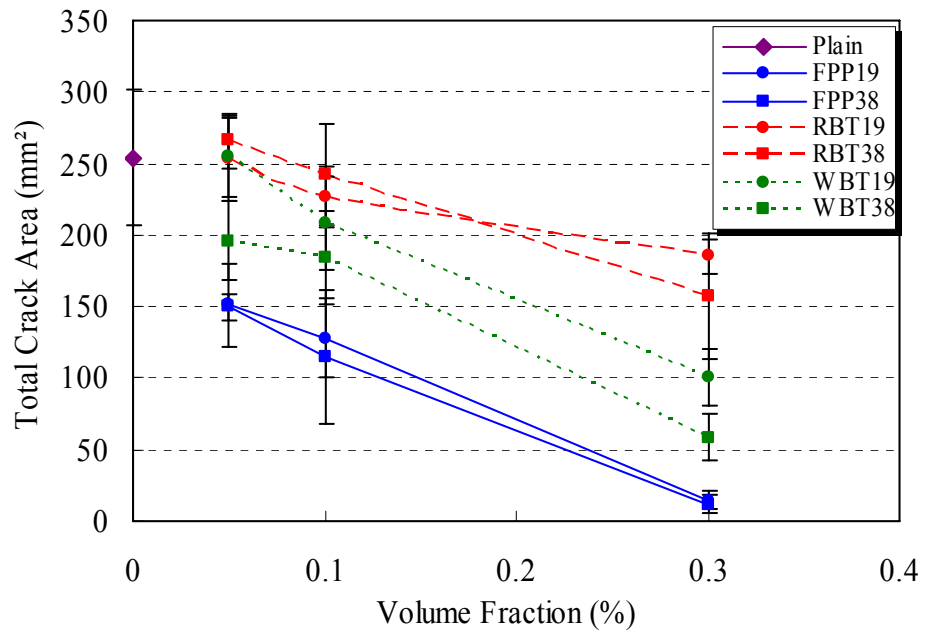


Figure 4.7. Total crack area of specimens with all fibre types plotted against volume fraction.

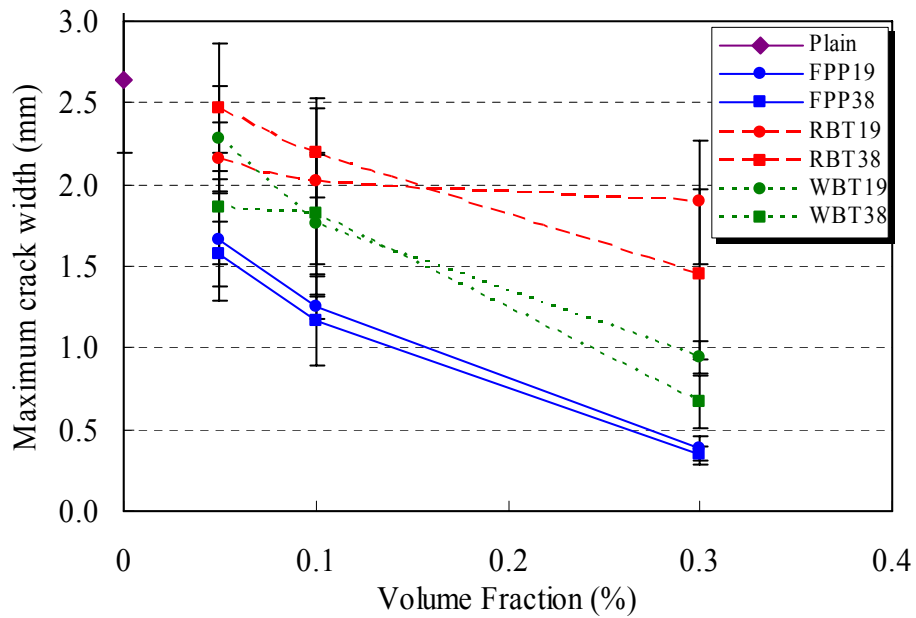


Figure 4.8. Maximum crack width of specimens with all fibre types plotted against volume fraction.

For all fibre types and lengths, maximum crack widths also consistently decreased with an increase in the fibre volume fraction. Similar to the total crack area, the reduction of maximum crack width was most striking when the fibre volume fraction increased from 0.1% to 0.3%. For specimens with a 0.05% volume fraction, except for 19 mm white baler twine and 38 mm red baler twine, all other fibre types and lengths reduced the maximum crack width by statistically significant amounts ranging from 18% to 40%. When 0.1% fibres were used, the maximum crack width was reduced by 17% to 57%. Further reductions ranging from 28% to 87% were observed when the volume fraction increased to 0.3%. All fibres reduced the maximum crack width by statistically significant amounts at volume fractions of 0.1% and 0.3%.

Figures 4.7 and 4.8 also show that changing the fibre length did not generally have a significant influence on the cracking behaviour. With the possible exception of white baler twine fibres, a clear and consistent trend cannot be observed in the test result. At a given volume fraction, only a slight improvement in performance was achieved in most cases with longer fibres. The improvements were most significant for the white baler twine fibres. However, the contrary trend was also observed in a few cases. For example, at the 0.05% and 0.1% volume fractions, the total crack area and maximum crack width both increased when the length of red baler twine fibres increased from 19 mm to 38 mm. The maximum crack width also increased slightly when the length of white baler twine increased from 19 mm to 38 mm at a volume fraction of 0.1%. The possible reason for these opposing trends is that the baler twine fibres which had been cut into shorter lengths (19 mm) were easier to shred and separate during the cut and mix procedure, and, therefore, dispersed more uniformly. However, this advantage vanished when the volume fraction of fibre increased to 0.3%, when the larger number of fibre bundles apparently compensated for the lack of dispersion.

The number of cracks generally increased with increasing fibre volume fraction, as illustrated in Table 4.1 and Fig. 4.6. Again, this trend was most obvious when the volume fraction increased from 0.1 to 0.3%. When 0.05 and 0.1% volume fractions were added, the increases in crack numbers were relatively small. At the 0.3% volume

fraction, fibres of all types and lengths caused multiple small cracks; and therefore, the crack numbers increased significantly. The reason for the occurrence of multiple small cracks is thought to be related to the bridging forces provided by the fibres. Since there were more fibres bridging a crack at high volume fractions, they effectively held the faces of the crack together, preventing it from growing. As a result, discontinuous small cracks formed instead of the continuous large cracks; because the dominant large cracks could not form on the specimen's surface, the tensile stresses in the specimens had to be relieved at multiple places instead of just at a small number of locations on the specimen's surface.

In order to better understand and compare the performance of the three fibre types, Figs. 4.9 and 4.10 show plots of the maximum crack width and total crack area, respectively, for the best fibre length (the fibre length that was most effective in controlling plastic shrinkage cracking) for a given fibre type and volume fraction. Note that the best fibre length varied with fibre type and volume fraction. For example, at a volume fraction of 0.05%, 19 mm red baler twine was more effective than the 38 mm red baler twine in reducing the maximum crack width and total crack area. However, for white baler twine, the 38 mm fibre length produced the best result at a volume fraction of 0.05%. When the volume fraction increased to 0.3%, 38 mm was the best fibre length for all fibre types. In this way, the performance of different fibre types can be compared, on the assumption that the best fibre length has been used at each volume fraction for a certain fibre type. Both figures show that the fibrillated polypropylene fibres were the most effective, the white baler twine was the second best, and the red baler twine was the least effective in controlling the maximum crack width and the total crack area. Further discussion of the performance of each fibre type provided in Section 4.4.

4.3. Unrestrained Plastic Shrinkage Test Results

The development of the free shrinkage strains over 22 hours after casting for representative plain specimens and specimens containing 38 mm white baler twine fibre is illustrated in Fig. 4.11. It shows that the shrinkage strains typically stabilized within the first five hours after casting. A similar trend was observed for all other specimens with different combinations of fibre type, volume fraction and length (See Appendix D). No cracking was found on any of the free plastic shrinkage specimens.

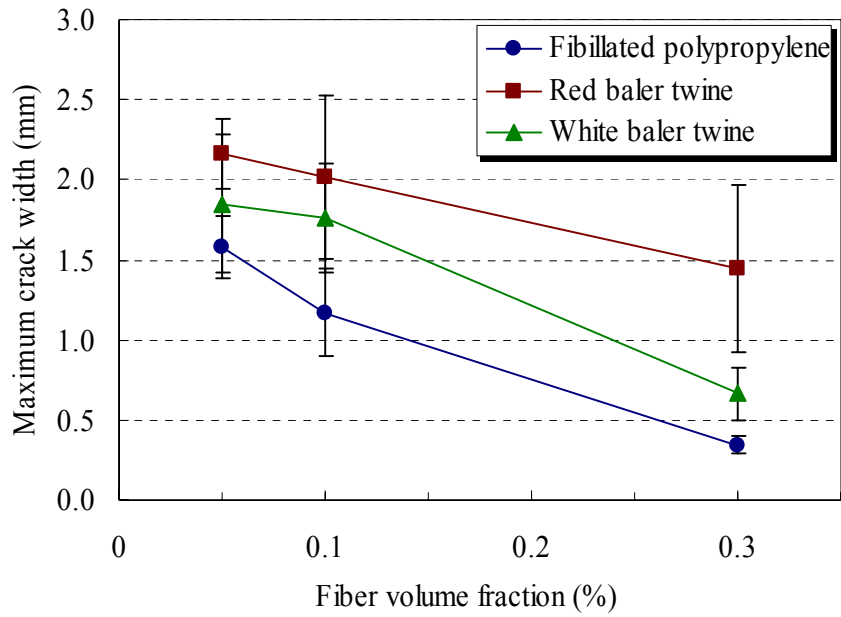


Figure 4.9. Comparison of maximum crack widths for specimens with the best fibre lengths.

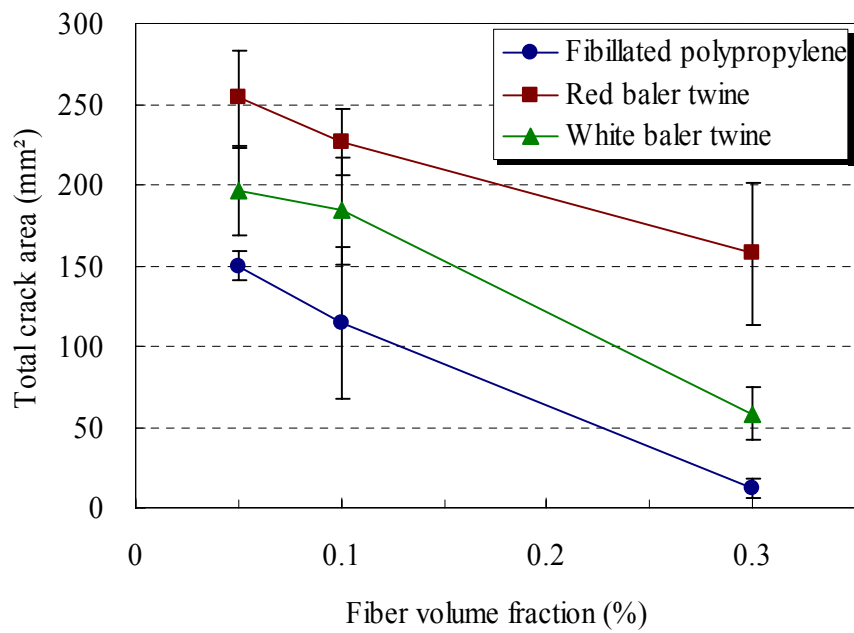


Figure 4.10. Comparison of total crack areas for specimens with the best fibre lengths.

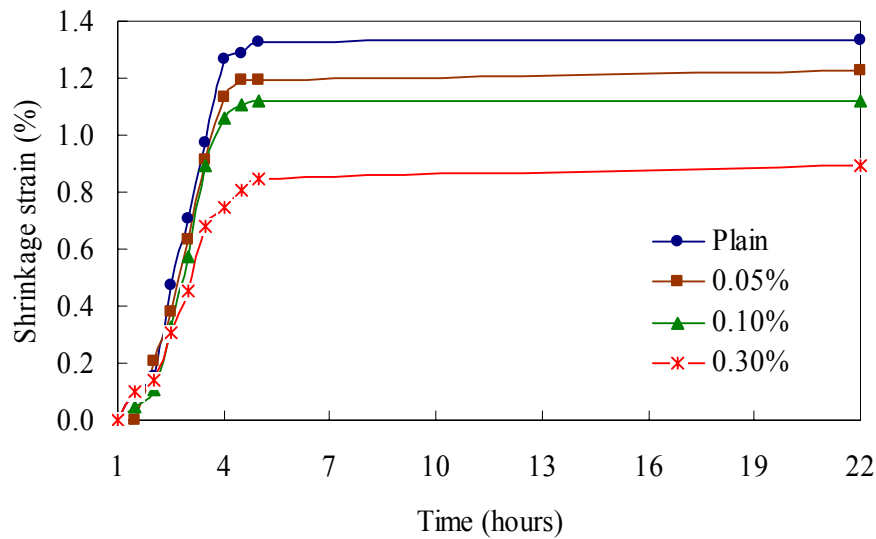


Figure 4.11. Typical development of free shrinkage over time for 38 mm white baler twine.

The unrestrained plastic shrinkage strains measured 22 hours after casting are summarized in Table 4.2. The shrinkage strains reported in this table are the averages of four specimens for the fibre reinforced mixtures and twenty-four specimens for the plain control mixtures. The change in the shrinkage strain is given as a percentage of that observed for plain specimens. Figure 4.12 shows a plot of the unrestrained plastic shrinkage test results. All unrestrained plastic shrinkage tests and T-test results are summarized in Appendix D.

As observed from Table 4.2 and Fig. 4.12, adding 0.05% fibres, regardless of fibre type and length, did not have a significant effect on free plastic shrinkage. At a volume fraction of 0.1%, all fibre types and lengths were observed to reduce the shrinkage strain slightly, but only the 38 mm fibrillated polypropylene and white baler twine fibres produced statistically significant reductions. When the volume of fibres increased from 0.1% to 0.3%, further reductions in shrinkage strains were observed for most cases. Except for the 19 mm red and white baler twine fibres, all other fibres reduced the shrinkage strains significantly.

Table 4.2. Unrestrained plastic shrinkage strains recorded 22 hours after casting.

Fibre Type	Fibre Length (mm)	Volume Fraction (%)	Number of Specimens	Shrinkage strain (mm/mm)	C.O.V. (%)	Change in Strain (%)
Plain	—	—	24	0.0125	10.9	—
Fibrillated Polypropylene	19	0.05	4	0.0128	2.4	2.1
		0.10	4	0.0121	3.5	-3.1
		0.30	4	0.0103	7.1	-17.7
	38	0.05	4	0.0114	12.8	-8.7
		0.10	4	0.0112	8.3	-10.7
		0.30	4	0.0087	10.7	-30.2
Red Baler Twine	19	0.05	4	0.0132	3.3	5.8
		0.10	4	0.0119	2.7	-5.1
		0.30	4	0.0120	6.4	-4.1
	38	0.05	4	0.0120	7.0	-3.6
		0.10	4	0.0113	15.7	-9.5
		0.30	4	0.0112	12.7	-10.7
White Baler Twine	19	0.05	4	0.0124	6.7	-0.8
		0.10	4	0.0118	4.3	-5.6
		0.30	4	0.0109	4.2	-12.5
	38	0.05	4	0.0113	13.4	-9.4
		0.10	4	0.0105	3.9	-16.0
		0.30	4	0.0083	6.1	-33.9

The influence of the fibre type, length and volume fraction on the shrinkage strains may be better understood by considering Fig. 4.13, in which shrinkage strain is plotted against volume fraction. It can be observed that there is a general decrease in total shrinkage strain due to fibre addition, particularly at higher volume fractions. In all cases, long fibres were observed to be more effective in reducing the shrinkage strain than short fibres. The effect of fibre type varied with the volume fraction when 19 mm fibres were used. However, when 38 mm fibres were used, at all volume fractions, the white baler twine fibres were always the most effective in reducing shrinkage strain. The fibrillated polypropylene fibres were slightly inferior to the white baler twine and the red baler twine fibres were the least effective.

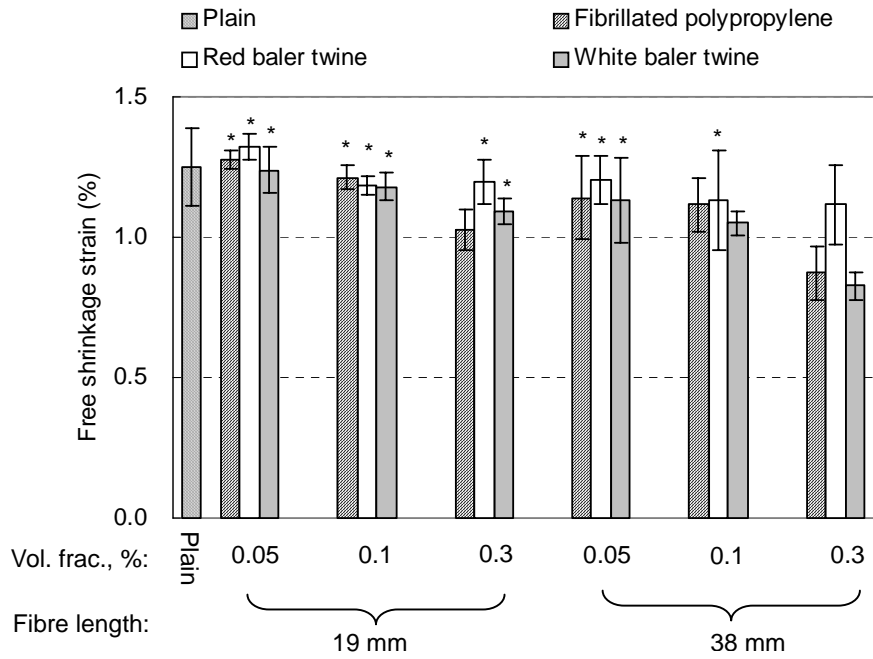


Figure 4.12. Measured unrestrained plastic shrinkage strains 22 hours after casting. Asterisks indicate cases that did not differ significantly from plain control specimens at the 95% level of confidence.

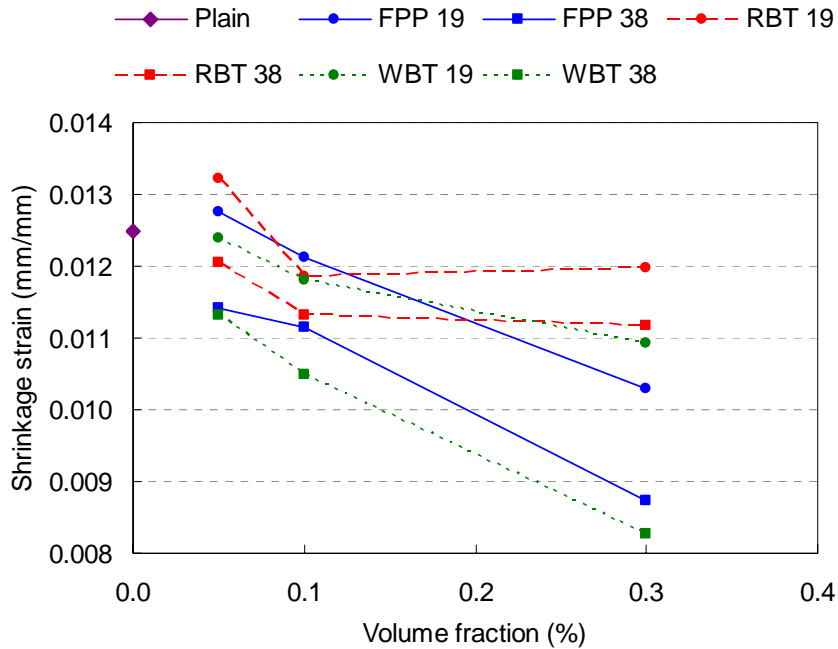


Figure 4.13. Unrestrained plastic shrinkage strains of all fibre types measured at 22 hours, plotted against volume fraction.

One explanation of the mechanism by which free strains are decreased by adding fibres is given by Mangat and Azari (1984). They believed that fibres can restrain shrinkage by shear stresses developing along the fibre-matrix interface. Qi et al. (2003) and Wongtanakitcharoen (2005) reported that the reduction in unrestrained shrinkage could be attributed to the large gap formed between fibre and matrix. This gap provided a path for bleeding water to rise to the concrete surface, which compensated for the moisture loss due to evaporation. As a result, the formation of a water meniscus at the surface was reduced, and shrinkage caused by capillary pressure was reduced.

4.4. Discussion and Analysis

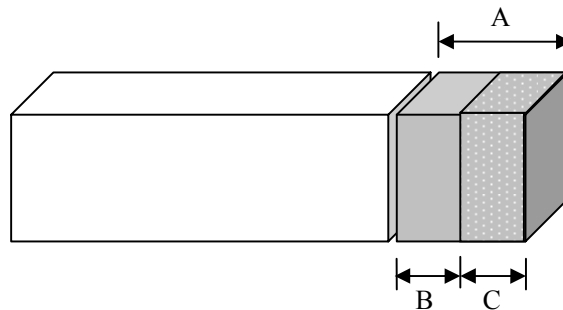
4.4.1. Role of reduced shrinkage tendency in the reduction of restrained shrinkage cracking

Based on the results of both the restrained and unrestrained shrinkage tests, it appears that the reduction in free shrinkage associated with fibre addition is a factor that contributes to the reduction of plastic shrinkage cracking observed in the restrained plastic shrinkage tests. The reduction in unrestrained shrinkage strain corresponds directly to an expected reduction in total crack area resulting from a reduced tendency to shrink. Under the assumption that the entire measured free shrinkage strain is accommodated in the restrained specimens by cracking, it is possible to calculate an expected total crack area as the product of the shrinkage strain, the specimen length (375 mm) and the specimen width (100 mm). The expected reductions in total crack area are then given as a percent of corresponding values on the plain specimens. Table 4.3 summarizes the expected and measured total crack areas, along with the expected and actual measured reductions in total crack area for all specimens. It is seen that, except for a few of the specimens with lower volume fractions of the baler twine fibres, the reductions in total crack area were greater than could be attributed to free strain reduction alone.

The above analysis assumed that the entire propensity for shrinkage, as

measured in the unrestrained specimens, was relieved by cracking in the restrained specimens. In fact, this was not the case, as seen by the ratio of actual to expected total crack areas in Table 4.3. In the case of plain specimens, for example, only 54.2% of the free shrinkage can be accounted for by the area of cracks on the surface.

Figure 4.14 illustrates this in schematic form. While the expected crack area on plain specimens was 469 mm² (illustrated by length A in the figure), the actual area was only 54% of this (length B). The remaining 46% (length C) must be attributed to other factors. Only two other factors are possible: 1) the restrained specimen actually shrank to some extent due to incomplete restraint, and 2) the mortar had some capacity to strain without cracking. The relative contribution of each of these factors cannot be precisely quantified. However, for the purpose of comparing the influence of different fibres, it may be assumed that the amount of restraint would not differ significantly from one specimen to the next. Differences among the ratios of actual to expected crack areas must therefore be attributed primarily to differences in the strain capacities of the mortars.



A: Expected crack area = $\varepsilon_f A_s$ (ε_f = free shrinkage, A_s = specimen area)

B: Actual crack area.

C: Shrinkage due to incomplete restraint and strain capacity of mortar.

Figure 4.14. Schematic of restrained specimen, showing the contribution of various factors to the expected crack area.

Figures 4.15 to 4.17 show plot of the free plastic shrinkage strains in a form that shows the portions of shrinkage that were accommodated by cracking in the restrained specimens along with portions attributable to a combination of incomplete restraint and strain capacity in the mortar. The strain accommodated by cracking was calculated as the ratio of the total crack area to the area of top surface of the specimen.

Table 4.3. The actual and expected reductions in total crack area for all specimens due to a reduced shrinkage tendency.

Fibre Type	Fibre Length (mm)	Volume Fraction (%)	Shrinkage Strain (mm/mm)	Expected Total Crack Area (mm ²)	Actual Total Crack Area (mm ²)	<u>Actual</u> <u>Expected</u>
Plain	—	Plain	0.0125	469	254.2	0.542
	19	0.05	0.0128	479	151.0	0.316
		0.10	0.0121	454	128.1	0.282
Fibrillated Polypropylene	38	0.30	0.0103	386	14.8	0.038
		0.05	0.0114	428	149.7	0.350
		0.10	0.0112	418	114.8	0.274
	19	0.30	0.0087	327	11.9	0.036
		0.05	0.0132	496	253.7	0.512
Red Baler Twine	38	0.10	0.0119	445	226.9	0.510
		0.30	0.0120	449	185.2	0.412
		0.05	0.0120	452	265.8	0.588
	19	0.10	0.0113	424	241.7	0.570
		0.30	0.0112	419	157.4	0.376
White Baler Twine	38	0.05	0.0124	465	255.0	0.549
		0.10	0.0118	442	208.6	0.471
		0.30	0.0109	410	100.7	0.245
	19	0.05	0.0113	425	195.8	0.461
		0.10	0.0105	394	184.3	0.468
		0.30	0.0083	310	58.3	0.188

Table 4.3. (Cont'd) The actual and expected reductions in total crack area for all specimens due to a reduced shrinkage tendency.

Fibre Type	Fibre Length (mm)	Volume Fraction (%)	Expected Reduction in Total Crack Area (%)	Actual Reduction in Total Crack Area (%)	<u>Actual</u> <u>Expected</u>
Plain	—	Plain	—	—	—
Fibrillated Polypropylene	19	0.05	-2.1	40.6	-19.20
		0.10	3.1	49.6	15.99
		0.30	17.7	94.2	5.33
	38	0.05	8.7	41.1	4.71
		0.10	10.7	54.8	5.11
		0.30	30.2	95.3	3.15
Red Baler Twine	19	0.05	-5.8	0.2	-0.03
		0.10	5.1	10.7	2.11
		0.30	4.1	27.2	6.55
	38	0.05	3.6	-4.6	-1.26
		0.10	9.5	4.9	0.51
		0.30	10.7	38.1	3.57
White Baler Twine	19	0.05	0.8	-0.3	-0.40
		0.10	5.6	17.9	3.20
		0.30	12.5	60.4	4.83
	38	0.05	9.4	23.0	2.45
		0.10	16.0	27.5	1.72
		0.30	33.9	77.1	2.27

It can be observed from these figures that the fibrillated polypropylene fibre was the most effective in increasing the mortar's strain capacity. When 38 mm fibrillated polypropylene fibre at a volume fraction 0.3% was added, 96% of the free shrinkage stain was attributed to incomplete restraint and strain capacity of mortar. The performance of white baler twine was slightly inferior to the fibrillated polypropylene

fibre. A maximum of 81% of the free shrinkage strain due to incomplete restraint and strain capacity of mortar was achieved when 0.3% white baler twine fibre cut to 38 mm was used. The effect of red baler twine in increasing the mortar's strain capacity was least among the three fibre types studied. When 0.3% red baler twine fibres at 38 mm was added, only 62% of the free shrinkage strain was accommodated by incomplete restraint and strain capacity of mortar.

Figures 4.15 to 4.17 also clearly show that the mortar's strain capacity consistently increased with an increase in the fibre volume fraction. The increase in strain capacity was most striking when the fibre's volume fraction increased from 0.1% to 0.3%. Changing the fibre length did not have a significant influence on the mortar's strain capacity and there is no consistent trend that can be observed in the test results.

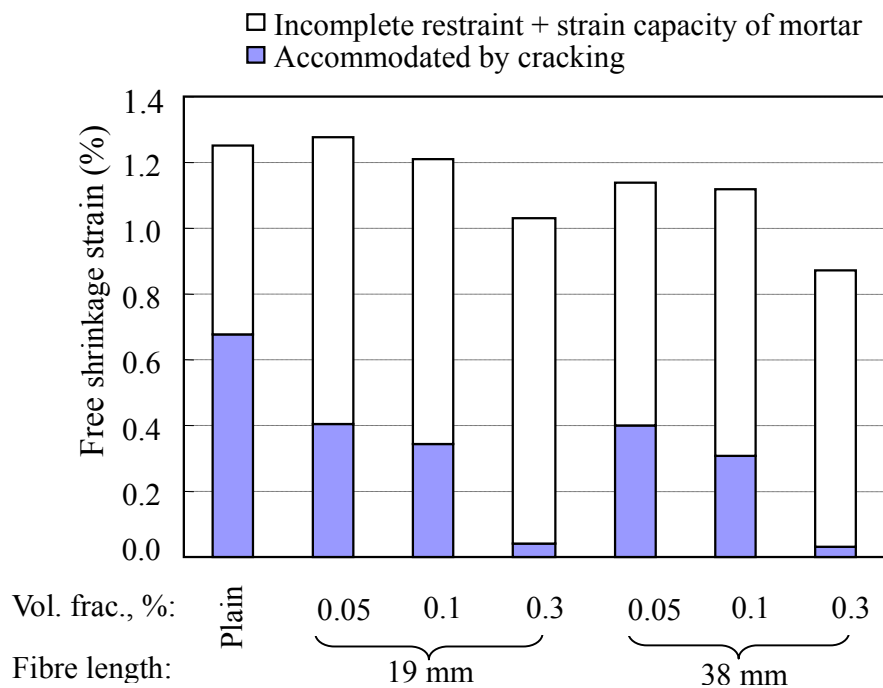


Figure 4.15. The contribution of various factors to the expected crack area for specimens reinforced with fibrillated polypropylene fibres.

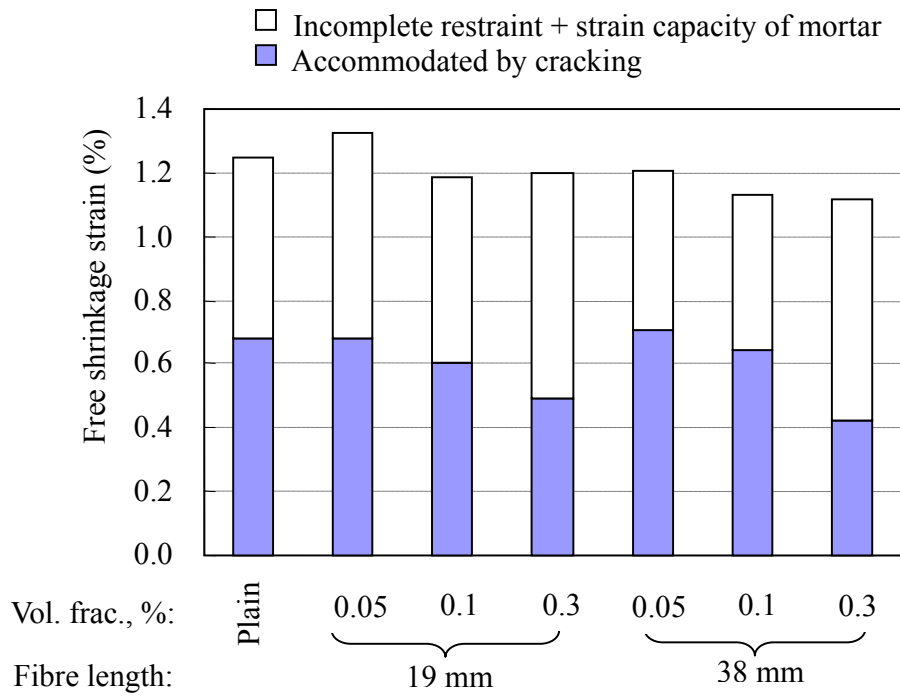


Figure 4.16. The contribution of various factors to the expected crack area for specimens reinforced with red baler twine fibres.

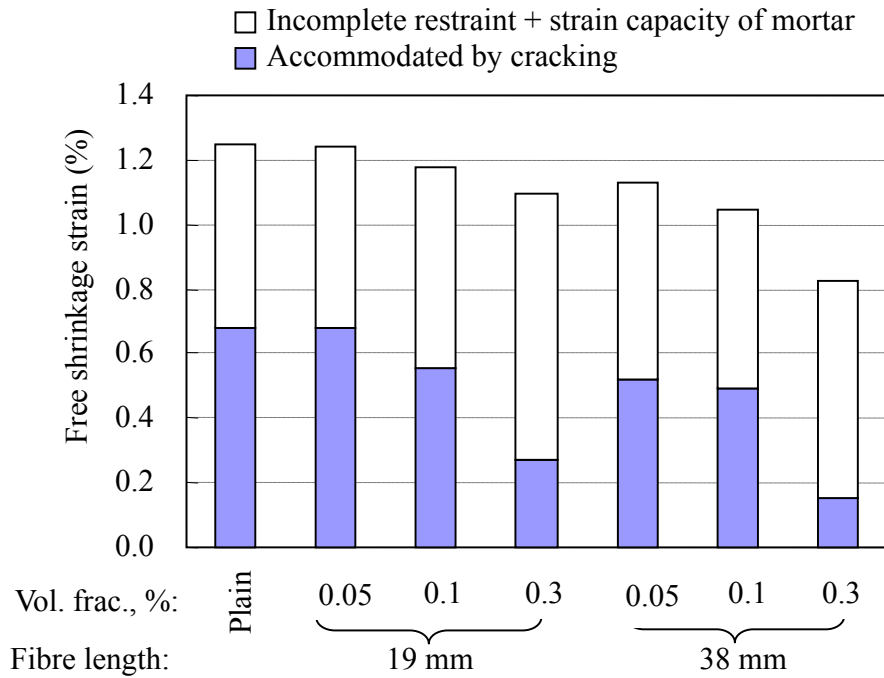


Figure 4.17. The contribution of various factors to the expected crack area for specimens reinforced with white baler twine fibres.

4.4.2. Performance of different fibre types

Even though all three types of fibres tested in this study were made from polypropylene, their performance in controlling plastic shrinkage cracking was quite different. The test results clearly showed that both types of baler twine fibres were not as effective as the fibrillated polypropylene fibres in controlling plastic shrinkage cracking, and that the white baler twine fibres performed better than the red baler twine fibres. The following discussion provides two possible reasons which might explain the different performance of the various fibres.

The most important reason for the differences in performance is the different fibre forms—that is, the arrangement of individual fibres. The fibrillated polypropylene fibres are composed of film sheets which are collated or held together by cross linking fine fibres along their length. This forms a continuous network or a woven mesh. As stated by Brown et al. (2002), “the cement matrix can therefore penetrate into the mesh structure between the individual fibrils and create a mechanical bond between fibre and matrix.” The white baler twine fibres are composed of a group of flat band-shaped strands which are twisted together. Many of the strands can separate from the fibre bundles during the cutting and mixing procedures. On the other hand, the red baler twine fibres are composed of a group of strands with a circular cross section. These strands are not only twisted together but also glued together at certain intervals along their length. As a result, only a few of the individual strands tend to separate from the fibre bundles during the cutting and mixing procedures, resulting in the inability of these fibres to distribute themselves as effectively.

The second reason for performance differences is related to the cross-sectional shape of individual fibre strands. The fibrillated polypropylene fibres and the white baler twine fibres are both composed of flat band-shaped strands, while the red baler twine is composed of strands with circular cross section. Qian et al. (2005) found that fibres with polygonal cross sections performed better than those with circular cross sections because of their higher surface areas for equivalent volumes. A higher surface

area produces more fibre-matrix interfaces in the paste. Consequently, tensile stresses will transfer to the fibres more efficiently.

Considering the two reasons mentioned above, at a given fibre volume fraction, the fibrillated polypropylene fibres in the form of woven meshes have a higher surface area and provide a better bond with the cement matrix than either of the two baler twine fibres, resulting in their superior performance. The surface area of the white baler twine fibres is also higher than that of the red baler twine fibres due to their greater propensity to separate into individual strands and their band-shaped cross section. This explains the white fibres' superior performance. Because the fibrillated and white baler twine fibres tend to separate and disperse, there are more fibres crossing a given cross section. This allows fibres to bridge matrix cracks more effectively, reducing stress concentrations and preventing cracks from growing (Banthia and Gupta 2006).

4.4.3. Analysis of the influence of fibre surface area

Since fibres interact with the surrounding matrix by the transfer of stress at the fibre – matrix interface, the surface area of fibres for a given volume is believed to be an important factor contributing to their effectiveness. The specific surface area of fibres in a fibre reinforced mortar is defined as the fibre surface area contained in a unit volume of the mortar. Based on how the different fibres tended to separate and the different shapes of fibre cross sections, the specific surface area of fibres in specimens containing different fibre types and different volume fractions was estimated. The relationship between the fibre specific surface area and total crack area was then evaluated and is discussed in this section.

As a first step in estimating the specific surface area of fibres, the mass of 20 pieces of 38 mm fibres of a given type was measured to the nearest 0.01g (Denver Instrument DI-4K, Denver, Colorado). This test was repeated five times for each fibre type. The average mass was then used to calculate a mass per unit length of fibre, also known as linear density. Results for each fibre type are given in Table 4.4.

Table 4.4. Weight of 20 pieces of 38 mm fibre and the resulting linear density of different fibre types.

	Average mass of 20 pieces (g)	C.O.V. (%)	Linear density, w (g/m)
Fibrillated polypropylene	0.87	1.3	1.15
White baler twine	1.36	2.7	1.79
Red baler twine	0.85	0.7	1.11

Because the red baler twine fibres tended to remain in bundled form, the effective surface area of the fibres was estimated by assuming that the fibre bundle acted as a single fibre with a circular cross section having the same linear density as the bundle. The equivalent diameter (d) of the red baler twine can then be calculated by the following formula:

$$d = 2\sqrt{\frac{w}{\rho \times \pi}} \quad , \quad [4.1]$$

where w = linear density and ρ = density of polypropylene (0.91 g/cm³).

The specific surface area of fibres (S) can be obtained from:

$$S = \frac{4v_f}{d} \quad , \quad [4.2]$$

where v_f = fibre volume fraction.

Since the fibrillated polypropylene and white baler twine fibres were derived from a tape form, the thickness of the tape (t) was measured to the nearest 0.02 mm with the aid of a handheld 50X microscope (EO Edmond Industrial Optics, 50X direct Measuring, Model 61210, Japan). The thickness of fibrillated polypropylene and white baler twine tape were found to be approximately 0.02mm and 0.04 mm, respectively. The number of pieces each fibre divided into (n) was measured 10 times for each fibre

type. A summary of the results is given in Table 4.5.

For fibres derived from tape form, the total length of fibres (L) in a unit volume of mortar can be calculated as follows:

$$L = \frac{v_f}{at}, \quad [4.3]$$

where a = width of fibre's cross section, v_f = fibre volume fraction, and t = thickness of the tape.

The specific surface area (S) is then obtained from:

$$S = \frac{2(a + nt)v_f}{at}, \quad [4.4]$$

where a = width of fibre's cross section, n = number of pieces each fibre divides into, and t = thickness of the tape.

Substituting $a = \frac{w}{t\rho}$ into Equation [4.4], the specific surface area (S) can be calculated by

$$S = 2v_f \left(\frac{1}{t} + \frac{nt\rho}{w} \right). \quad [4.5]$$

Table 4.5. The average number of pieces that different fibre types divided into.

Fibre type	Average number of pieces the fibre divided into (n)	C.O.V. (%)
Fibrillated polypropylene	39	8.3
White baler twine	9	26.0

The estimated specific surface areas associated with different fibre types and volume fractions are listed in Table 4.6. It can be seen that for a given fibre volume fraction, the fibrillated polypropylene has the largest specific surface area, white baler twine has the second largest and red baler twine has the smallest. This order corresponds to their order of effectiveness in controlling plastic shrinkage cracking.

The total crack area for 38 mm fibres is plotted against specific surface area in Fig 4.17. A clear trend can be observed of decreasing total crack area with increasing the fiber specific surface area.

4.4.4. Improving the effectiveness of baler twine fibres

The white baler twine fibres proved to be more effective than the red baler twine fibres for controlling plastic shrinkage cracking. However, they were still inferior to the fibrillated polypropylene fibres. To achieve the same performance as fibrillated polypropylene fibres, two methods might be considered. Firstly, a higher volume fraction of white baler twine fibres could be used. For example, to achieve the same reduction in maximum crack width produced by 38 mm fibrillated polypropylene fibres at 0.1%, a volume fraction of 38 mm white baler twine of 0.21% is required (see Fig. 4.8). Secondly, if the white baler twine can be separated into individual fibres effectively and inexpensively, using the separated baler twine should be more effective in controlling plastic shrinkage cracking compared with the original white baler twine fibres because the separated baler twine fibres have more surface area than the original baler twine fibres for a given fibre volume fraction.

Table 4.6. Specific surface area (mm^2/mm^3) of different fibre types and volume fractions.

Volume fraction (%)	Fibrillated polypropylene	White baler twine	Red baler twine
0.05	0.051	0.025	0.002
0.10	0.101	0.050	0.003
0.30	0.304	0.151	0.010

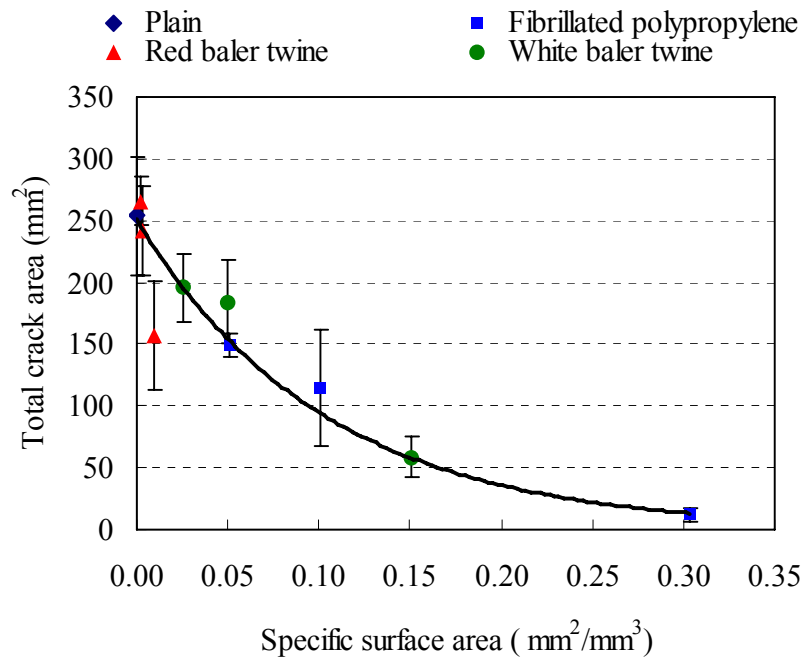


Figure 4.18. Effect of specific surface area of fibres on total crack area for 38 mm long fibres.

CHAPTER 5 CONCLUSIONS AND RECOMMENDATIONS

5.1. Summary and Conclusions

The plastic shrinkage properties of portland cement mortar reinforced with two types of baler twine fibres were compared with those of mortar reinforced with conventional fibrillated polypropylene fibres at equal lengths (19 mm and 38 mm) and volume fractions (0.05, 0.1, and 0.3%). Fresh mortar specimens were cast over a rough substrate and subjected to hot, dry, and windy conditions for a period of 22 hours, after which the size and number of cracks were measured.

Test results showed that both types of baler twine fibres were effective in reducing the plastic shrinkage cracking, especially when a high volume fraction of fibres were added to the cement mortar specimens. In terms of controlling the plastic shrinkage cracking, white baler twine fibres, composed of flat band-shaped strands twisted together, were more effective than the red baler twine fibres, which consisted of bundles of strands with circular cross sections, and both types of baler twine fibres were inferior to the fibrillated polypropylene fibres. At a volume fraction of 0.3% and with the fibre length found to be most effective for a given fibre type, the fibrillated polypropylene, white baler twine and red baler twine fibres reduced the maximum crack widths by 87.0% to less than 0.34 mm, 74.8% to less than 0.67 mm and 45.1% to less than 1.45mm, respectively, compared with plain mortar specimens. The reduction of total crack area reached 95.3%, 77.1% and 38.1%, respectively. A significant improvement in controlling the plastic shrinkage cracking was found by increasing the fibre volume fraction over a range from 0.05% to 0.3%. However, fibre length did not

have a significant influence on the cracking behaviour.

A slight decrease in unrestrained plastic shrinkage strain was generally found by adding fibres, particularly at higher fibre volume fractions and with longer fibre lengths. At a volume fraction of 0.1%, there was a statistically significant reduction in shrinkage strain experienced by specimens reinforced by 38 mm fibrillated polypropylene and white baler twine fibres when compared with plain specimens. When the volume fraction increased from 0.1% to 0.3%, all fibres, except for the 19 mm baler twine fibres, reduced the free shrinkage strain significantly. Maximum reductions were achieved at a volume fraction of 0.3% and length of 38 mm, at which the fibrillated polypropylene, white baler twine, and red baler twine fibres reduced plastic shrinkage strains by 30.2, 33.9, and 10.7%, respectively.

It is possible to conclude that the ability of fibres to control the restrained plastic shrinkage cracking could to a small extent be attributed to their ability to reduce the free shrinkage strain. However, the ability of fibres to improve the tensile capacity of fresh mortars and prevent the cracks from growing are believed to be the primary reasons for the reduction in restrained plastic shrinkage cracking. The reductions expected from a reduced tendency to shrink accounted for between 15 and 44% of the total crack area reductions when specimens with a 0.3% fibre volume fraction are considered.

All three types of fibre controlled plastic shrinkage cracking to some extent. However the different types of fibres performed differently due to their different fibre forms. Fibrillated polypropylene had a continuous network form when incorporated into the cement matrix. This, in turn, produced more fibre-matrix interfaces in the paste than the baler twine fibres at a given volume fraction. White baler twine fibres were composed of a group of flat band-shaped strands which were twisted together. These could be separated more easily into individual strands during cutting and mixing than could the red baler twine. The red baler twine was composed of a group of cylinder-shaped strands which were not only twisted together but also glued together at certain intervals along their length. As a result, white baler twine had more surface area

than red baler twine at a given volume fraction. They were therefore able to improve the tensile strength of matrix and bridge the cracks more effectively. As a result, the improved performance of certain fibre types can be attributed largely to their increased surface area relative to other fibre types. Higher surface areas permit the fibres to improve the tensile strength of the matrix and bridge the cracks more effectively.

5.2. Suggestions for Future Work

Because of the different specimen geometries, environmental conditions, and measurement methods that have been used by researchers to investigate plastic shrinkage cracking, test results differ widely, and there is no consensus regarding how to properly interpret the data. Therefore, there is an urgent need to develop a standardized test method to measure the plastic shrinkage properties of fibre reinforced concrete.

In this research, only new baler twine fibres were studied for their effect on controlling plastic shrinkage. If used baler twine can be studied in future research, it will permit a better evaluation of the technical feasibility of using recycled baler twine fibres as a concrete reinforcement. According to the research carried out by Randall Conrad & Assoc. Ltd. (2000), the cost of recycling of baler twine into a concrete fibre additive is about \$ 330 per tonne. Changes to the economy in recent years would warrant an updated cost analysis and a market study to assess the economic feasibility of this idea.

Separated baler twine fibres should be more effective in controlling plastic shrinkage cracking than the original baler twine fibres, which remain in bundles, because separated fibres have more surface area to bond with the cement matrix at a given volume fraction. Therefore, a method should be found to effectively separate the baler twine into individual strands, and the plastic shrinkage properties of the mortar reinforced with separated baler twine fibres needs to be studied in the future.

REFERENCES

ACI Committee 305R. (1999). Hot weather concreting. American concrete Institute, Farmington Hills, MI.

ASTM C157. 2004. Standard test method for length change of hardened hydraulic-cement mortar and concrete. Annual Book of ASTM Standards, 04-02.

ASTM C192. 2002. Standard practice for making and curing concrete test specimens in the laboratory. Annual Book of ASTM Standards, 04-02.

ASTM C29. 1997. Standard test method for bulk density (“unit weight”) and voids in aggregate. Annual Book of ASTM Standards, 04-02.

ASTM C136. 2001. Standard test method for sieve analysis of fine and coarse aggregates. Annual Book of ASTM Standards, 04-02.

ASTM C33-03. 2003. Standard specification for concrete aggregates. Annual Book of ASTM Standards, 04-02.

Al-Amoudi, O.S.B., Abiola, T.O., and Maslehuddin, M. 2006. Effect of superplasticizer on plastic shrinkage of plain and silica fume cement concretes. *Construction and Building Materials*, 20: 642-647.

Al-Amoudi, O.S.B., Maslehuddin, M., and Abiola, T.O. 2004. Effect of type and dosage of silica fume on plastic shrinkage in concrete exposed to hot weather. *Construction and Building Materials*, 18: 737-743.

Balaguru, P. 1994. Contribution of fibres to crack reduction of cement composites during the initial and final setting period. *ACI Materials Journal*, 91(3): 280-288.

Balaguru, P.N. and Bhatt, D. 2000. Rapid hardening concrete, final report. Center for advanced infrastructure and technology, New Jersey, U.S.

Banthia, N. and Gupta, R. 2006. Influence of polypropylene fibre geometry on plastic

shrinkage cracking in concrete. *Cement and Concrete Research*, 36: 1263-1267.

Banthia, N. and Yan, C. 2000. Shrinkage cracking in polyolefin fibre-reinforced concrete. *ACI Materials Journal*, 97(4): 432-437.

Banthia, N., Azzabi, M., and Pigeon, M. 1993. Restrained shrinkage cracking in fibre reinforced cementitious composites. *Materials and Structures*, 26: 405-413.

Banthia, N., Yan, C., and Mindess, S. 1996. Restrained shrinkage cracking in fibre reinforced concrete: a novel test technique. *Cement and Concrete Research*, 26(1): 9-14.

Bayasi, Z. and McIntyre, M. 2002. Application of fibrillated polypropylene fibres for restraint of plastic shrinkage cracking in silica fume concrete. *ACI Materials Journal*, 99(4): 337-344.

Berke, N.S. and Dalliare, M.P. 1994. The effect of low addition rate of polypropylene fibres on plastic shrinkage cracking and mechanical properties of concrete. *Fibre reinforced concrete: development and innovations*, ACI SP-142-2, pp.19-41.

Boghossiaan, E. 2004. Plastic shrinkage cracking of flax fibre reinforced concrete. M.Sc. Thesis, Department of Civil and Geological Engineering, University of Saskatchewan, Canada.

Boghossian, E. and Wegner, L.D. 2003. Plastic shrinkage properties of flax fibre reinforced concrete. *Proceedings of Annual Conference of the Canadian Society for Civil Engineering*, Moncton, NB, Paper GCE-399.

Brown, R., Shukla, A., and Natarajan, K.R. 2002. Fibre reinforcement of concrete structures. URITIC project NO. 536101, Department of Transportation, University of Rhode Island, U.S.

Carlson, R.W. and Reading, T. J. 1988. Model study of shrinkage cracking in concrete building walls. *ACI Structural Journal*, 85(4): 395-404.

Cohen, M.D., Olek, J., and Dolch, W.L. 1990. Mechanism of plastic shrinkage cracking

in portland-cement and portland cement-silica fume paste and mortar. *Cement and Concrete Research*, 20: 103-119.

Groth, P. 2000. Fibre reinforced concrete. Ph.D. Thesis, Department of Civil and Mining Engineering, Luleå University of Technology, Sweden.

Hameed, A. 2002. Flexural toughness of baler twine fibre reinforced concrete. M.Sc. Thesis, Department of Civil and Geological Engineering, University of Saskatchewan, Canada.

Holt, E. 2004. Contribution of mixture design to chemical and autogenous shrinkage of concrete at early ages. *Cement and Concrete Research*, 35: 464-472.

Kraai, P.P. 1985. A proposed test to determine the cracking potential due to drying shrinkage of concrete. *Concrete Construction*, 30(9): 775-778.

Ma, Y., Qiu, J., Wang, P., Yang, Q., Sun, Z., and Jiang, Z. 2005. Effect of polypropylene fibre on the plastic shrinkage stress and plastic shrinkage ratio of mortar. *Jianzhu Cailiao Xuebao/Journal of Building Materials*, 8(5): 499-507.

Mangat, P.S. and Azari, M.M. 1984. A theory for the free shrinkage of steel fibre reinforced cement matrices. *Material Science*, 19:2183-3194.

Naaman, A.E., Wongtanakitcharoen, T., and Hauser, G. 2005. Influence of different fibres on plastic shrinkage cracking of concrete. *ACI Materials Journal*, 102(1): 49-58.

Najm, H. and Balaguru, P. 2002. Effect of large-diameter polymeric fibres on shrinkage cracking of cement composites. *ACI Materials Journal*, 99(4): 345-351.

Qi, C. 2003. Quantitative assessment of plastic shrinkage cracking and its impact on the corrosion of steel reinforcement. Ph.D. Thesis, Department of Civil Engineering, Purdue University, West Lafayette, Indiana, USA.

Qi, C., Weiss, J., and Olek, J. 2003. Characterization of plastic shrinkage cracking in fibre reinforced concrete using image analysis and a modified Weibull function.

Materials and Structures, 36: 386-395.

Qian, C., Geng, F., and Li, L. 2005. Mechanism research on improvement of resistance to plastic shrinkage and cracking of cement mortar by polypropylene fibres. *Dongnan Daxue Xuebao (Ziran Kexue Ban)/Journal of Southeast University, China, (Natural Science Edition)*, 35(5): 786-791.

Randall Conrad & Assoc. Ltd. 2000. Citing online sources: The market feasibility of recycling/recovering post consumer polypropylene baler twin in Alberta [online]. Available from http://www.cpia.ca/files/files/files_baler_twine_study.pdf [cited 15 March 2000].

Sanjuán, M.A., and Moragues, A. 1997. Polypropylene fibre reinforced mortar mixes: optimization to control plastic shrinkage. *Composites Science and Technology*, 57(6): 655-660.

Shaeles, C.A. and Hover, K.C. 1988. Influence of mix proportions and construction operations on plastic shrinkage cracking in thin slabs. *ACI Materials Journal*, 85(6): 495-504.

Soroushian, P., Mirza, F., and Alhozaimy, A. 1995. Plastic shrinkage cracking of polypropylene fibre reinforced concrete. *ACI Materials Journal*, 92(5): 553-560.

Swamy, R.N. and Stravides H. 1979. Influence of fibre reinforcement on restrained shrinkage, *ACI Journal*, 86: 443-460.

Tia, M., Subramanian, R., Brown, D., Broward, C. 2005. Evaluation of shrinkage cracking potential of concrete used in bridge decks in Florida. Final report. Department of Civil and Coastal Engineering, University of Florida, Gainesville, Florida, United States.

Toledo Filho, R.D. and Sanjuán, M.A. 1999. Effect of low modulus sisal and polypropylene fibre on the free and restrained shrinkage of mortars at early age. *Cement and Concrete Research*, 29(10): 1597-1604.

Toledo Filho, R.D., Ghavami, K., Sanjuán, M.A., and England, G.L. 2005. Free, restrained and drying shrinkage of cement mortar composites reinforced with vegetable fibres. *Cement and Concrete Composites*, 27(5): 537-546.

Wang, K., Shah, S.P., and Phuaksuk, P. 2001. Plastic shrinkage cracking in concrete materials - Influence of fly ash and fibres. *ACI Materials Journal*, 98(6): 458-464.

Wang, T. 2003. Flexural toughness of flax fibre reinforced concrete. M.Sc. Thesis, Department of Civil and Geological Engineering, University of Saskatchewan, Canada.

Waris, M.A. 1996. Plastic shrinkage cracking in hot weather conditions. M.Sc. Thesis, Department of Civil Engineering, King Fahd University of Petroleum and minerals, India.

Weyers, R.E., Conway, J.C. and Cady, P.D. 1982. Photoelastic analysis of rigid inclusions in fresh concrete. *Cement and Concrete Research*, 12: 475-484.

Wongtanakitcharoen, T. 2005. Effect of randomly distributed fibres on plastic shrinkage cracking of cement composites. Ph.D. Thesis, Department of Civil Engineering, University of Michigan, Ann Arbor, Michigan, United States.

APPENDIX A — Comparison of Different Settings for Crack Measurement

Different settings of dot per inch (dpi) and gray scale values were tried before the specimens were digitized. The results are listed in Table A.1. Based on the minimum crack width that could be detected and scanning time, a scanning resolution of 1200 dpi and 8 bit gray scale were selected when the samples were scanned. With these settings, crack widths smaller than 0.0212 mm were not detectable. A total of 256 gray levels were assigned to the pixels in the digital image.

Table A.1. Comparison of different settings for crack measurement.

Dpi	Gray Scale	Minimum crack width could be detected (mm/pixel)	Time for scanning a whole sample (minutes)
800	8	0.0318	2
800	16	0.0318	8
1200	8	0.0212	10
1200	16	0.0212	50

APPENDIX B — Environmental Conditions

Some trial and error was required to achieve the desired environmental conditions and evaporation rate. A detailed description of this process is provided in this section.

First the temperature and relative humidity in the chamber were held constant at $45\pm 2^{\circ}\text{C}$ and less than 3%, respectively. The average wind speed on the top surface of the specimen was around 6.1 m/s in tunnel A and tunnel B. The measured average evaporation rate was around 1.9 kg/m²/h. Under this environmental condition, the use of 19 mm fibrillated polypropylene at 0.1% caused a reduction of approximately 17% and 39% in the maximum crack width and the crack area, respectively, as shown in Table B.1. The effectiveness of adding fibres was not obvious. The high evaporation rate used in this test increased plastic shrinkage of mortar significantly, which may have caused that result. Thus, the tendency of cracking is so strong that fibres cannot stop it effectively. In order to enhance the ability to compare the performance of different fibres, the evaporation rate was reduced by reducing the temperature and wind speed.

The temperature was reduced by shutting down two heaters. Only the one connected to the computer was open. In this way, the average temperature was reduced from 45°C to 35°C and the relative humidity remained less than 3%.

The wind speed was reduced by opening the inlet of a fume hood in another room. This inlet was also connected to the same building ventilation system. In this way, the average wind speed on the top surface of the specimen was reduced from around 6.1 m/s to 2.6 m/s.

After the temperature and wind speed were changed, the evaporation rate was measured again. The measured average evaporation rate in both tunnels was reduced from 1.9 kg/m²/h to 0.8 kg/m²/h.

The restrained shrinkage test, containing plain specimens and specimens with

19 mm fibrillated polypropylene fibres at 0.1% volume fraction, were tested under the changed environmental conditions which had lower evaporation rates. Table B.1 compares the restrained plastic shrinkage test results when subjected to the two evaporation rates. It can be observed that under a low evaporation rate, the effectiveness of 0.1% fibrillated polypropylene fibre in reducing maximum crack width and total crack area reached 58% and 66%, respectively. The differences between plain samples and fibre reinforced samples were more obvious under the low evaporation rate. Thus, the environmental conditions with a low evaporation rate was used for all tests.

Prior to conducting the tests, the wind speeds were measured at nine different points in each wind tunnel. At each point, wind speeds were measured at three different depths: top, middle and bottom. The changes of wind speed at different point and depths of each tunnel are illustrated in Figs B.1 to B.18.

Table B.1. The comparison of restrained shrinkage test results under high and low evaporation rates.

Evaporation rate	Sample	Crack Numbers	C.O.V. (%)	Max Crack Width (mm)	C.O.V. (%)
High	Plain	3.8	40.0	3.0	16.3
	0.1% FPP	9.8	34.9	2.5	14.8
Low	Plain	6.3	54.5	2.0	6.1
	0.1% FPP	11.3	26.5	0.8	33.8

Table B.1. (Cont'd) The comparison of restrained shrinkage test results under high and low evaporation rates.

Evaporation rate	Sample	Crack Area (mm ²)	C.O.V. (%)	Decrease in Max Crack width (%)	Decrease in Total Crack Area (%)
High	Plain	232.4	9.1	17	39
	0.1% FPP	141.6	21.3		
Low	Plain	189.1	19.2	58	66
	0.1% FPP	63.9	54.5		

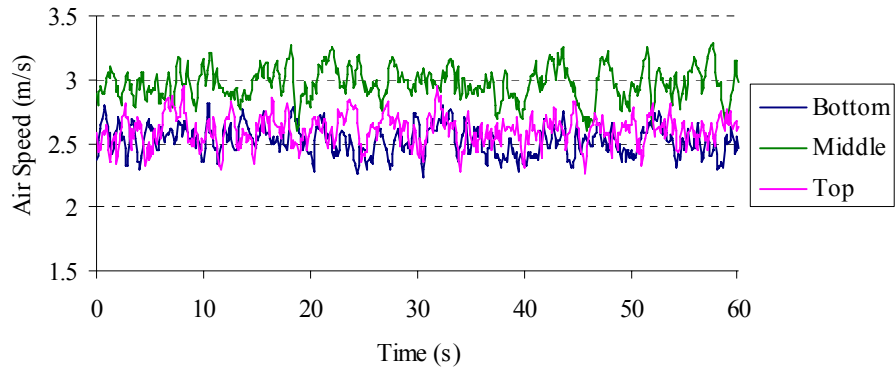


Figure B.1. Record of wind speed at Point 1 in tunnel A.

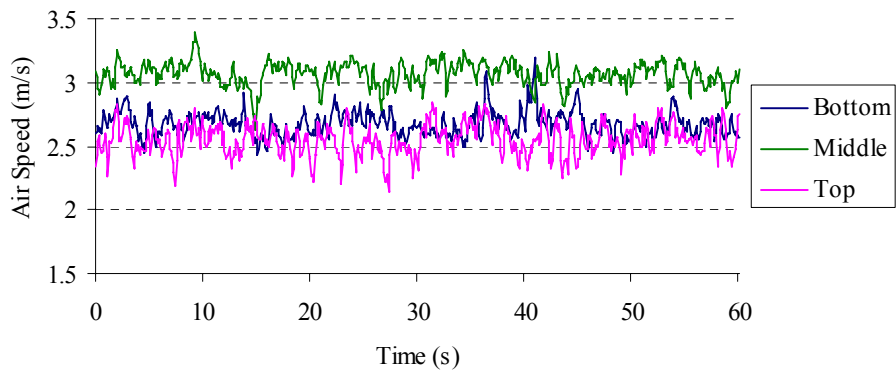


Figure B.2. Record of wind speed at Point 2 in tunnel A.

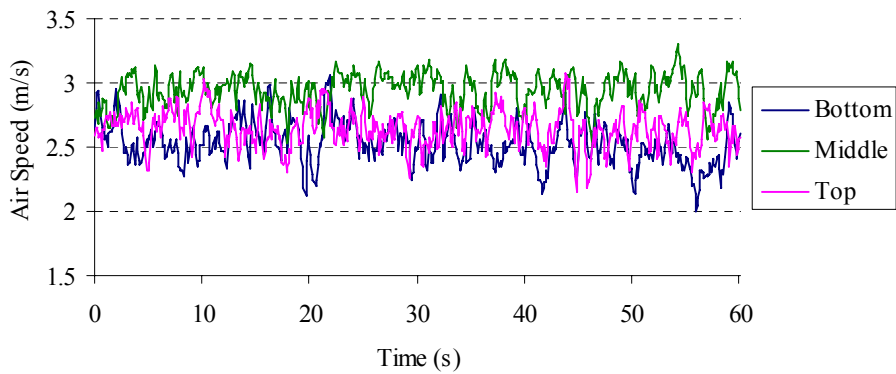


Figure B.3. Record of wind speed at Point 3 in tunnel A.

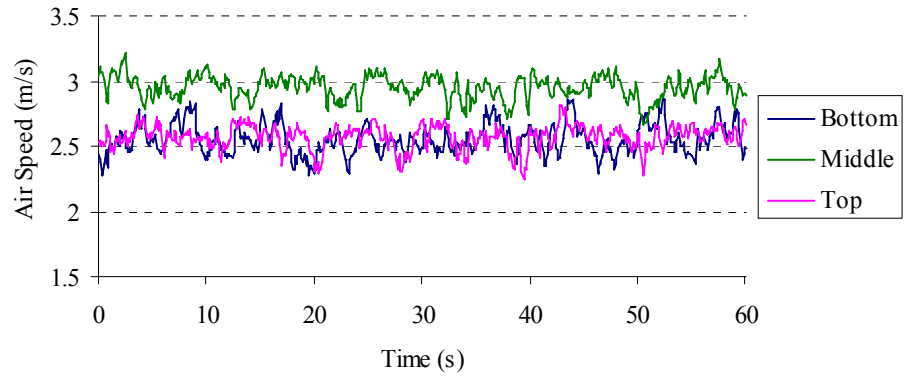


Figure B.4. Record of wind speed at Point 4 in tunnel A.

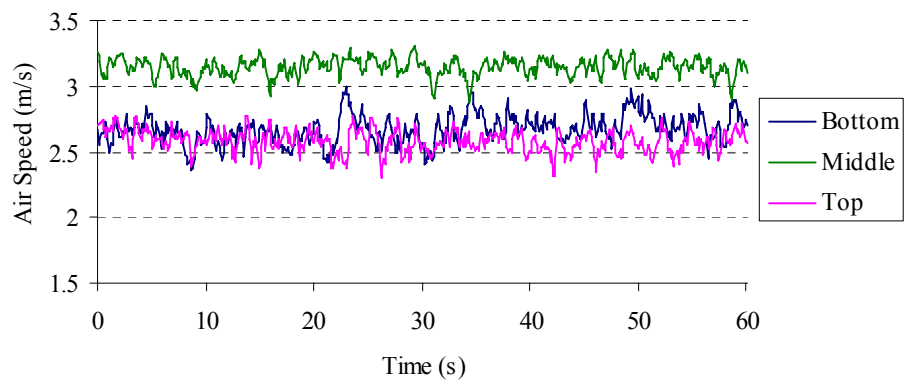


Figure B.5. Record of wind speed at Point 5 in tunnel A.

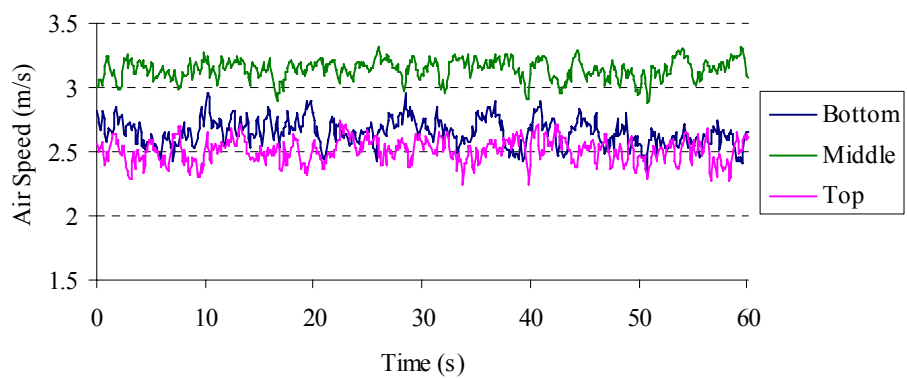


Figure B.6. Record of wind speed at Point 6 in tunnel A.

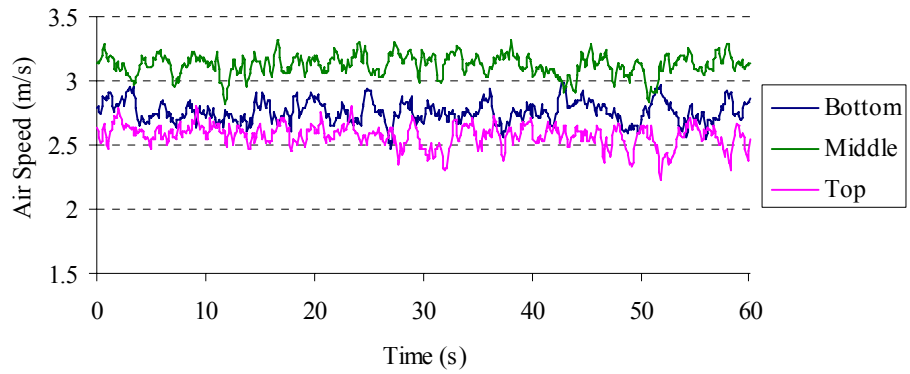


Figure B.7. Record of wind speed at Point 7 in tunnel A.

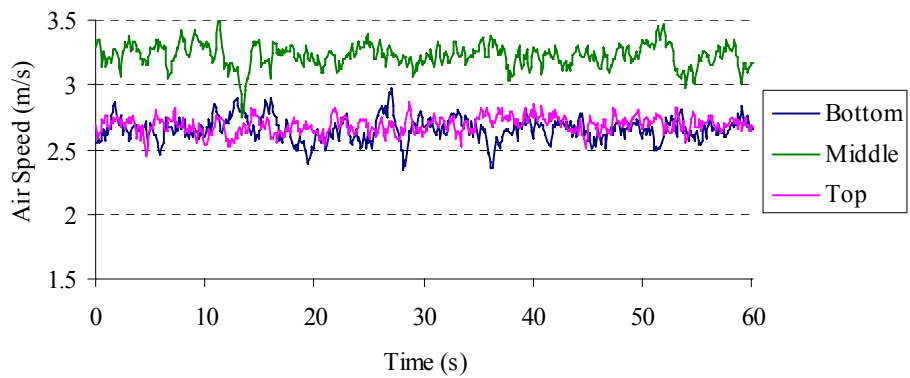


Figure B.8. Record of wind speed at Point 8 in tunnel A.

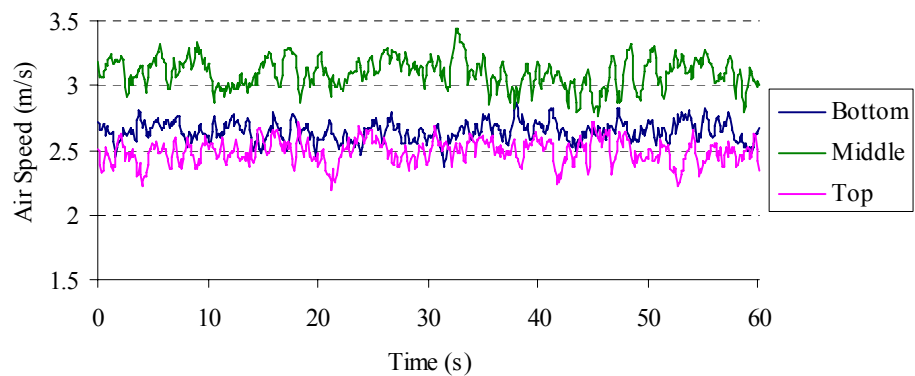


Figure B.9. Record of wind speed at Point 9 in tunnel A.

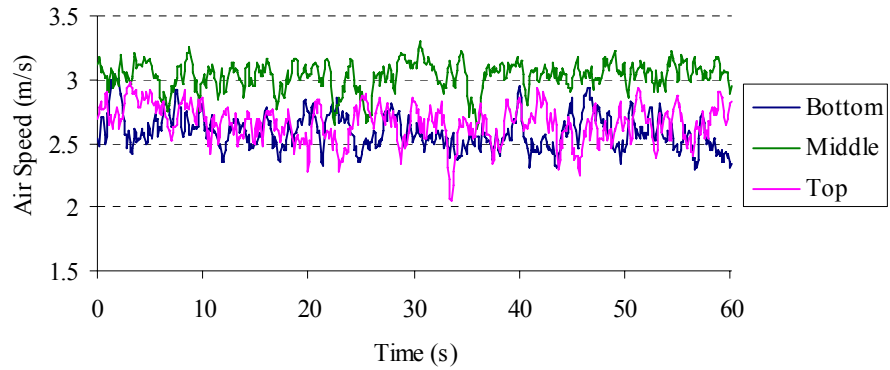


Figure B.10. Record of wind speed at Point 1 in tunnel B.

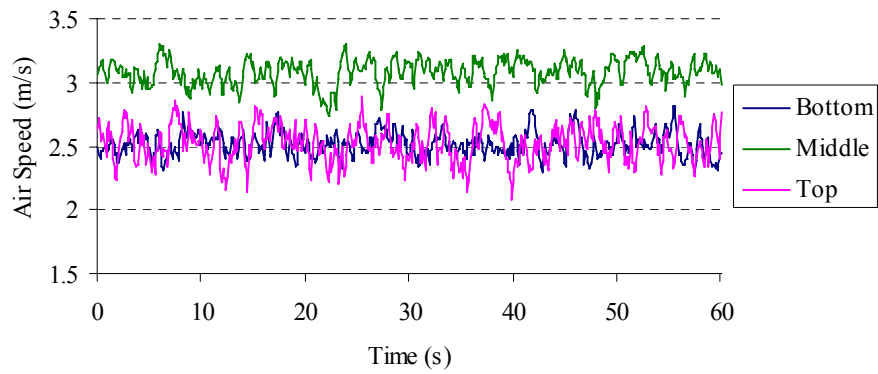


Figure B.11. Record of wind speed at Point 2 in tunnel B.

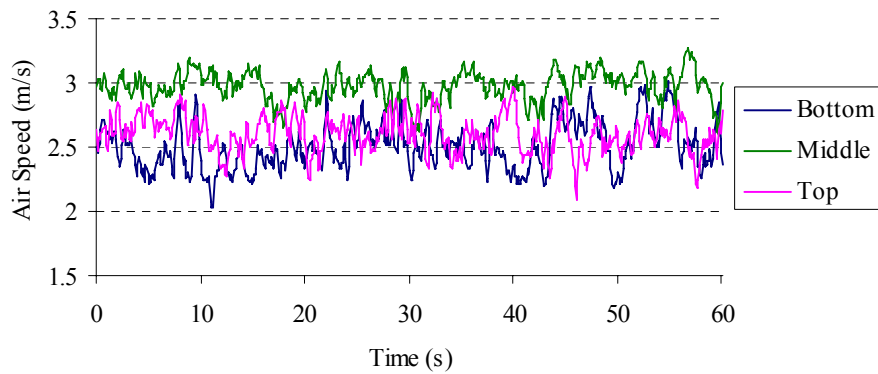


Figure B.12. Record of wind speed at Point 3 in tunnel B.

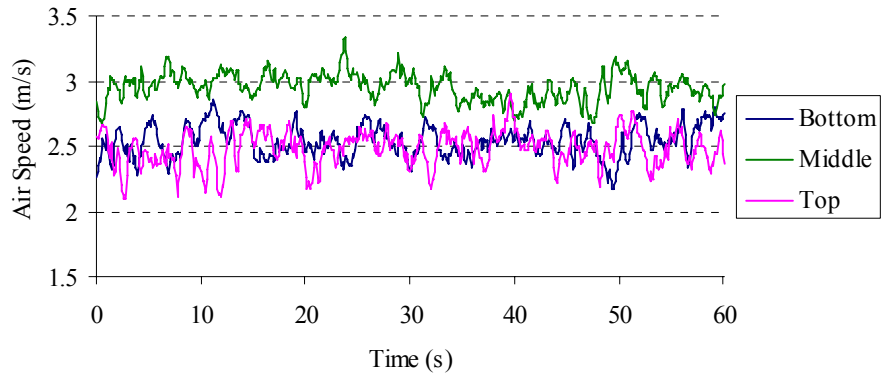


Figure B.13. Record of wind speed at Point 4 in tunnel B.

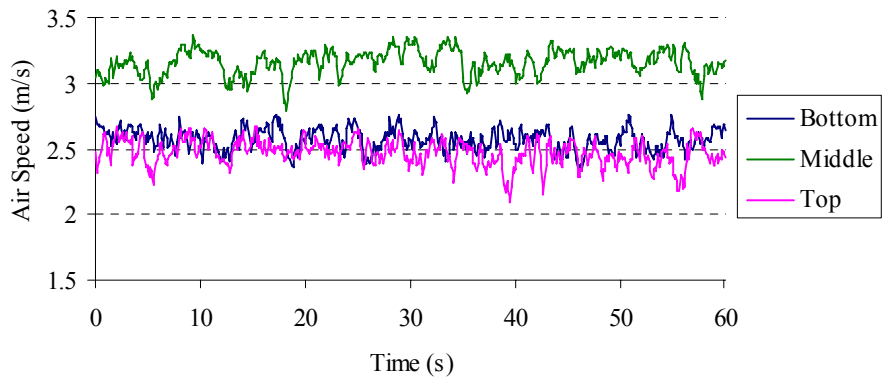


Figure B.14. Record of wind speed at Point 5 in tunnel B.

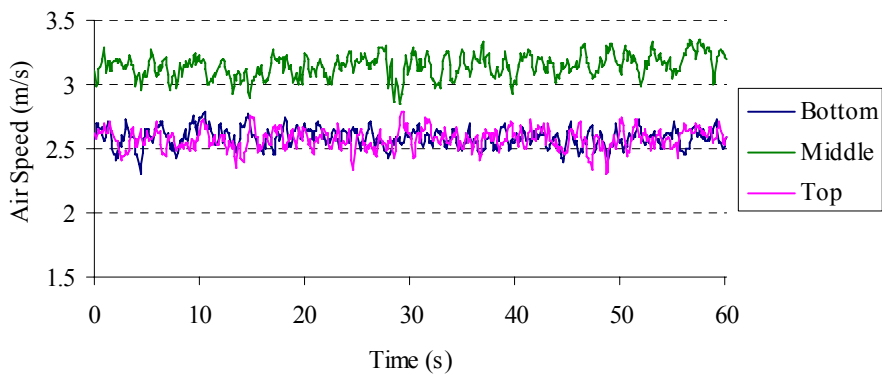


Figure B.15. Record of wind speed at Point 6 in tunnel B.

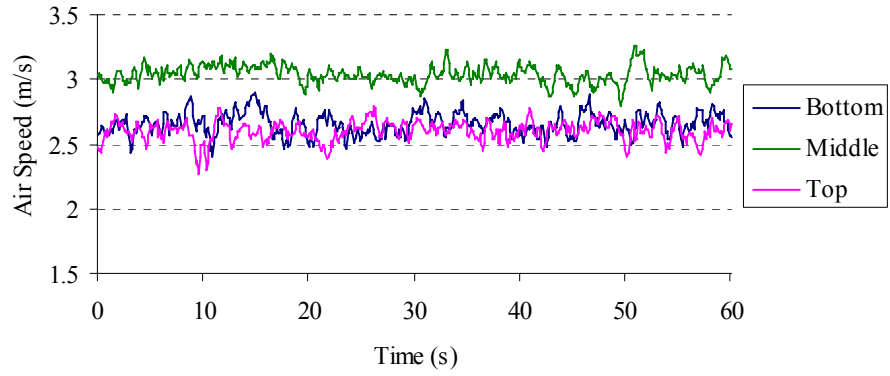


Figure B.16. Record of wind speed at Point 7 in tunnel B.

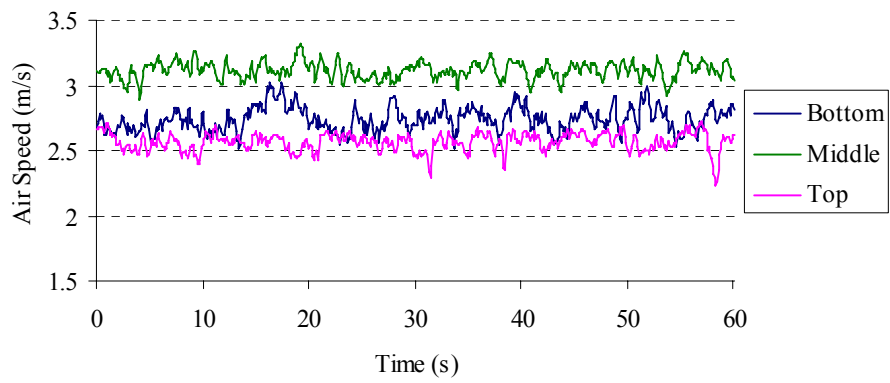


Figure B.17. Record of wind speed at Point 8 in tunnel B.

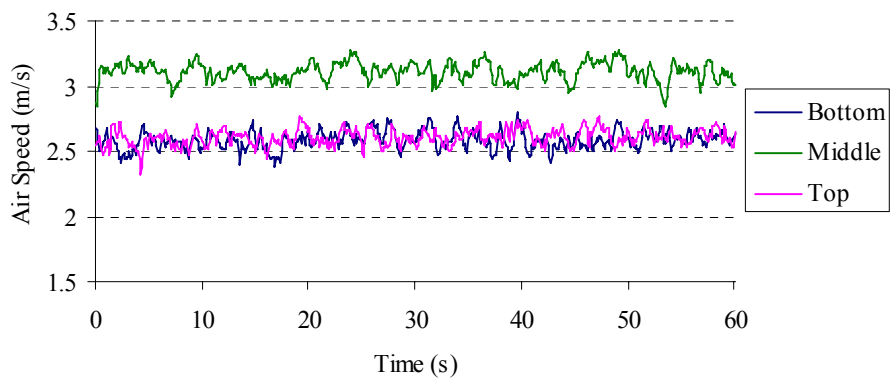


Figure B.18. Record of wind speed at Point 9 in tunnel B.

T-tests were carried out to assess whether the means of the evaporation rates at different points of each tunnel were statistically different from each other. The calculated results are summarized in Table B.2. In this table S is standard deviation, C.O.V. denotes coefficient of variation, n is number of samples in each group, ν is total degrees of freedom, S_c is the pooled standard deviation, S_d denotes standard error of the difference between two means, t is difference between means divided by standard error of sample means, and t_{crit} denotes t test critical value. If the t value is larger than t test critical value it can be concluded that the difference between the means for the two groups is significant.

Table B.2. Evaporation rate, 95% confidence limit (one-sided), comparison between different points of each tunnel.

Group 1	Group 2	Group 1	C.O.V.	S_1	Group 2	C.O.V.	S_2	n_1	n_2	ν
A1	A2	0.831	4.94%	0.0410	0.844	4.43%	0.0374	6	6	10
A1	A3	0.831	4.94%	0.0410	0.776	6.00%	0.0465	6	6	10
A1	A4	0.831	4.94%	0.0410	0.769	3.58%	0.0275	6	6	10
A1	B1	0.831	4.94%	0.0410	0.838	4.55%	0.0381	6	6	10
A1	B2	0.831	4.94%	0.0410	0.802	5.50%	0.0442	6	6	10
A1	B3	0.831	4.94%	0.0410	0.749	3.07%	0.0230	6	6	10
A1	B4	0.831	4.94%	0.0410	0.744	2.64%	0.0196	6	6	10
A2	A3	0.844	4.43%	0.0374	0.776	6.00%	0.0465	6	6	10
A2	A4	0.844	4.43%	0.0374	0.769	3.58%	0.0275	6	6	10
A2	B1	0.844	4.43%	0.0374	0.838	4.55%	0.0381	6	6	10
A2	B2	0.844	4.43%	0.0374	0.802	5.50%	0.0442	6	6	10
A2	B3	0.844	4.43%	0.0374	0.749	3.07%	0.0230	6	6	10
A2	B4	0.844	4.43%	0.0374	0.744	2.64%	0.0196	6	6	10
A3	A4	0.776	6.00%	0.0465	0.769	3.58%	0.0275	6	6	10
A3	B1	0.776	6.00%	0.0465	0.838	4.55%	0.0381	6	6	10
A3	B2	0.776	6.00%	0.0465	0.802	5.50%	0.0442	6	6	10
A3	B3	0.776	6.00%	0.0465	0.749	3.07%	0.0230	6	6	10
A3	B4	0.776	6.00%	0.0465	0.744	2.64%	0.0196	6	6	10
A4	B1	0.769	3.58%	0.0275	0.838	4.55%	0.0381	6	6	10
A4	B2	0.769	3.58%	0.0275	0.802	5.50%	0.0442	6	6	10
A4	B3	0.769	3.58%	0.0275	0.749	3.07%	0.0230	6	6	10
A4	B4	0.769	3.58%	0.0275	0.744	2.64%	0.0196	6	6	10
B1	B2	0.838	4.55%	0.0381	0.802	5.50%	0.0442	6	6	10
B1	B3	0.838	4.55%	0.0381	0.749	3.07%	0.0230	6	6	10
B1	B4	0.838	4.55%	0.0381	0.744	2.64%	0.0196	6	6	10
B2	B3	0.802	5.50%	0.0442	0.749	3.07%	0.0230	6	6	10
B2	B4	0.802	5.50%	0.0442	0.744	2.64%	0.0196	6	6	10
B3	B4	0.749	3.07%	0.0230	0.744	2.64%	0.0196	6	6	10

Table B.2. (Cont'd) Evaporation rate, 95% confidence limit (one-sided), comparison between different points of each tunnel.

Group 1	Group 2	S_c^2	S_d	t	t_{crit}	t/t_{crit}	Significant	Probability from same set
A1	A2	1.54E-03	2.27E-02	0.588	1.812	0.325	NO	28.5%
A1	A3	1.92E-03	2.53E-02	-2.194	1.812	1.211	YES	2.6%
A1	A4	1.22E-03	2.02E-02	-3.085	1.812	1.702	YES	0.6%
A1	B1	1.57E-03	2.29E-02	0.292	1.812	0.161	NO	38.8%
A1	B2	1.82E-03	2.46E-02	-1.174	1.812	0.648	NO	13.4%
A1	B3	1.11E-03	1.92E-02	-4.284	1.812	2.364	YES	0.1%
A1	B4	1.03E-03	1.86E-02	-4.668	1.812	2.576	YES	0.0%
A2	A3	1.78E-03	2.44E-02	-2.828	1.812	1.560	YES	0.9%
A2	A4	1.08E-03	1.90E-02	-3.985	1.812	2.199	YES	0.1%
A2	B1	1.43E-03	2.18E-02	-0.306	1.812	0.169	NO	38.3%
A2	B2	1.67E-03	2.36E-02	-1.787	1.812	0.986	NO	5.2%
A2	B3	9.63E-04	1.79E-02	-5.333	1.812	2.943	YES	0.0%
A2	B4	8.92E-04	1.72E-02	-5.800	1.812	3.201	YES	0.0%
A3	A4	1.46E-03	2.21E-02	-0.302	1.812	0.167	NO	38.4%
A3	B1	1.81E-03	2.45E-02	2.535	1.812	1.399	YES	1.5%
A3	B2	2.06E-03	2.62E-02	1.019	1.812	0.562	NO	16.6%
A3	B3	1.35E-03	2.12E-02	-1.259	1.812	0.695	NO	11.8%
A3	B4	1.27E-03	2.06E-02	-1.510	1.812	0.833	NO	8.1%
A4	B1	1.11E-03	1.92E-02	3.589	1.812	1.981	YES	0.2%
A4	B2	1.35E-03	2.12E-02	1.569	1.812	0.866	NO	7.4%
A4	B3	6.43E-04	1.46E-02	-1.366	1.812	0.754	NO	10.1%
A4	B4	5.72E-04	1.38E-02	-1.771	1.812	0.977	NO	5.4%
B1	B2	1.70E-03	2.38E-02	-1.493	1.812	0.824	NO	8.3%
B1	B3	9.90E-04	1.82E-02	-4.894	1.812	2.701	YES	0.0%
B1	B4	9.19E-04	1.75E-02	-5.334	1.812	2.944	YES	0.0%
B2	B3	1.24E-03	2.03E-02	-2.625	1.812	1.449	YES	1.3%
B2	B4	1.17E-03	1.97E-02	-2.929	1.812	1.616	YES	0.8%
B3	B4	4.56E-04	1.23E-02	-0.360	1.812	0.199	NO	36.3%

APPENDIX C — Restrained Shrinkage Test Results

For the restrained shrinkage tests, the fresh fibre-reinforced overlay mortars were cast over the hardened and roughened substrate bases and transferred to the chamber with hot, dry and windy conditions. The maximum crack widths and total crack area were measured using the image analysis method 22 hours later after the specimens were transferred to the environmental chamber. Crack numbers were recorded at the same time.

Table C.1 to C.19 summarize the test results of all restrained plastic shrinkage tests which include 19 different kinds of specimens. Except for plain specimens, each one had a different combination of fibre type, length, and volume fraction.

T-tests were carried out to assess whether the means of two groups were statistically different from each other. The calculated results are summarized in Table C.21 to Table C.25. The abbreviations used to represent the mortar mixtures with different fibre type, fibre length and fibre volume fraction are shown in Table C.20.

Table C.1. Restrained shrinkage test results for plain specimens.

Sample	Crack numbers	Max Crack Width (mm)	Total Crack Area (mm ²)
1	7	3.22	258.68
2	5	1.91	194.81
3	9	2.30	208.49
4	2	2.88	293.50
5	5	2.58	250.46
6	1	2.10	136.49
7	6	2.62	221.06
8	5	2.53	184.83
9	8	2.34	283.62
10	2	2.32	337.33
11	12	2.30	282.65
12	4	2.02	264.80
13	1	3.24	239.84
14	5	2.55	243.19
15	6	2.83	228.18
16	4	3.24	243.26
17	3	3.56	271.20
18	5	3.20	346.28
19	7	2.77	251.50
20	5	2.17	312.67
21	6	2.47	254.52
22	8	2.36	242.01
23	6	2.85	312.82
24	1	2.92	237.77
Mean	5.13	2.64	254.17
S.D.	2.69	0.44	47.93
C.O.V.	52.5%	16.7%	18.9%

Table C.2. Restrained shrinkage test results for specimens with 0.05% fibrillated polypropylene fibres cut to 19 mm.

Sample	Crack numbers	Max Crack Width (mm)	Total Crack Area (mm ²)
1	5	1.59	176.04
2	8	1.18	175.69
3	2	1.85	124.98
4	2	2.04	127.43
Mean	4.25	1.66	151.04
S.D.	2.87	0.37	28.69
C.O.V.	67.6%	22.3%	19.0%

Table C.3. Restrained shrinkage test results for specimens with 0.1% fibrillated polypropylene fibres cut to 19 mm.

Sample	Crack numbers	Max Crack Width (mm)	Total Crack Area (mm ²)
1	10	1.32	149.91
2	7	1.20	134.70
3	14	1.18	139.70
4	9	1.29	87.93
Mean	10.00	1.25	128.06
S.D.	2.94	0.07	27.49
C.O.V.	29.4%	5.3%	21.5%

Table C.4. Restrained shrinkage test results for specimens with 0.3% fibrillated polypropylene fibres cut to 19 mm.

Sample	Crack numbers	Max Crack Width (mm)	Total Crack Area (mm ²)
1	7	0.30	23.97
2	9	0.45	14.07
3	9	0.45	9.95
4	9	0.34	11.20
Mean	8.50	0.38	14.80
S.D.	1.00	0.08	6.36
C.O.V.	11.8%	20.2%	43.0%

Table C.5. Restrained shrinkage test results for specimens with 0.05% fibrillated polypropylene fibres cut to 38 mm.

Sample	Crack numbers	Max Crack Width (mm)	Total Crack Area (mm ²)
1	7	1.80	148.70
2	15	1.37	136.98
3	10	1.46	155.15
4	6	1.67	157.85
Mean	9.50	1.58	149.67
S.D.	4.04	0.20	9.29
C.O.V.	42.5%	12.4%	6.2%

Table C.6. Restrained shrinkage test results for specimens with 0.1% fibrillated polypropylene fibres cut to 38 mm.

Sample	Crack numbers	Max Crack Width (mm)	Total Crack Area (mm ²)
1	14	1.09	95.48
2	11	1.48	148.34
3	15	0.84	57.81
4	21	1.27	157.42
Mean	15.25	1.17	114.76
S.D.	4.19	0.27	46.77
C.O.V.	27.5%	23.3%	40.8%

Table C.7. Restrained shrinkage test results for specimens with 0.3% fibrillated polypropylene fibres cut to 38 mm.

Sample	Crack numbers	Max Crack Width (mm)	Total Crack Area (mm ²)
1	17	0.32	7.39
2	13	0.41	9.58
3	24	0.28	20.42
4	14	0.36	10.34
Mean	17.00	0.34	11.93
S.D.	4.97	0.06	5.79
C.O.V.	29.2%	16.1%	48.5%

Table C.8. Restrained shrinkage test results for specimens with 0.05% red baler twine fibres cut to 19 mm.

Sample	Crack numbers	Max Crack Width (mm)	Total Crack Area (mm ²)
1	9	2.08	213.14
2	11	2.00	251.78
3	7	2.08	276.98
4	5	2.48	272.84
Mean	8.00	2.16	253.68
S.D.	2.58	0.22	29.19
C.O.V.	32.3%	10.1%	11.5%

Table C.9. Restrained shrinkage test results for specimens with 0.1% red baler twine fibres cut to 19 mm.

Sample	Crack numbers	Max Crack Width (mm)	Total Crack Area (mm ²)
1	1	2.64	219.63
2	6	1.44	207.06
3	7	1.83	255.72
4	8	2.17	225.07
Mean	5.50	2.02	226.87
S.D.	3.11	0.51	20.66
C.O.V.	56.5%	25.3%	9.1%

Table C.10. Restrained shrinkage test results for specimens with 0.3% red baler twine fibres cut to 19 mm.

Sample	Crack numbers	Max Crack Width (mm)	Total Crack Area (mm ²)
1	10	1.57	178.39
2	22	2.05	173.40
3	12	1.61	199.67
4	18	2.36	189.17
Mean	15.50	1.90	185.16
S.D.	5.51	0.38	11.70
C.O.V.	35.5%	19.9%	6.3%

Table C.11. Restrained shrinkage test results for specimens with 0.05% red baler twine fibres cut to 38 mm.

Sample	Crack numbers	Max Crack Width (mm)	Total Crack Area (mm ²)
1	11	2.75	257.15
2	8	2.81	244.53
3	4	1.97	272.89
4	7	2.34	288.53
Mean	7.50	2.47	265.77
S.D.	2.89	0.39	19.10
C.O.V.	38.5%	15.8%	7.2%

Table C.12. Restrained shrinkage test results for specimens with 0.1% red baler twine fibres cut to 38 mm.

Sample	Crack numbers	Max Crack Width (mm)	Total Crack Area (mm ²)
1	6	2.10	294.68
2	10	2.58	229.05
3	12	2.17	226.25
4	12	1.93	216.76
Mean	10.00	2.19	241.69
S.D.	2.83	0.27	35.72
C.O.V.	28.3%	12.4%	14.8%

Table C.13. Restrained shrinkage test results for specimens with 0.3% red baler twine fibres cut to 38 mm.

Sample	Crack numbers	Max Crack Width (mm)	Total Crack Area (mm ²)
1	20	1.48	191.89
2	18	1.27	140.97
3	22	2.15	194.06
4	30	0.90	102.67
Mean	22.50	1.45	157.40
S.D.	5.26	0.52	43.96
C.O.V.	23.4%	36.1%	27.9%

Table C.14. Restrained shrinkage test results for specimens with 0.05% white baler twine fibres cut to 19 mm.

Sample	Crack numbers	Max Crack Width (mm)	Total Crack Area (mm ²)
1	4	2.60	223.01
2	9	2.19	273.69
3	7	2.45	282.07
4	5	1.87	241.28
Mean	6.25	2.28	255.02
S.D.	2.22	0.32	27.65
C.O.V.	35.5%	14.2%	10.8%

Table C.15. Restrained shrinkage test results for specimens with 0.1% white baler twine fibres cut to 19 mm.

Sample	Crack numbers	Max Crack Width (mm)	Total Crack Area (mm ²)
1	6	1.85	252.48
2	13	1.22	179.38
3	14	1.70	188.12
4	8	2.27	214.24
Mean	10.25	1.76	208.55
S.D.	3.86	0.43	32.81
C.O.V.	37.7%	24.7%	15.7%

Table C.16. Restrained shrinkage test results for specimens with 0.3% white baler twine fibres cut to 19 mm.

Sample	Crack numbers	Max Crack Width (mm)	Total Crack Area (mm ²)
1	31	0.86	90.19
2	24	0.86	99.94
3	15	1.05	127.91
4	28	1.01	84.61
Mean	24.50	0.94	100.66
S.D.	6.95	0.10	19.24
C.O.V.	28.4%	10.7%	19.1%

Table C.17. Restrained shrinkage test results for specimens with 0.05% white baler twine fibres cut to 38 mm.

Sample	Crack numbers	Max Crack Width (mm)	Total Crack Area (mm ²)
1	9	1.57	222.15
2	21	1.78	160.89
3	12	2.35	212.40
4	11	1.72	187.71
Mean	13.25	1.85	195.79
S.D.	5.32	0.34	27.41
C.O.V.	40.1%	18.5%	14.0%

Table C.18. Restrained shrinkage test results for specimens with 0.1% white baler twine fibres cut to 38 mm.

Sample	Crack numbers	Max Crack Width (mm)	Total Crack Area (mm ²)
1	10	1.42	144.55
2	8	2.10	201.28
3	6	2.15	219.75
4	15	1.61	171.54
Mean	9.75	1.82	184.28
S.D.	3.86	0.36	33.11
C.O.V.	39.6%	19.9%	18.0%

Table C.19. Restrained shrinkage test results for specimens with 0.3% white baler twine fibres cut to 38 mm.

Sample	Crack numbers	Max Crack Width (mm)	Total Crack Area (mm ²)
1	20	0.43	34.29
2	28	0.79	61.55
3	17	0.73	69.57
4	22	0.71	67.86
Mean	21.75	0.67	58.32
S.D.	4.65	0.16	16.39
C.O.V.	21.4%	24.3%	28.1%

Table C.20. The meaning of the abbreviations used in the following table.

	Fiber type	Length (mm)	Volume fraction
FIB 1905	fibrillated polypropylene	19	0.05%
FIB 3805	fibrillated polypropylene	38	0.05%
FIB 1910	fibrillated polypropylene	19	0.10%
FIB 3810	fibrillated polypropylene	38	0.10%
FIB 1930	fibrillated polypropylene	19	0.30%
FIB 3830	fibrillated polypropylene	38	0.30%
RBT 1905	red baler twine	19	0.05%
RBT 3805	red baler twine	38	0.05%
RBT 1910	red baler twine	19	0.10%
RBT 3810	red baler twine	38	0.10%
RBT 1930	red baler twine	19	0.30%
RBT 3830	red baler twine	38	0.30%
WBT 1905	white baler twine	19	0.05%
WBT 3805	white baler twine	38	0.05%
WBT 1910	white baler twine	19	0.10%
WBT 3810	white baler twine	38	0.10%
WBT 1930	white baler twine	19	0.30%
WBT 3830	white baler twine	38	0.30%

Table C.21. Number of cracks, 95% confidence limit (one-sided), comparison to plain control.

FRC	Plain	C.O.V.	S_1	FRC	C.O.V.	S_2	n_1	n_2	v
FIB 1905	5.1	0.525	2.69	4.3	0.676	2.87	24	4	26
FIB 3805	5.1	0.525	2.69	9.5	0.425	4.04	24	4	26
FIB 1910	5.1	0.525	2.69	10.0	0.294	2.94	24	4	26
FIB 3810	5.1	0.525	2.69	15.3	0.275	4.19	24	4	26
FIB 1930	5.1	0.525	2.69	8.5	0.118	1.00	24	4	26
FIB 3830	5.1	0.525	2.69	17.0	0.292	4.96	24	4	26
RBT 1905	5.1	0.525	2.69	8.0	0.323	2.58	24	4	26
RBT 3805	5.1	0.525	2.69	7.5	0.385	2.89	24	4	26
RBT 1910	5.1	0.525	2.69	5.5	0.565	3.11	24	4	26
RBT 3810	5.1	0.525	2.69	10.0	0.283	2.83	24	4	26
RBT 1930	5.1	0.525	2.69	15.5	0.355	5.50	24	4	26
RBT 3830	5.1	0.525	2.69	22.5	0.234	5.27	24	4	26
WBT 1905	5.1	0.525	2.69	6.3	0.355	2.22	24	4	26
WBT 3805	5.1	0.525	2.69	13.3	0.401	5.31	24	4	26
WBT 1910	5.1	0.525	2.69	10.3	0.377	3.86	24	4	26
WBT 3810	5.1	0.525	2.69	9.8	0.396	3.86	24	4	26
WBT 1930	5.1	0.525	2.69	24.5	0.284	6.96	24	4	26
WBT 3830	5.1	0.525	2.69	21.8	0.214	4.65	24	4	26

Table C.21. (Cont'd) Number of cracks, 95% confidence limit (one-sided), comparison to plain control.

FRC	S_c^2	S_d	t	t_{crit}	t/t_{crit}	Significant	Probability from same set
FIB 1905	7.37	1.47	-0.600	1.706	0.352	NO	27.7%
FIB 3805	8.30	1.56	2.809	1.706	1.647	YES	0.5%
FIB 1910	7.41	1.47	3.312	1.706	1.941	YES	0.1%
FIB 3810	8.45	1.57	6.448	1.706	3.779	YES	0.0%
FIB 1930	6.53	1.38	2.441	1.706	1.431	YES	1.1%
FIB 3830	9.26	1.64	7.223	1.706	4.234	YES	0.0%
RBT 1905	7.19	1.45	1.982	1.706	1.162	YES	2.9%
RBT 3805	7.38	1.47	1.616	1.706	0.947	NO	5.9%
RBT 1910	7.53	1.48	0.250	1.706	0.146	NO	40.2%
RBT 3810	7.34	1.46	3.328	1.706	1.951	YES	0.1%
RBT 1930	9.91	1.70	6.099	1.706	3.575	YES	0.0%
RBT 3830	9.62	1.67	10.372	1.706	6.080	YES	0.0%
WBT 1905	6.98	1.43	0.785	1.706	0.460	NO	22.0%
WBT 3805	9.67	1.68	4.834	1.706	2.834	YES	0.0%
WBT 1910	8.14	1.54	3.323	1.706	1.948	YES	0.1%
WBT 3810	8.14	1.54	2.999	1.706	1.758	YES	0.3%
WBT 1930	12.00	1.87	10.352	1.706	6.068	YES	0.0%
WBT 3830	8.92	1.61	10.306	1.706	6.041	YES	0.0%

Table C.22. Maximum crack width, 95% confidence limit (one-sided), comparison to plain control.

FRC	Plain	C.O.V.	S ₁	FRC	C.O.V.	S ₂	n ₁	n ₂	v
FIB 1905	2.64	0.167	0.44	1.66	0.223	0.37	24	4	26
FIB 3805	2.64	0.167	0.44	1.58	0.124	0.20	24	4	26
FIB 1910	2.64	0.167	0.44	1.25	0.053	0.07	24	4	26
FIB 3810	2.64	0.167	0.44	1.17	0.233	0.27	24	4	26
FIB 1930	2.64	0.167	0.44	0.38	0.202	0.08	24	4	26
FIB 3830	2.64	0.167	0.44	0.34	0.161	0.05	24	4	26
RBT 1905	2.64	0.167	0.44	2.16	0.101	0.22	24	4	26
RBT 3805	2.64	0.167	0.44	2.47	0.158	0.39	24	4	26
RBT 1910	2.64	0.167	0.44	2.02	0.253	0.51	24	4	26
RBT 3810	2.64	0.167	0.44	2.19	0.124	0.27	24	4	26
RBT 1930	2.64	0.167	0.44	1.90	0.199	0.38	24	4	26
RBT 3830	2.64	0.167	0.44	1.45	0.361	0.52	24	4	26
WBT 1905	2.64	0.167	0.44	2.28	0.142	0.32	24	4	26
WBT 3805	2.64	0.167	0.44	1.85	0.185	0.34	24	4	26
WBT 1910	2.64	0.167	0.44	1.76	0.247	0.43	24	4	26
WBT 3810	2.64	0.167	0.44	1.82	0.199	0.36	24	4	26
WBT 1930	2.64	0.167	0.44	0.94	0.107	0.10	24	4	26
WBT 3830	2.64	0.167	0.44	0.67	0.243	0.16	24	4	26

Table C.22. (Cont'd) Maximum crack width, 95% confidence limit (one-sided), comparison to plain control.

FRC	S_c^2	S_d	t	t_{crit}	t/t_{crit}	Significant	Probability from same set
FIB 1905	0.19	0.23	-4.188	1.706	2.455	YES	0.0%
FIB 3805	0.18	0.23	-4.674	1.706	2.739	YES	0.0%
FIB 1910	0.17	0.22	-6.198	1.706	3.633	YES	0.0%
FIB 3810	0.18	0.23	-6.406	1.706	3.755	YES	0.0%
FIB 1930	0.17	0.22	-10.072	1.706	5.904	YES	0.0%
FIB 3830	0.17	0.22	-10.260	1.706	6.014	YES	0.0%
RBT 1905	0.18	0.23	-2.110	1.706	1.237	YES	2.2%
RBT 3805	0.19	0.24	-0.723	1.706	0.424	NO	23.8%
RBT 1910	0.20	0.24	-2.554	1.706	1.497	YES	0.8%
RBT 3810	0.18	0.23	-1.961	1.706	1.150	YES	3.0%
RBT 1930	0.19	0.23	-3.156	1.706	1.850	YES	0.2%
RBT 3830	0.20	0.24	-4.884	1.706	2.863	YES	0.0%
WBT 1905	0.18	0.23	-1.554	1.706	0.911	NO	6.6%
WBT 3805	0.19	0.23	-3.397	1.706	1.991	YES	0.1%
WBT 1910	0.19	0.24	-3.702	1.706	2.170	YES	0.1%
WBT 3810	0.19	0.23	-3.510	1.706	2.058	YES	0.1%
WBT 1930	0.17	0.22	-7.566	1.706	4.435	YES	0.0%
WBT 3830	0.18	0.23	-8.720	1.706	5.111	YES	0.0%

Table C.23. Total crack area, 95% confidence limit (one-sided), comparison to plain control.

FRC	Plain	C.O.V.	S ₁	FRC	C.O.V.	S ₂	n ₁	n ₂	v
FIB 1905	254.17	0.189	48.04	151.04	0.190	28.70	24	4	26
FIB 3805	254.17	0.189	48.04	149.67	0.062	9.28	24	4	26
FIB 1910	254.17	0.189	48.04	128.06	0.215	27.53	24	4	26
FIB 3810	254.17	0.189	48.04	114.76	0.408	46.82	24	4	26
FIB 1930	254.17	0.189	48.04	14.80	0.430	6.36	24	4	26
FIB 3830	254.17	0.189	48.04	11.93	0.485	5.79	24	4	26
RBT 1905	254.17	0.189	48.04	253.68	0.115	29.17	24	4	26
RBT 3805	254.17	0.189	48.04	265.77	0.072	19.14	24	4	26
RBT 1910	254.17	0.189	48.04	226.87	0.091	20.65	24	4	26
RBT 3810	254.17	0.189	48.04	241.69	0.148	35.77	24	4	26
RBT 1930	254.17	0.189	48.04	185.16	0.063	11.67	24	4	26
RBT 3830	254.17	0.189	48.04	157.40	0.279	43.91	24	4	26
WBT 1905	254.17	0.189	48.04	255.02	0.108	27.54	24	4	26
WBT 3805	254.17	0.189	48.04	195.79	0.140	27.41	24	4	26
WBT 1910	254.17	0.189	48.04	208.55	0.157	32.74	24	4	26
WBT 3810	254.17	0.189	48.04	184.28	0.180	33.17	24	4	26
WBT 1930	254.17	0.189	48.04	100.66	0.191	19.23	24	4	26
WBT 3830	254.17	0.189	48.04	58.32	0.281	16.39	24	4	26

Table C.23. (Cont'd) Total crack area, 95% confidence limit (one-sided), comparison to plain control.

FRC	S_c^2	S_d	t	t_{crit}	t/t_{crit}	Significant	Probability from same set
FIB 1905	2136.42	24.96	-4.131	1.706	2.422	YES	0.0%
FIB 3805	2051.33	24.46	-4.272	1.706	2.504	YES	0.0%
FIB 1910	2128.86	24.92	-5.061	1.706	2.967	YES	0.0%
FIB 3810	2294.35	25.87	-5.389	1.706	3.159	YES	0.0%
FIB 1930	2046.07	24.43	-9.799	1.706	5.744	YES	0.0%
FIB 3830	2045.26	24.42	-9.918	1.706	5.814	YES	0.0%
RBT 1905	2139.59	24.98	-0.020	1.706	0.011	NO	49.2%
RBT 3805	2083.64	24.65	0.471	1.706	0.276	NO	32.1%
RBT 1910	2090.57	24.69	-1.106	1.706	0.648	NO	14.0%
RBT 3810	2189.03	25.27	-0.494	1.706	0.290	NO	31.3%
RBT 1930	2057.09	24.49	-2.817	1.706	1.651	YES	0.5%
RBT 3830	2263.91	25.70	-3.766	1.706	2.207	YES	0.0%
WBT 1905	2128.92	24.92	0.034	1.706	0.020	NO	48.7%
WBT 3805	2128.09	24.91	-2.343	1.706	1.374	YES	1.4%
WBT 1910	2165.09	25.13	-1.815	1.706	1.064	YES	4.1%
WBT 3810	2168.35	25.15	-2.779	1.706	1.629	YES	0.5%
WBT 1930	2084.04	24.65	-6.226	1.706	3.650	YES	0.0%
WBT 3830	2072.38	24.59	-7.966	1.706	4.669	YES	0.0%

Table C.24. Maximum crack width, 95% confidence limit (one-sided), influence of length.

FRC	19 mm	C.O.V.	S_1	38 mm	C.O.V.	S_2	n_1	n_2	v
FIB 05	1.66	0.223	0.37	1.58	0.124	0.20	4	4	6
FIB 10	1.25	0.053	0.07	1.17	0.233	0.27	4	4	6
FIB 30	0.38	0.202	0.08	0.34	0.161	0.05	4	4	6
RBT 05	2.16	0.101	0.22	2.47	0.158	0.39	4	4	6
RBT 10	2.02	0.253	0.51	2.19	0.124	0.27	4	4	6
RBT 30	1.90	0.199	0.38	1.45	0.361	0.52	4	4	6
WBT 05	2.28	0.142	0.32	1.85	0.185	0.34	4	4	6
WBT 10	1.76	0.247	0.43	1.82	0.199	0.36	4	4	6
WBT 30	0.94	0.107	0.10	0.67	0.243	0.16	4	4	6

Table C.24. (Cont'd) Maximum crack width, 95% confidence limit (one-sided), influence of length.

FRC	S_c^2	S_d	t	t_{crit}	t/t_{crit}	Significant	Probability from same set
FIB 05	0.09	0.21	-0.382	1.943	0.197	NO	35.8%
FIB 10	0.04	0.14	-0.570	1.943	0.294	NO	29.5%
FIB 30	0.00	0.05	-0.849	1.943	0.437	NO	21.4%
RBT 05	0.10	0.22	1.387	1.943	0.714	NO	10.7%
RBT 10	0.17	0.29	0.587	1.943	0.302	NO	28.9%
RBT 30	0.21	0.32	-1.394	1.943	0.717	NO	10.6%
WBT 05	0.11	0.24	-1.825	1.943	0.939	NO	5.9%
WBT 10	0.16	0.28	0.212	1.943	0.109	NO	42.0%
WBT 30	0.02	0.10	-2.822	1.943	1.452	YES	1.5%

Table C.25. Total crack area, 95% confidence limit (one-sided), influence of length.

FRC	19 mm	C.O.V.	S ₁	38 mm	C.O.V.	S ₂	n ₁	n ₂	v
FIB 05	151.04	0.190	28.70	149.67	0.062	9.28	4	4	6
FIB 10	128.06	0.215	27.53	114.76	0.408	46.82	4	4	6
FIB 30	14.80	0.430	6.36	11.93	0.485	5.79	4	4	6
RBT 05	253.68	0.115	29.17	265.77	0.072	19.14	4	4	6
RBT 10	226.87	0.091	20.65	241.69	0.148	35.77	4	4	6
RBT 30	185.16	0.063	11.67	157.40	0.279	43.91	4	4	6
WBT 05	255.02	0.108	27.54	195.79	0.140	27.41	4	4	6
WBT 10	208.55	0.157	32.74	184.28	0.180	33.17	4	4	6
WBT 30	100.66	0.191	19.23	58.32	0.281	16.39	4	4	6

Table C.25. (Cont'd) Total crack area, 95% confidence limit (one-sided), influence of length.

FRC	S _c ²	S _d	t	t _{crit}	t/t _{crit}	Significant	Probability from same set
FIB 05	454.83	15.08	-0.091	1.943	0.047	NO	46.5%
FIB 10	1475.18	27.16	-0.490	1.943	0.252	NO	32.1%
FIB 30	36.99	4.30	-0.667	1.943	0.343	NO	26.5%
RBT 05	608.62	17.44	0.693	1.943	0.357	NO	25.7%
RBT 10	852.86	20.65	0.718	1.943	0.369	NO	25.0%
RBT 30	1032.28	22.72	-1.222	1.943	0.629	NO	13.4%
WBT 05	754.96	19.43	-3.049	1.943	1.569	YES	1.1%
WBT 10	1086.17	23.30	-1.041	1.943	0.536	NO	16.9%
WBT 30	319.10	12.63	-3.352	1.943	1.725	YES	0.8%

APPENDIX D — Unrestrained Shrinkage Test Results

The unrestrained plastic shrinkage tests were carried out to determine whether the reduction in restrained plastic shrinkage cracking could be partially attributed to the overall reduction in free plastic shrinkage.

Nineteen different kinds of specimens were tested in the unrestrained plastic shrinkage tests. Except for plain specimens, each one had a different combination of fibre type, length, and volume fraction. The test results are summarized in Table D.1 to D.96.

Table D.1. Unrestrained shrinkage test results for plain specimens, fibrillated polypropylene, 19 mm, batch 1-tunnel 1.

T (min)	L (mm)	ΔL (mm)	$e=\Delta L /L_0$
0.0	199.430	0.000	0.000
30.0	199.370	0.060	0.000
60.0	198.950	0.480	0.002
90.0	198.630	0.800	0.004
120.0	198.120	1.310	0.007
150.0	197.560	1.870	0.009
180.0	197.000	2.430	0.012
210.0	196.900	2.530	0.013
240.0	196.890	2.540	0.013
1260.0	196.850	2.580	0.013

Table D.2. Unrestrained shrinkage test results for plain specimens, fibrillated polypropylene, 19 mm, batch 1-tunnel 2.

T (min)	L (mm)	ΔL (mm)	$e=\Delta L /L_0$
0.0	200.800	0.000	0.000
30.0	200.730	0.070	0.000
60.0	200.510	0.290	0.001
90.0	200.350	0.450	0.002
120.0	199.500	1.300	0.006
150.0	199.010	1.790	0.009
180.0	198.410	2.390	0.012
210.0	198.370	2.430	0.012
240.0	198.210	2.590	0.013
1260.0	198.210	2.590	0.013

Table D.3. Unrestrained shrinkage test results for plain specimens, fibrillated polypropylene, 19 mm, batch 2-tunnel 1.

T (min)	L (mm)	ΔL (mm)	$e=\Delta L / L_0$
0.0	202.090	0.000	0.000
30.0	201.800	0.290	0.001
60.0	201.240	0.850	0.004
90.0	200.740	1.350	0.007
120.0	200.300	1.790	0.009
150.0	199.790	2.300	0.011
180.0	199.550	2.540	0.013
210.0	199.360	2.730	0.014
240.0	199.360	2.730	0.014
1260.0	199.340	2.750	0.014

Table D.4. Unrestrained shrinkage test results for plain specimens, fibrillated polypropylene, 19 mm, batch 2-tunnel 2.

T (min)	L (mm)	ΔL (mm)	$e=\Delta L / L_0$
0.0	201.320	0.000	0.000
30.0	201.230	0.090	0.000
60.0	200.730	0.590	0.003
90.0	200.050	1.270	0.006
120.0	199.380	1.940	0.010
150.0	198.850	2.470	0.012
180.0	198.660	2.660	0.013
210.0	198.450	2.870	0.014
240.0	198.410	2.910	0.014
1260.0	198.400	2.920	0.015

Table D.5. Unrestrained shrinkage test results for 0.05% fibrillated polypropylene, 19 mm, batch 1-tunnel 1.

T (min)	L (mm)	ΔL (mm)	$e=\Delta L / L_0$
0.0	200.610	0.000	0.000
30.0	200.530	0.080	0.000
60.0	200.340	0.270	0.001
90.0	199.560	1.050	0.005
120.0	199.090	1.520	0.008
150.0	198.540	2.070	0.010
180.0	198.150	2.460	0.012
210.0	198.050	2.560	0.013
240.0	198.050	2.560	0.013
1260.0	198.050	2.560	0.013

Table D.6. Unrestrained shrinkage test results for 0.05% fibrillated polypropylene, 19 mm, batch 1-tunnel 2.

T (min)	L (mm)	ΔL (mm)	$e=\Delta L / L_0$
0.0	199.980	0.000	0.000
30.0	199.820	0.160	0.001
60.0	199.500	0.480	0.002
90.0	198.850	1.130	0.006
120.0	198.400	1.580	0.008
150.0	198.000	1.980	0.010
180.0	197.850	2.130	0.011
210.0	197.660	2.320	0.012
240.0	197.550	2.430	0.012
1260.0	197.510	2.470	0.012

Table D.7. Unrestrained shrinkage test results for 0.05% fibrillated polypropylene, 19 mm, batch 2-tunnel 1.

T (min)	L (mm)	ΔL (mm)	$e=\Delta L / L_0$
0.0	204.450	0.000	0.000
30.0	204.240	0.210	0.001
60.0	204.080	0.370	0.002
90.0	203.450	1.000	0.005
120.0	202.910	1.540	0.008
150.0	202.210	2.240	0.011
180.0	201.930	2.520	0.012
210.0	201.820	2.630	0.013
240.0	201.840	2.610	0.013
1260.0	201.820	2.630	0.013

Table D.8. Unrestrained shrinkage test results for 0.05% fibrillated polypropylene, 19 mm, batch 2-tunnel 2.

T (min)	L (mm)	ΔL (mm)	$e=\Delta L / L_0$
0.0	201.900	0.000	0.000
30.0	201.860	0.040	0.000
60.0	201.520	0.380	0.002
90.0	201.010	0.890	0.004
120.0	200.760	1.140	0.006
150.0	200.310	1.590	0.008
180.0	199.840	2.060	0.010
210.0	199.470	2.430	0.012
240.0	199.330	2.570	0.013
1260.0	199.260	2.640	0.013

Table D.9. Unrestrained shrinkage test results for 0.1% fibrillated polypropylene, 19 mm, batch 1-tunnel 1.

T (min)	L (mm)	ΔL (mm)	$e=\Delta L / L_0$
0.0	200.210	0.000	0.000
30.0	200.120	0.090	0.000
60.0	199.880	0.330	0.002
90.0	199.220	0.990	0.005
120.0	198.810	1.400	0.007
150.0	198.390	1.820	0.009
180.0	197.890	2.320	0.012
210.0	197.800	2.410	0.012
240.0	197.780	2.430	0.012
1260.0	197.780	2.430	0.012

Table D.10. Unrestrained shrinkage test results for 0.1% fibrillated polypropylene, 19 mm, batch 1-tunnel 2.

T (min)	L (mm)	ΔL (mm)	$e=\Delta L / L_0$
0.0	199.810	0.000	0.000
30.0	199.720	0.090	0.000
60.0	199.500	0.310	0.002
90.0	199.010	0.800	0.004
120.0	198.450	1.360	0.007
150.0	197.980	1.830	0.009
180.0	197.750	2.060	0.010
210.0	197.510	2.300	0.012
240.0	197.510	2.300	0.012
1260.0	197.510	2.300	0.012

Table D.11. Unrestrained shrinkage test results for 0.1% fibrillated polypropylene, 19 mm, batch 2-tunnel 1.

T (min)	L (mm)	ΔL (mm)	$e=\Delta L / L_0$
0.0	199.540	0.000	0.000
30.0	199.480	0.060	0.000
60.0	199.350	0.190	0.001
90.0	198.710	0.830	0.004
120.0	198.050	1.490	0.007
150.0	197.490	2.050	0.010
180.0	197.250	2.290	0.011
210.0	197.170	2.370	0.012
240.0	197.170	2.370	0.012
1260.0	197.090	2.450	0.012

Table D.12. Unrestrained shrinkage test results for 0.1% fibrillated polypropylene, 19 mm, batch 2-tunnel 2.

T (min)	L (mm)	ΔL (mm)	$e=\Delta L / L_0$
0.0	200.510	0.000	0.000
30.0	200.510	0.000	0.000
60.0	199.990	0.520	0.003
90.0	199.210	1.300	0.006
120.0	198.820	1.690	0.008
150.0	198.390	2.120	0.011
180.0	198.330	2.180	0.011
210.0	198.150	2.360	0.012
240.0	198.000	2.510	0.013
1260.0	198.000	2.510	0.013

Table D.13. Unrestrained shrinkage test results for 0.3% fibrillated polypropylene, 19 mm, batch 1-tunnel 1.

T (min)	L (mm)	ΔL (mm)	$e=\Delta L / L_0$
0.0	199.870	0.000	0.000
30.0	199.850	0.020	0.000
60.0	199.570	0.300	0.002
90.0	199.460	0.410	0.002
120.0	198.850	1.020	0.005
150.0	198.360	1.510	0.008
180.0	198.010	1.860	0.009
210.0	197.850	2.020	0.010
240.0	197.850	2.020	0.010
1260.0	197.850	2.020	0.010

Table D.14. Unrestrained shrinkage test results for 0.3% fibrillated polypropylene, 19 mm, batch 1-tunnel 2.

T (min)	L (mm)	ΔL (mm)	$e=\Delta L / L_0$
0.0	200.130	0.000	0.000
30.0	199.830	0.300	0.001
60.0	199.490	0.640	0.003
90.0	199.310	0.820	0.004
120.0	198.850	1.280	0.006
150.0	198.450	1.680	0.008
180.0	198.390	1.740	0.009
210.0	198.230	1.900	0.009
240.0	198.230	1.900	0.009
1260.0	198.230	1.900	0.009

Table D.15. Unrestrained shrinkage test results for 0.3% fibrillated polypropylene, 19 mm, batch 2-tunnel 1.

T (min)	L (mm)	ΔL (mm)	$e=\Delta L / L_0$
0.0	200.750	0.000	0.000
30.0	200.750	0.000	0.000
60.0	200.530	0.220	0.001
90.0	199.900	0.850	0.004
120.0	199.640	1.110	0.006
150.0	199.210	1.540	0.008
180.0	198.630	2.120	0.011
210.0	198.760	1.990	0.010
240.0	198.680	2.070	0.010
1260.0	198.680	2.070	0.010

Table D.16. Unrestrained shrinkage test results for 0.3% fibrillated polypropylene, 19 mm, batch 2-tunnel 2.

T (min)	L (mm)	ΔL (mm)	$e=\Delta L / L_0$
0.0	200.060	0.000	0.000
30.0	199.900	0.160	0.001
60.0	199.660	0.400	0.002
90.0	199.030	1.030	0.005
120.0	198.450	1.610	0.008
150.0	197.980	2.080	0.010
180.0	197.930	2.130	0.011
210.0	197.900	2.160	0.011
240.0	197.810	2.250	0.011
1260.0	197.810	2.250	0.011

Table D.17. Unrestrained shrinkage test results for plain specimens, fibrillated polypropylene, 38 mm, batch 1-tunnel 1.

T (min)	L (mm)	ΔL (mm)	$e=\Delta L / L_0$
0.0	202.910	0.000	0.000
30.0	202.890	0.020	0.000
60.0	202.620	0.290	0.001
90.0	202.080	0.810	0.004
120.0	201.500	0.830	0.004
150.0	200.740	1.410	0.007
180.0	200.360	2.170	0.011
210.0	200.250	2.550	0.013
240.0	200.250	2.660	0.013
1260.0	200.250	2.660	0.013

Table D.18. Unrestrained shrinkage test results for plain specimens, fibrillated polypropylene, 38 mm, batch 1-tunnel 2.

T (min)	L (mm)	ΔL (mm)	$e=\Delta L / L_0$
0.0	202.840	0.000	0.000
30.0	202.770	0.070	0.000
60.0	202.570	0.270	0.001
90.0	202.220	0.620	0.003
120.0	201.430	1.410	0.007
150.0	200.890	1.950	0.010
180.0	200.410	2.430	0.012
210.0	200.410	2.430	0.012
240.0	200.380	2.460	0.012
1260.0	200.300	2.540	0.013

Table D.19. Unrestrained shrinkage test results for plain specimens, fibrillated polypropylene, 38 mm, batch 2-tunnel 1.

T (min)	L (mm)	ΔL (mm)	$e=\Delta L / L_0$
0.0	203.670	0.000	0.000
30.0	203.410	0.260	0.001
60.0	203.090	0.580	0.003
90.0	202.750	0.920	0.005
120.0	202.270	1.400	0.007
150.0	201.610	2.060	0.010
180.0	201.310	2.360	0.012
210.0	201.200	2.470	0.012
240.0	201.140	2.530	0.012
1260.0	201.140	2.530	0.012

Table D.20. Unrestrained shrinkage test results for plain specimens, fibrillated polypropylene, 38 mm, batch 2-tunnel 2.

T (min)	L (mm)	ΔL (mm)	$e=\Delta L / L_0$
0.0	200.980	0.000	0.000
30.0	200.950	0.030	0.000
60.0	200.460	0.520	0.003
90.0	200.250	0.730	0.004
120.0	199.600	1.380	0.007
150.0	198.940	2.040	0.010
180.0	198.730	2.250	0.011
210.0	198.540	2.440	0.012
240.0	198.480	2.500	0.012
1260.0	198.480	2.500	0.012

Table D.21. Unrestrained shrinkage test results for 0.05% fibrillated polypropylene, 38 mm, batch 1-tunnel 1.

T (min)	L (mm)	ΔL (mm)	$e=\Delta L / L_0$
0.0	200.230	0.000	0.000
30.0	200.070	0.160	0.001
60.0	199.930	0.300	0.001
90.0	199.500	0.730	0.004
120.0	198.700	1.530	0.008
150.0	198.260	1.970	0.010
180.0	197.670	2.560	0.013
210.0	197.630	2.600	0.013
240.0	197.630	2.600	0.013
1260.0	197.630	2.600	0.013

Table D.22. Unrestrained shrinkage test results for 0.05% fibrillated polypropylene, 38 mm, batch 1-tunnel 2.

T (min)	L (mm)	ΔL (mm)	$e=\Delta L / L_0$
0.0	202.240	0.000	0.000
30.0	202.110	0.130	0.001
60.0	201.730	0.510	0.003
90.0	201.190	1.050	0.005
120.0	200.310	1.930	0.010
150.0	199.970	2.270	0.011
180.0	199.880	2.360	0.012
210.0	199.760	2.480	0.012
240.0	199.760	2.480	0.012
1260.0	199.760	2.480	0.012

Table D.23. Unrestrained shrinkage test results for 0.05% fibrillated polypropylene, 38 mm, batch 2-tunnel 1.

T (min)	L (mm)	ΔL (mm)	$e=\Delta L / L_0$
0.0	204.040	0.000	0.000
30.0	204.010	0.030	0.000
60.0	203.930	0.110	0.001
90.0	203.550	0.490	0.002
120.0	202.930	1.110	0.005
150.0	202.460	1.580	0.008
180.0	202.060	1.980	0.010
210.0	202.060	1.980	0.010
240.0	202.020	2.020	0.010
1260.0	202.020	2.020	0.010

Table D.24. Unrestrained shrinkage test results for 0.05% fibrillated polypropylene, 38 mm, batch 2-tunnel 2.

T (min)	L (mm)	ΔL (mm)	$e=\Delta L / L_0$
0.0	204.190	0.000	0.000
30.0	204.190	0.000	0.000
60.0	203.750	0.440	0.002
90.0	203.440	0.750	0.004
120.0	202.980	1.210	0.006
150.0	202.530	1.660	0.008
180.0	202.190	2.000	0.010
210.0	202.080	2.110	0.010
240.0	202.050	2.140	0.010
1260.0	202.050	2.140	0.010

Table D.25. Unrestrained shrinkage test results for 0.1% fibrillated polypropylene, 38 mm, batch 1-tunnel 1.

T (min)	L (mm)	ΔL (mm)	$e=\Delta L / L_0$
0.0	199.700	0.000	0.000
30.0	199.390	0.310	0.002
60.0	199.320	0.380	0.002
90.0	198.790	0.910	0.005
120.0	198.100	1.600	0.008
150.0	197.540	2.160	0.011
180.0	197.310	2.390	0.012
210.0	197.310	2.390	0.012
240.0	197.310	2.390	0.012
1260.0	197.300	2.400	0.012

Table D.26. Unrestrained shrinkage test results for 0.1% fibrillated polypropylene, 38 mm, batch 1-tunnel 2.

T (min)	L (mm)	ΔL (mm)	$e=\Delta L / L_0$
0.0	201.870	0.000	0.000
30.0	201.510	0.360	0.002
60.0	201.280	0.590	0.003
90.0	200.940	0.930	0.005
120.0	200.530	1.340	0.007
150.0	199.950	1.920	0.010
180.0	199.790	2.080	0.010
210.0	199.750	2.120	0.011
240.0	199.680	2.190	0.011
1260.0	199.630	2.240	0.011

Table D.27. Unrestrained shrinkage test results for 0.1% fibrillated polypropylene, 38 mm, batch 2-tunnel 1.

T (min)	L (mm)	ΔL (mm)	$e=\Delta L / L_0$
0.0	203.330	0.000	0.000
30.0	203.000	0.330	0.002
60.0	202.900	0.430	0.002
90.0	202.500	0.830	0.004
120.0	201.950	1.380	0.007
150.0	201.620	1.710	0.008
180.0	201.330	2.000	0.010
210.0	201.320	2.010	0.010
240.0	201.320	2.010	0.010
1260.0	201.320	2.010	0.010

Table D.28. Unrestrained shrinkage test results for 0.1% fibrillated polypropylene, 38 mm, batch 2-tunnel 2.

T (min)	L (mm)	ΔL (mm)	$e=\Delta L / L_0$
0.0	202.110	0.000	0.000
30.0	202.090	0.020	0.000
60.0	201.660	0.450	0.002
90.0	201.200	0.910	0.005
120.0	200.650	1.460	0.007
150.0	200.010	2.100	0.010
180.0	199.800	2.310	0.011
210.0	199.760	2.350	0.012
240.0	199.760	2.350	0.012
1260.0	199.760	2.350	0.012

Table D.29. Unrestrained shrinkage test results for 0.3% fibrillated polypropylene, 38 mm, batch 1-tunnel 1.

T (min)	L (mm)	ΔL (mm)	$e=\Delta L / L_0$
0.0	201.790	0.000	0.000
30.0	201.650	0.140	0.001
60.0	201.550	0.240	0.001
90.0	201.220	0.570	0.003
120.0	200.730	1.060	0.005
150.0	200.380	1.410	0.007
180.0	200.170	1.620	0.008
210.0	200.170	1.620	0.008
240.0	200.170	1.620	0.008
1260.0	200.130	1.660	0.008

Table D.30. Unrestrained shrinkage test results for 0.3% fibrillated polypropylene, 38 mm, batch 1-tunnel 2.

T (min)	L (mm)	ΔL (mm)	$e=\Delta L / L_0$
0.0	202.860	0.000	0.000
30.0	202.400	0.460	0.002
60.0	202.330	0.530	0.003
90.0	201.850	1.010	0.005
120.0	201.340	1.520	0.007
150.0	201.080	1.780	0.009
180.0	200.890	1.970	0.010
210.0	200.890	1.970	0.010
240.0	200.810	2.050	0.010
1260.0	200.810	2.050	0.010

Table D.31. Unrestrained shrinkage test results for 0.3% fibrillated polypropylene, 38 mm, batch 2-tunnel 1.

T (min)	L (mm)	ΔL (mm)	$e=\Delta L / L_0$
0.0	203.460	0.000	0.000
30.0	203.460	0.000	0.000
60.0	203.100	0.360	0.002
90.0	202.700	0.760	0.004
120.0	202.280	1.180	0.006
150.0	202.000	1.460	0.007
180.0	201.900	1.560	0.008
210.0	201.840	1.620	0.008
240.0	201.810	1.650	0.008
1260.0	201.810	1.650	0.008

Table D.32. Unrestrained shrinkage test results for 0.3% fibrillated polypropylene, 38 mm, batch 2-tunnel 2.

T (min)	L (mm)	ΔL (mm)	$e=\Delta L / L_0$
0.0	202.650	0.000	0.000
30.0	202.510	0.140	0.001
60.0	202.130	0.520	0.003
90.0	201.850	0.800	0.004
120.0	201.480	1.170	0.006
150.0	201.050	1.600	0.008
180.0	201.000	1.650	0.008
210.0	200.980	1.670	0.008
240.0	200.940	1.710	0.008
1260.0	200.940	1.710	0.008

Table D.33. Unrestrained shrinkage test results for plain specimens, red baler twine, 19 mm, batch 1-tunnel 1.

T (min)	L (mm)	ΔL (mm)	$e=\Delta L / L_0$
0.0	202.520	0.000	0.000
30.0	202.250	0.270	0.001
60.0	201.590	0.930	0.005
90.0	201.280	1.240	0.006
120.0	201.050	1.470	0.007
150.0	200.600	1.920	0.009
180.0	200.280	2.240	0.011
210.0	200.170	2.350	0.012
240.0	200.070	2.450	0.012
1260.0	199.980	2.540	0.013

Table D.34. Unrestrained shrinkage test results for plain specimens, red baler twine, 19 mm, batch 1-tunnel 2.

T (min)	L (mm)	ΔL (mm)	$e=\Delta L / L_0$
0.0	200.330	0.000	0.000
30.0	200.150	0.180	0.001
60.0	199.740	0.590	0.003
90.0	199.360	0.970	0.005
120.0	198.800	1.530	0.008
150.0	198.340	1.990	0.010
180.0	198.560	1.770	0.009
210.0	198.060	2.270	0.011
240.0	197.850	2.480	0.012
1260.0	197.850	2.480	0.012

Table D.35. Unrestrained shrinkage test results for plain specimens, red baler twine, 19 mm, batch 2-tunnel 1.

T (min)	L (mm)	ΔL (mm)	$e=\Delta L / L_0$
0.0	199.660	0.000	0.000
30.0	199.500	0.160	0.001
60.0	199.460	0.200	0.001
90.0	199.100	0.560	0.003
120.0	198.750	0.910	0.005
150.0	198.260	1.400	0.007
180.0	197.800	1.860	0.009
210.0	197.450	2.210	0.011
240.0	197.380	2.280	0.011
1260.0	197.330	2.330	0.012

Table D.36. Unrestrained shrinkage test results for plain specimens, red baler twine, 19 mm, batch 2-tunnel 2.

T (min)	L (mm)	ΔL (mm)	$e=\Delta L / L_0$
0.0	202.530	0.000	0.000
30.0	202.230	0.300	0.001
60.0	202.140	0.390	0.002
90.0	201.650	0.880	0.004
120.0	201.010	1.520	0.008
150.0	200.460	2.070	0.010
180.0	199.860	2.670	0.013
210.0	199.770	2.760	0.014
240.0	199.730	2.800	0.014
1260.0	199.670	2.860	0.014

Table D.37. Unrestrained shrinkage test results for 0.05% red baler twine, 19 mm, batch 1-tunnel 1.

T (min)	L (mm)	ΔL (mm)	$e=\Delta L / L_0$
0.0	202.890	0.000	0.000
30.0	202.570	0.320	0.002
60.0	202.410	0.480	0.002
90.0	201.950	0.940	0.005
120.0	201.240	1.650	0.008
150.0	200.770	2.120	0.010
180.0	200.370	2.520	0.012
210.0	200.190	2.700	0.013
240.0	200.190	2.700	0.013
1260.0	200.190	2.700	0.013

Table D.38. Unrestrained shrinkage test results for 0.05% red baler twine, 19 mm, batch 1-tunnel 2.

T (min)	L (mm)	ΔL (mm)	$e=\Delta L / L_0$
0.0	201.920	0.000	0.000
30.0	201.760	0.160	0.001
60.0	201.210	0.710	0.004
90.0	200.660	1.260	0.006
120.0	200.210	1.710	0.008
150.0	199.630	2.290	0.011
180.0	199.190	2.730	0.014
210.0	199.170	2.750	0.014
240.0	199.160	2.760	0.014
1260.0	199.160	2.760	0.014

Table D.39. Unrestrained shrinkage test results for 0.05% red baler twine, 19 mm, batch 2-tunnel 1.

T (min)	L (mm)	ΔL (mm)	$e=\Delta L /L_0$
0.0	202.820	0.000	0.000
30.0	202.740	0.080	0.000
60.0	202.600	0.220	0.001
90.0	202.270	0.550	0.003
120.0	201.770	1.050	0.005
150.0	201.030	1.790	0.009
180.0	200.640	2.180	0.011
210.0	200.440	2.380	0.012
240.0	200.270	2.550	0.013
1260.0	200.260	2.560	0.013

Table D.40. Unrestrained shrinkage test results for 0.05% red baler twine, 19 mm, batch 2-tunnel 2.

T (min)	L (mm)	ΔL (mm)	$e=\Delta L /L_0$
0.0	198.080	0.000	0.000
30.0	198.050	0.030	0.000
60.0	197.980	0.100	0.001
90.0	197.310	0.770	0.004
120.0	196.880	1.200	0.006
150.0	196.390	1.690	0.009
180.0	195.850	2.230	0.011
210.0	195.540	2.540	0.013
240.0	195.480	2.600	0.013
1260.0	195.450	2.630	0.013

Table D.41. Unrestrained shrinkage test results for 0.1% red baler twine, 19 mm, batch 1-tunnel 1.

T (min)	L (mm)	ΔL (mm)	$e=\Delta L /L_0$
0.0	200.250	0.000	0.000
30.0	200.150	0.100	0.000
60.0	199.610	0.640	0.003
90.0	199.240	1.010	0.005
120.0	198.720	1.530	0.008
150.0	198.100	2.150	0.011
180.0	197.850	2.400	0.012
210.0	197.830	2.420	0.012
240.0	197.810	2.440	0.012
1260.0	197.810	2.440	0.012

Table D.42. Unrestrained shrinkage test results for 0.1% red baler twine, 19 mm, batch 1-tunnel 2.

T (min)	L (mm)	ΔL (mm)	$e=\Delta L / L_0$
0.0	200.600	0.000	0.000
30.0	200.580	0.020	0.000
60.0	200.310	0.290	0.001
90.0	199.890	0.710	0.004
120.0	199.330	1.270	0.006
150.0	198.700	1.900	0.009
180.0	198.380	2.220	0.011
210.0	198.260	2.340	0.012
240.0	198.260	2.340	0.012
1260.0	198.260	2.340	0.012

Table D.43. Unrestrained shrinkage test results for 0.1% red baler twine, 19 mm, batch 2-tunnel 1.

T (min)	L (mm)	ΔL (mm)	$e=\Delta L / L_0$
0.0	201.030	0.000	0.000
30.0	200.920	0.110	0.001
60.0	200.750	0.280	0.001
90.0	200.450	0.580	0.003
120.0	199.960	1.070	0.005
150.0	199.410	1.620	0.008
180.0	198.930	2.100	0.010
210.0	198.670	2.360	0.012
240.0	198.670	2.360	0.012
1260.0	198.600	2.430	0.012

Table D.44. Unrestrained shrinkage test results for 0.1% red baler twine, 19 mm, batch 2-tunnel 2.

T (min)	L (mm)	ΔL (mm)	$e=\Delta L / L_0$
0.0	203.170	0.000	0.000
30.0	203.070	0.100	0.000
60.0	203.000	0.170	0.001
90.0	202.360	0.810	0.004
120.0	201.950	1.220	0.006
150.0	201.520	1.650	0.008
180.0	201.020	2.150	0.011
210.0	200.940	2.230	0.011
240.0	200.940	2.230	0.011
1260.0	200.830	2.340	0.012

Table D.45. Unrestrained shrinkage test results for 0.3% red baler twine, 19 mm, batch 1-tunnel 1.

T (min)	L (mm)	ΔL (mm)	$e=\Delta L / L_0$
0.0	200.890	0.000	0.000
30.0	200.690	0.200	0.001
60.0	200.250	0.640	0.003
90.0	199.910	0.980	0.005
120.0	199.450	1.440	0.007
150.0	198.960	1.930	0.010
180.0	198.610	2.280	0.011
210.0	198.510	2.380	0.012
240.0	198.460	2.430	0.012
1260.0	198.460	2.430	0.012

Table D.46. Unrestrained shrinkage test results for 0.3% red baler twine, 19 mm, batch 1-tunnel 2.

T (min)	L (mm)	ΔL (mm)	$e=\Delta L / L_0$
0.0	202.500	0.000	0.000
30.0	202.240	0.260	0.001
60.0	202.060	0.440	0.002
90.0	201.630	0.870	0.004
120.0	201.120	1.380	0.007
150.0	200.630	1.870	0.009
180.0	200.360	2.140	0.011
210.0	200.360	2.140	0.011
240.0	200.300	2.200	0.011
1260.0	200.300	2.200	0.011

Table D.47. Unrestrained shrinkage test results for 0.3% red baler twine, 19 mm, batch 2-tunnel 1.

T (min)	L (mm)	ΔL (mm)	$e=\Delta L / L_0$
0.0	204.050	0.000	0.000
30.0	203.830	0.220	0.001
60.0	203.690	0.360	0.002
90.0	203.400	0.650	0.003
120.0	202.900	1.150	0.006
150.0	202.310	1.740	0.009
180.0	201.750	2.300	0.011
210.0	201.550	2.500	0.012
240.0	201.530	2.520	0.012
1260.0	201.490	2.560	0.013

Table D.48. Unrestrained shrinkage test results for 0.3% red baler twine, 19 mm, batch 2-tunnel 2.

T (min)	L (mm)	ΔL (mm)	$e=\Delta L / L_0$
0.0	200.540	0.000	0.000
30.0	200.540	0.000	0.000
60.0	200.410	0.130	0.001
90.0	199.910	0.630	0.003
120.0	199.560	0.980	0.005
150.0	198.920	1.620	0.008
180.0	198.320	2.220	0.011
210.0	198.060	2.480	0.012
240.0	198.050	2.490	0.012
1260.0	198.050	2.490	0.012

Table D.49. Unrestrained shrinkage test results for plain specimens, red baler twine, 38 mm, batch 1-tunnel 1.

T (min)	L (mm)	ΔL (mm)	$e=\Delta L / L_0$
0.0	199.130	0.000	0.000
30.0	198.880	0.250	0.001
60.0	198.690	0.440	0.002
90.0	198.300	0.580	0.003
120.0	197.900	0.830	0.004
150.0	197.650	1.230	0.006
180.0	197.220	1.480	0.007
210.0	197.050	1.910	0.010
240.0	196.990	2.080	0.010
1260.0	196.990	2.140	0.011

Table D.50. Unrestrained shrinkage test results for plain specimens, red baler twine, 38 mm, batch 1-tunnel 2.

T (min)	L (mm)	ΔL (mm)	$e=\Delta L / L_0$
0.0	198.330	0.000	0.000
30.0	198.320	0.010	0.000
60.0	198.020	0.310	0.002
90.0	197.800	0.530	0.003
120.0	197.450	0.880	0.004
150.0	197.070	1.260	0.006
180.0	196.760	1.570	0.008
210.0	196.680	1.650	0.008
240.0	196.600	1.730	0.009
1260.0	196.600	1.730	0.009

Table D.51. Unrestrained shrinkage test results for plain specimens, red baler twine, 38 mm, batch 2-tunnel 1.

T (min)	L (mm)	ΔL (mm)	$e=\Delta L / L_0$
0.0	199.570	0.000	0.000
30.0	199.490	0.080	0.000
60.0	199.180	0.390	0.002
90.0	198.820	0.750	0.004
120.0	198.430	1.140	0.006
150.0	198.010	1.560	0.008
180.0	197.670	1.900	0.010
210.0	197.470	2.100	0.011
240.0	197.360	2.210	0.011
1260.0	197.320	2.250	0.011

Table D.52. Unrestrained shrinkage test results for plain specimens, red baler twine, 38 mm, batch 2-tunnel 2.

T (min)	L (mm)	ΔL (mm)	$e=\Delta L / L_0$
0.0	202.070	0.000	0.000
30.0	202.000	0.070	0.000
60.0	201.390	0.680	0.003
90.0	201.000	1.070	0.005
120.0	200.420	1.650	0.008
150.0	199.860	2.210	0.011
180.0	199.370	2.700	0.013
210.0	199.370	2.700	0.013
240.0	199.220	2.850	0.014
1260.0	199.170	2.900	0.014

Table D.53. Unrestrained shrinkage test results for 0.05% red baler twine, 38 mm, batch 1-tunnel 1.

T (min)	L (mm)	ΔL (mm)	$e=\Delta L / L_0$
0.0	201.090	0.000	0.000
30.0	200.950	0.140	0.001
60.0	200.760	0.330	0.002
90.0	200.410	0.680	0.003
120.0	200.090	1.000	0.005
150.0	199.640	1.450	0.007
180.0	199.280	1.810	0.009
210.0	198.980	2.110	0.010
240.0	198.920	2.170	0.011
1260.0	198.900	2.190	0.011

Table D.54. Unrestrained shrinkage test results for 0.05% red baler twine, 38 mm, batch 1-tunnel 2.

T (min)	L (mm)	ΔL (mm)	$e=\Delta L / L_0$
0.0	202.840	0.000	0.000
30.0	202.810	0.030	0.000
60.0	202.540	0.300	0.001
90.0	201.950	0.890	0.004
120.0	201.430	1.410	0.007
150.0	200.980	1.860	0.009
180.0	200.470	2.370	0.012
210.0	200.460	2.380	0.012
240.0	200.450	2.490	0.012
1260.0	200.400	2.440	0.012

Table D.55. Unrestrained shrinkage test results for 0.05% red baler twine, 38 mm, batch 2-tunnel 1.

T (min)	L (mm)	ΔL (mm)	$e=\Delta L / L_0$
0.0	200.820	0.000	0.000
30.0	200.820	0.000	0.000
60.0	200.480	0.340	0.002
90.0	200.090	0.730	0.004
120.0	199.490	1.330	0.007
150.0	199.010	1.810	0.009
180.0	198.480	2.340	0.012
210.0	198.300	2.520	0.013
240.0	198.320	2.500	0.012
1260.0	198.240	2.580	0.013

Table D.56. Unrestrained shrinkage test results for 0.05% red baler twine, 38 mm, batch 2-tunnel 2.

T (min)	L (mm)	ΔL (mm)	$e=\Delta L / L_0$
0.0	201.430	0.000	0.000
30.0	201.420	0.010	0.000
60.0	200.910	0.520	0.003
90.0	200.480	0.950	0.005
120.0	199.990	1.440	0.007
150.0	199.760	1.670	0.008
180.0	199.260	2.170	0.011
210.0	199.080	2.350	0.012
240.0	198.900	2.530	0.013
1260.0	198.930	2.500	0.012

Table D.57. Unrestrained shrinkage test results for 0.1% red baler twine, 38 mm, batch 1-tunnel 1.

T (min)	L (mm)	ΔL (mm)	$e=\Delta L /L_0$
0.0	201.090	0.000	0.000
30.0	200.950	0.140	0.001
60.0	200.710	0.380	0.002
90.0	200.500	0.590	0.003
120.0	200.150	0.940	0.005
150.0	199.680	1.410	0.007
180.0	199.280	1.810	0.009
210.0	199.270	1.820	0.009
240.0	199.270	1.820	0.009
1260.0	199.200	1.890	0.009

Table D.58. Unrestrained shrinkage test results for 0.1% red baler twine, 38 mm, batch 1-tunnel 2.

T (min)	L (mm)	ΔL (mm)	$e=\Delta L /L_0$
0.0	201.240	0.000	0.000
30.0	201.180	0.060	0.000
60.0	200.910	0.330	0.002
90.0	200.560	0.680	0.003
120.0	200.260	0.980	0.005
150.0	199.820	1.420	0.007
180.0	199.320	1.920	0.010
210.0	199.290	1.950	0.010
240.0	199.280	1.960	0.010
1260.0	199.190	2.050	0.010

Table D.59. Unrestrained shrinkage test results for 0.1% red baler twine, 38 mm, batch 2-tunnel 1.

T (min)	L (mm)	ΔL (mm)	$e=\Delta L /L_0$
0.0	200.420	0.000	0.000
30.0	200.390	0.030	0.000
60.0	199.860	0.560	0.003
90.0	199.510	0.910	0.005
120.0	199.060	1.360	0.007
150.0	198.620	1.800	0.009
180.0	198.200	2.220	0.011
210.0	197.960	2.460	0.012
240.0	197.890	2.530	0.013
1260.0	197.840	2.580	0.013

Table D.60. Unrestrained shrinkage test results for 0.1% red baler twine, 38 mm, batch 2-tunnel 2.

T (min)	L (mm)	ΔL (mm)	$e=\Delta L / L_0$
0.0	199.750	0.000	0.000
30.0	199.720	0.030	0.000
60.0	199.120	0.630	0.003
90.0	198.820	0.930	0.005
120.0	198.260	1.490	0.007
150.0	197.780	1.970	0.010
180.0	197.350	2.400	0.012
210.0	197.230	2.520	0.013
240.0	197.210	2.540	0.013
1260.0	197.200	2.550	0.013

Table D.61. Unrestrained shrinkage test results for 0.3% red baler twine, 38 mm, batch 1-tunnel 1.

T (min)	L (mm)	ΔL (mm)	$e=\Delta L / L_0$
0.0	202.260	0.000	0.000
30.0	202.120	0.140	0.001
60.0	201.980	0.280	0.001
90.0	201.620	0.640	0.003
120.0	201.160	1.100	0.005
150.0	200.850	1.410	0.007
180.0	200.420	1.840	0.009
210.0	200.270	1.990	0.010
240.0	200.270	1.990	0.010
1260.0	200.270	1.990	0.010

Table D.62. Unrestrained shrinkage test results for 0.3% red baler twine, 38 mm, batch 1-tunnel 2.

T (min)	L (mm)	ΔL (mm)	$e=\Delta L / L_0$
0.0	197.140	0.000	0.000
30.0	197.020	0.120	0.001
60.0	196.940	0.200	0.001
90.0	196.430	0.710	0.004
120.0	195.990	1.150	0.006
150.0	195.570	1.570	0.008
180.0	195.300	1.840	0.009
210.0	195.160	1.980	0.010
240.0	195.160	1.980	0.010
1260.0	195.160	1.980	0.010

Table D.63. Unrestrained shrinkage test results for 0.3% red baler twine, 38 mm, batch 2-tunnel 1.

T (min)	L (mm)	ΔL (mm)	$e=\Delta L /L_0$
0.0	199.560	0.000	0.000
30.0	199.480	0.080	0.000
60.0	198.870	0.690	0.003
90.0	198.420	1.140	0.006
120.0	198.040	1.520	0.008
150.0	197.510	2.050	0.010
180.0	197.190	2.370	0.012
210.0	197.190	2.370	0.012
240.0	197.110	2.450	0.012
1260.0	197.100	2.460	0.012

Table D.64. Unrestrained shrinkage test results for 0.3% red baler twine, 38 mm, batch 2-tunnel 2.

T (min)	L (mm)	ΔL (mm)	$e=\Delta L /L_0$
0.0	200.730	0.000	0.000
30.0	200.610	0.120	0.001
60.0	200.020	0.710	0.004
90.0	199.690	1.040	0.005
120.0	199.110	1.620	0.008
150.0	198.580	2.150	0.011
180.0	198.280	2.450	0.012
210.0	198.230	2.500	0.012
240.0	198.230	2.500	0.012
1260.0	198.230	2.500	0.012

Table D.65. Unrestrained shrinkage test results for plain specimens, white baler twine, 19 mm, batch 1-tunnel 1.

T (min)	L (mm)	ΔL (mm)	$e=\Delta L /L_0$
0.0	200.880	0.000	0.000
30.0	200.740	0.140	0.001
60.0	200.330	0.550	0.003
90.0	199.560	1.320	0.007
120.0	198.990	1.890	0.009
150.0	198.410	2.470	0.012
180.0	198.310	2.570	0.013
210.0	198.290	2.590	0.013
240.0	198.280	2.600	0.013
1260.0	198.270	2.610	0.013

Table D.66. Unrestrained shrinkage test results for plain specimens, white baler twine, 19 mm, batch 1-tunnel 2.

T (min)	L (mm)	ΔL (mm)	$e=\Delta L / L_0$
0.0	198.680	0.000	0.000
30.0	198.600	0.080	0.000
60.0	198.120	0.560	0.003
90.0	197.760	0.920	0.005
120.0	197.180	1.500	0.008
150.0	196.730	1.950	0.010
180.0	196.330	2.350	0.012
210.0	196.200	2.480	0.012
240.0	196.150	2.530	0.013
1260.0	196.080	2.600	0.013

Table D.67. Unrestrained shrinkage test results for plain specimens, white baler twine, 19 mm, batch 2-tunnel 1.

T (min)	L (mm)	ΔL (mm)	$e=\Delta L / L_0$
0.0	199.710	0.000	0.000
30.0	199.620	0.090	0.000
60.0	199.410	0.300	0.002
90.0	198.930	0.780	0.004
120.0	198.420	1.290	0.006
150.0	198.020	1.690	0.008
180.0	197.500	2.210	0.011
210.0	197.290	2.420	0.012
240.0	197.290	2.420	0.012
1260.0	197.290	2.420	0.012

Table D.68. Unrestrained shrinkage test results for plain specimens, white baler twine, 19 mm, batch 2-tunnel 2.

T (min)	L (mm)	ΔL (mm)	$e=\Delta L / L_0$
0.0	199.460	0.000	0.000
30.0	199.230	0.230	0.001
60.0	198.620	0.840	0.004
90.0	198.120	1.340	0.007
120.0	197.460	2.000	0.010
150.0	197.040	2.420	0.012
180.0	196.640	2.820	0.014
210.0	196.580	2.880	0.014
240.0	196.580	2.880	0.014
1260.0	196.580	2.880	0.014

Table D.69. Unrestrained shrinkage test results for 0.05% white baler twine, 19 mm, batch 1-tunnel 1.

T (min)	L (mm)	ΔL (mm)	$e=\Delta L / L_0$
0.0	202.400	0.000	0.000
30.0	202.220	0.180	0.001
60.0	201.660	0.740	0.004
90.0	201.150	1.250	0.006
120.0	200.800	1.600	0.008
150.0	200.290	2.110	0.010
180.0	199.860	2.540	0.013
210.0	199.680	2.720	0.013
240.0	199.680	2.720	0.013
1260.0	199.680	2.720	0.013

Table D.70. Unrestrained shrinkage test results for 0.05% white baler twine, 19 mm, batch 1-tunnel 2.

T (min)	L (mm)	ΔL (mm)	$e=\Delta L / L_0$
0.0	200.170	0.000	0.000
30.0	199.950	0.220	0.001
60.0	199.660	0.510	0.003
90.0	199.230	0.940	0.005
120.0	198.690	1.480	0.007
150.0	198.200	1.970	0.010
180.0	197.870	2.300	0.011
210.0	197.670	2.500	0.012
240.0	197.660	2.510	0.013
1260.0	197.640	2.530	0.013

Table D.71. Unrestrained shrinkage test results for 0.05% white baler twine, 19 mm, batch 2-tunnel 1.

T (min)	L (mm)	ΔL (mm)	$e=\Delta L / L_0$
0.0	200.000	0.000	0.000
30.0	199.920	0.080	0.000
60.0	199.760	0.240	0.001
90.0	199.130	0.870	0.004
120.0	198.740	1.260	0.006
150.0	198.210	1.790	0.009
180.0	197.730	2.270	0.011
210.0	197.660	2.340	0.012
240.0	197.610	2.390	0.012
1260.0	197.610	2.390	0.012

Table D.72. Unrestrained shrinkage test results for 0.05% white baler twine, 19 mm, batch 2-tunnel 2.

T (min)	L (mm)	ΔL (mm)	$e=\Delta L / L_0$
0.0	199.190	0.000	0.000
30.0	199.210	-0.020	0.000
60.0	198.800	0.390	0.002
90.0	198.340	0.850	0.004
120.0	198.000	1.190	0.006
150.0	197.500	1.690	0.008
180.0	197.240	1.950	0.010
210.0	196.930	2.260	0.011
240.0	196.930	2.260	0.011
1260.0	196.890	2.300	0.012

Table D.73. Unrestrained shrinkage test results for 0.1% white baler twine, 19 mm, batch 1-tunnel 1.

T (min)	L (mm)	ΔL (mm)	$e=\Delta L / L_0$
0.0	200.870	0.000	0.000
30.0	200.760	0.110	0.001
60.0	200.510	0.360	0.002
90.0	199.910	0.960	0.005
120.0	199.510	1.360	0.007
150.0	198.950	1.920	0.010
180.0	198.570	2.300	0.011
210.0	198.480	2.390	0.012
240.0	198.440	2.430	0.012
1260.0	198.350	2.520	0.013

Table D.74. Unrestrained shrinkage test results for 0.1% white baler twine, 19 mm, batch 1-tunnel 2.

T (min)	L (mm)	ΔL (mm)	$e=\Delta L / L_0$
0.0	200.160	0.000	0.000
30.0	199.980	0.180	0.001
60.0	199.770	0.390	0.002
90.0	199.350	0.810	0.004
120.0	198.850	1.310	0.007
150.0	198.210	1.950	0.010
180.0	198.030	2.130	0.011
210.0	197.980	2.180	0.011
240.0	197.900	2.260	0.011
1260.0	197.850	2.310	0.012

Table D.75. Unrestrained shrinkage test results for 0.1% white baler twine, 19 mm, batch 2-tunnel 1.

T (min)	L (mm)	ΔL (mm)	$e=\Delta L / L_0$
0.0	201.140	0.000	0.000
30.0	201.090	0.050	0.000
60.0	200.830	0.310	0.002
90.0	200.500	0.640	0.003
120.0	200.120	1.020	0.005
150.0	199.700	1.440	0.007
180.0	199.240	1.900	0.009
210.0	198.900	2.240	0.011
240.0	198.890	2.250	0.011
1260.0	198.840	2.300	0.011

Table D.76. Unrestrained shrinkage test results for 0.1% white baler twine, 19 mm, batch 2-tunnel 2.

T (min)	L (mm)	ΔL (mm)	$e=\Delta L / L_0$
0.0	200.550	0.000	0.000
30.0	200.340	0.210	0.001
60.0	200.030	0.520	0.003
90.0	199.820	0.730	0.004
120.0	199.300	1.250	0.006
150.0	198.850	1.700	0.008
180.0	198.430	2.120	0.011
210.0	198.320	2.230	0.011
240.0	198.270	2.280	0.011
1260.0	198.210	2.340	0.012

Table D.77. Unrestrained shrinkage test results for 0.3% white baler twine, 19 mm, batch 1-tunnel 1.

T (min)	L (mm)	ΔL (mm)	$e=\Delta L / L_0$
0.0	201.210	0.000	0.000
30.0	201.070	0.140	0.001
60.0	200.620	0.590	0.003
90.0	200.280	0.930	0.005
120.0	200.000	1.210	0.006
150.0	199.540	1.670	0.008
180.0	199.280	1.930	0.010
210.0	199.150	2.060	0.010
240.0	199.110	2.100	0.010
1260.0	198.960	2.250	0.011

Table D.78. Unrestrained shrinkage test results for 0.3% white baler twine, 19 mm, batch 1-tunnel 2.

T (min)	L (mm)	ΔL (mm)	$e=\Delta L /L_0$
0.0	199.230	0.000	0.000
30.0	199.210	0.020	0.000
60.0	198.870	0.360	0.002
90.0	198.530	0.700	0.004
120.0	198.090	1.140	0.006
150.0	197.650	1.580	0.008
180.0	197.410	1.820	0.009
210.0	197.260	1.970	0.010
240.0	197.210	2.020	0.010
1260.0	197.160	2.070	0.010

Table D.79. Unrestrained shrinkage test results for 0.3% white baler twine, 19 mm, batch 2-tunnel 1.

T (min)	L (mm)	ΔL (mm)	$e=\Delta L /L_0$
0.0	200.000	0.000	0.000
30.0	199.930	0.070	0.000
60.0	199.760	0.240	0.001
90.0	199.300	0.700	0.003
120.0	198.830	1.170	0.006
150.0	198.400	1.600	0.008
180.0	198.010	1.990	0.010
210.0	197.930	2.070	0.010
240.0	197.900	2.100	0.011
1260.0	197.850	2.150	0.011

Table D.80. Unrestrained shrinkage test results for 0.3% white baler twine, 19 mm, batch 2-tunnel 2.

T (min)	L (mm)	ΔL (mm)	$e=\Delta L /L_0$
0.0	200.570	0.000	0.000
30.0	200.560	0.010	0.000
60.0	200.170	0.400	0.002
90.0	199.840	0.730	0.004
120.0	199.380	1.190	0.006
150.0	198.900	1.670	0.008
180.0	198.460	2.110	0.011
210.0	198.280	2.290	0.011
240.0	198.280	2.290	0.011
1260.0	198.280	2.290	0.011

Table D.81. Unrestrained shrinkage test results for plain specimens, white baler twine, 38 mm, batch 1-tunnel 1.

T (min)	L (mm)	ΔL (mm)	$e=\Delta L / L_0$
0.0	199.470	0.000	0.000
30.0	199.360	0.110	0.001
60.0	199.190	0.280	0.001
90.0	198.920	0.550	0.003
120.0	198.470	1.000	0.005
150.0	197.920	1.550	0.008
180.0	197.500	1.970	0.010
210.0	197.490	1.980	0.010
240.0	197.280	2.190	0.011
1260.0	197.270	2.200	0.011

Table D.82. Unrestrained shrinkage test results for plain specimens, white baler twine, 38 mm, batch 1-tunnel 2.

T (min)	L (mm)	ΔL (mm)	$e=\Delta L / L_0$
0.0	201.770	0.000	0.000
30.0	201.570	0.200	0.001
60.0	201.460	0.310	0.002
90.0	200.820	0.950	0.005
120.0	200.360	1.410	0.007
150.0	199.820	1.950	0.010
180.0	199.240	2.530	0.013
210.0	199.210	2.560	0.013
240.0	199.130	2.640	0.013
1260.0	199.110	2.660	0.013

Table D.83. Unrestrained shrinkage test results for plain specimens, white baler twine, 38 mm, batch 2-tunnel 1.

T (min)	L (mm)	ΔL (mm)	$e=\Delta L / L_0$
0.0	203.650	0.000	0.000
30.0	203.600	0.050	0.000
60.0	203.490	0.160	0.001
90.0	203.310	0.340	0.002
120.0	202.960	0.690	0.003
150.0	202.580	1.070	0.005
180.0	202.010	1.640	0.008
210.0	201.690	1.960	0.010
240.0	201.570	2.080	0.010
1260.0	201.530	2.120	0.010

Table D.84. Unrestrained shrinkage test results for plain specimens, white baler twine, 38 mm, batch 2-tunnel 2.

T (min)	L (mm)	ΔL (mm)	$e=\Delta L /L_0$
0.0	199.730	0.000	0.000
30.0	199.730	0.000	0.000
60.0	199.480	0.250	0.001
90.0	199.130	0.600	0.003
120.0	198.690	1.040	0.005
150.0	198.050	1.680	0.008
180.0	197.440	2.290	0.011
210.0	197.290	2.440	0.012
240.0	197.260	2.470	0.012
1260.0	197.240	2.490	0.012

Table D.85. Unrestrained shrinkage test results for 0.05% white baler twine, 38 mm, batch 1-tunnel 1.

T (min)	L (mm)	ΔL (mm)	$e=\Delta L /L_0$
0.0	200.430	0.000	0.000
30.0	200.430	0.000	0.000
60.0	200.020	0.410	0.002
90.0	199.670	0.760	0.004
120.0	199.170	1.260	0.006
150.0	198.610	1.820	0.009
180.0	198.180	2.250	0.011
210.0	198.060	2.370	0.012
240.0	198.060	2.370	0.012
1260.0	198.000	2.430	0.012

Table D.86. Unrestrained shrinkage test results for 0.05% white baler twine, 38 mm, batch 1-tunnel 2.

T (min)	L (mm)	ΔL (mm)	$e=\Delta L /L_0$
0.0	202.090	0.000	0.000
30.0	202.080	0.010	0.000
60.0	201.620	0.470	0.002
90.0	201.360	0.730	0.004
120.0	200.700	1.390	0.007
150.0	200.160	1.930	0.010
180.0	199.720	2.370	0.012
210.0	199.580	2.510	0.012
240.0	199.580	2.510	0.012
1260.0	199.510	2.580	0.013

Table D.87. Unrestrained shrinkage test results for 0.05% white baler twine, 38 mm, batch 2-tunnel 1.

T (min)	L (mm)	ΔL (mm)	$e=\Delta L / L_0$
0.0	202.220	0.000	0.000
30.0	202.150	0.070	0.000
60.0	202.070	0.150	0.001
90.0	201.900	0.320	0.002
120.0	201.430	0.790	0.004
150.0	200.700	1.520	0.008
180.0	200.220	2.000	0.010
210.0	200.040	2.180	0.011
240.0	199.970	2.250	0.011
1260.0	199.970	2.250	0.011

Table D.88. Unrestrained shrinkage test results for 0.05% white baler twine, 38 mm, batch 2-tunnel 2.

T (min)	L (mm)	ΔL (mm)	$e=\Delta L / L_0$
0.0	200.090	0.000	0.000
30.0	199.880	0.210	0.001
60.0	199.770	0.320	0.002
90.0	199.690	0.400	0.002
120.0	199.490	0.600	0.003
150.0	199.120	0.970	0.005
180.0	198.740	1.350	0.007
210.0	198.390	1.700	0.008
240.0	198.260	1.830	0.009
1260.0	198.230	1.860	0.009

Table D.89. Unrestrained shrinkage test results for 0.1% white baler twine, 38 mm, batch 1-tunnel 1.

T (min)	L (mm)	ΔL (mm)	$e=\Delta L / L_0$
0.0	200.530	0.000	0.000
30.0	200.430	0.100	0.000
60.0	200.320	0.210	0.001
90.0	199.880	0.650	0.003
120.0	199.390	1.140	0.006
150.0	198.760	1.770	0.009
180.0	198.430	2.100	0.010
210.0	198.330	2.200	0.011
240.0	198.310	2.220	0.011
1260.0	198.310	2.220	0.011

Table D.90. Unrestrained shrinkage test results for 0.1% white baler twine, 38 mm, batch 1-tunnel 2.

T (min)	L (mm)	ΔL (mm)	$e=\Delta L /L_0$
0.0	197.160	0.000	0.000
30.0	197.130	0.030	0.000
60.0	197.030	0.130	0.001
90.0	196.550	0.610	0.003
120.0	196.460	0.700	0.004
150.0	195.900	1.260	0.006
180.0	195.440	1.720	0.009
210.0	195.170	1.990	0.010
240.0	195.090	2.070	0.010
1260.0	195.090	2.070	0.010

Table D.91. Unrestrained shrinkage test results for 0.1% white baler twine, 38 mm, batch 2-tunnel 1.

T (min)	L (mm)	ΔL (mm)	$e=\Delta L /L_0$
0.0	202.970	0.000	0.000
30.0	202.970	0.000	0.000
60.0	202.680	0.290	0.001
90.0	202.590	0.380	0.002
120.0	202.150	0.820	0.004
150.0	201.850	1.120	0.006
180.0	201.400	1.570	0.008
210.0	200.890	2.080	0.010
240.0	200.890	2.080	0.010
1260.0	200.890	2.080	0.010

Table D.92. Unrestrained shrinkage test results for 0.1% white baler twine, 38 mm, batch 2-tunnel 2.

T (min)	L (mm)	ΔL (mm)	$e=\Delta L /L_0$
0.0	200.410	0.000	0.000
30.0	200.400	0.010	0.000
60.0	200.320	0.090	0.000
90.0	199.900	0.510	0.003
120.0	199.570	0.840	0.004
150.0	199.110	1.300	0.006
180.0	198.570	1.840	0.009
210.0	198.430	1.980	0.010
240.0	198.430	1.980	0.010
1260.0	198.370	2.040	0.010

Table D.93. Unrestrained shrinkage test results for 0.3% white baler twine, 38 mm, batch 1-tunnel 1.

T (min)	L (mm)	ΔL (mm)	$e=\Delta L / L_0$
0.0	198.130	0.000	0.000
30.0	197.930	0.200	0.001
60.0	197.850	0.280	0.001
90.0	197.520	0.610	0.003
120.0	197.230	0.900	0.005
150.0	196.790	1.340	0.007
180.0	196.660	1.470	0.007
210.0	196.540	1.590	0.008
240.0	196.470	1.660	0.008
1260.0	196.380	1.750	0.009

Table D.94. Unrestrained shrinkage test results for 0.3% white baler twine, 38 mm, batch 1-tunnel 2.

T (min)	L (mm)	ΔL (mm)	$e=\Delta L / L_0$
0.0	200.620	0.000	0.000
30.0	200.590	0.030	0.000
60.0	200.450	0.170	0.001
90.0	199.830	0.790	0.004
120.0	199.560	1.060	0.005
150.0	199.180	1.440	0.007
180.0	199.040	1.580	0.008
210.0	199.040	1.580	0.008
240.0	199.000	1.620	0.008
1260.0	198.910	1.710	0.009

Table D.95. Unrestrained shrinkage test results for 0.3% white baler twine, 38 mm, batch 2-tunnel 1.

T (min)	L (mm)	ΔL (mm)	$e=\Delta L / L_0$
0.0	203.260	0.000	0.000
30.0	203.230	0.030	0.000
60.0	203.090	0.170	0.001
90.0	202.930	0.330	0.002
120.0	202.720	0.540	0.003
150.0	202.220	1.040	0.005
180.0	201.750	1.510	0.007
210.0	201.710	1.550	0.008
240.0	201.710	1.550	0.008
1260.0	201.680	1.580	0.008

Table D.96. Unrestrained shrinkage test results for 0.3% white baler twine, 38 mm batch 2-tunnel 2.

T (min)	L (mm)	ΔL (mm)	$e = \Delta L / L_0$
0.0	201.000	0.000	0.000
30.0	200.930	0.070	0.000
60.0	200.840	0.160	0.001
90.0	200.500	0.500	0.002
120.0	200.370	0.630	0.003
150.0	199.900	1.100	0.005
180.0	199.600	1.400	0.007
210.0	199.500	1.500	0.007
240.0	199.460	1.540	0.008
1260.0	199.410	1.590	0.008

Development of free shrinkage over time for all specimens with different fibre types, lengths and volume fractions are illustrated in Figs D.1 to D.5.

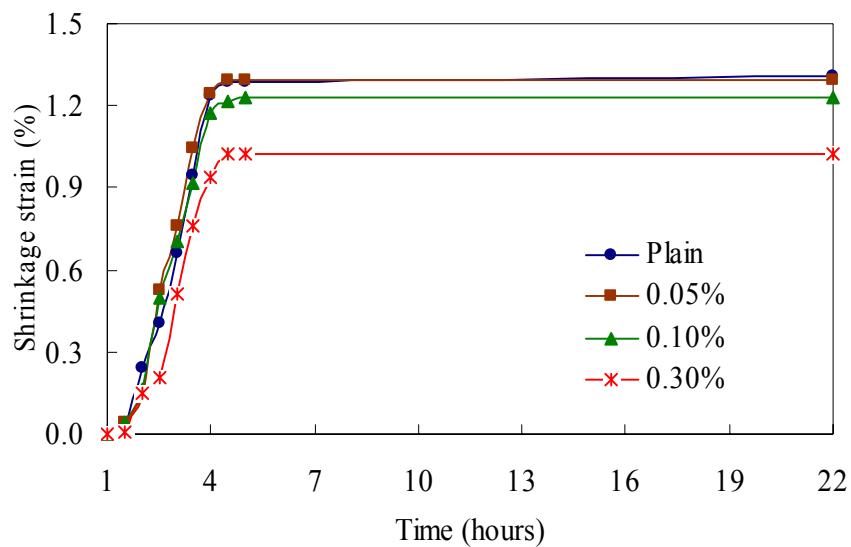


Figure D.1. Development of free shrinkage over time for 19 mm fibrillated polypropylene.

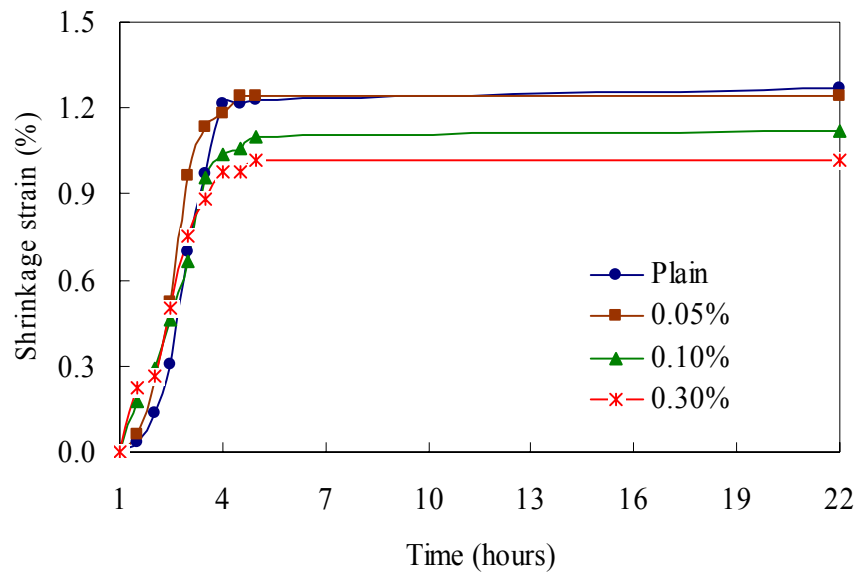


Figure D.2. Development of free shrinkage over time for 38 mm fibrillated polypropylene.

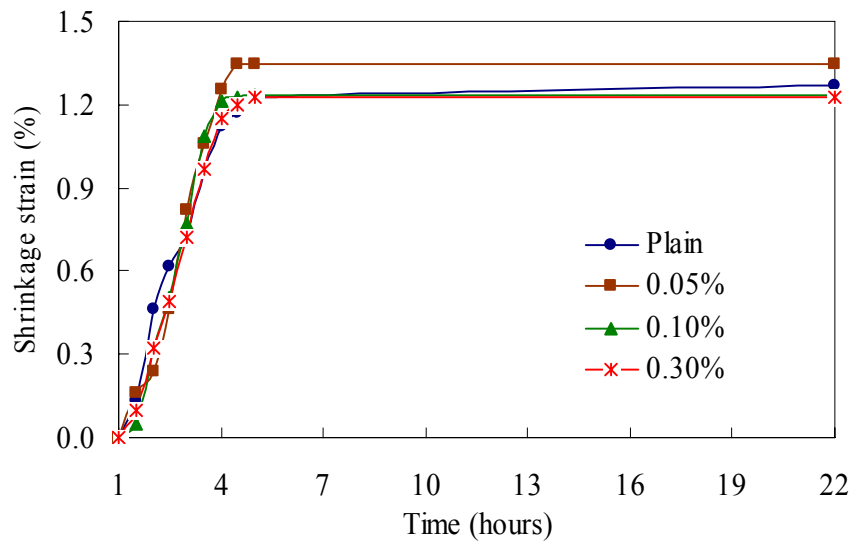


Figure D.3. Development of free shrinkage over time for 19 mm red baler twine.

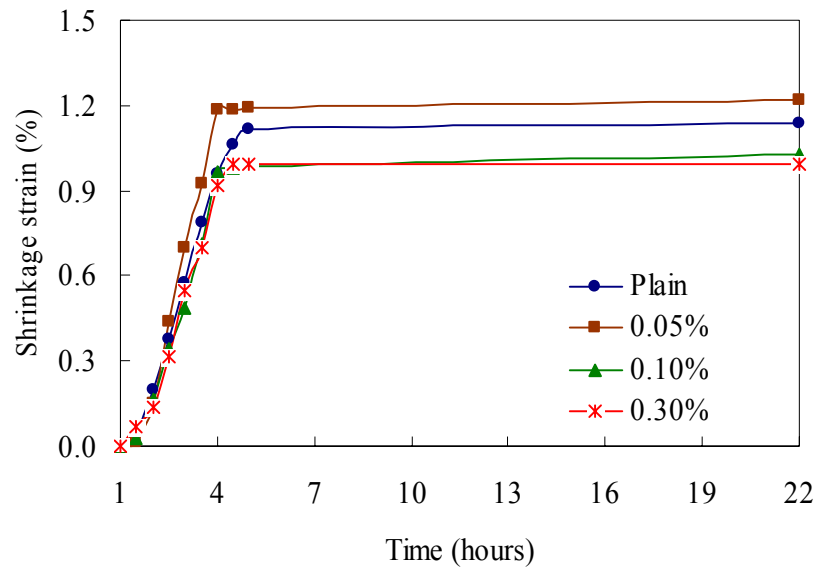


Figure D.4. Development of free shrinkage over time for 38 mm red baler twine.

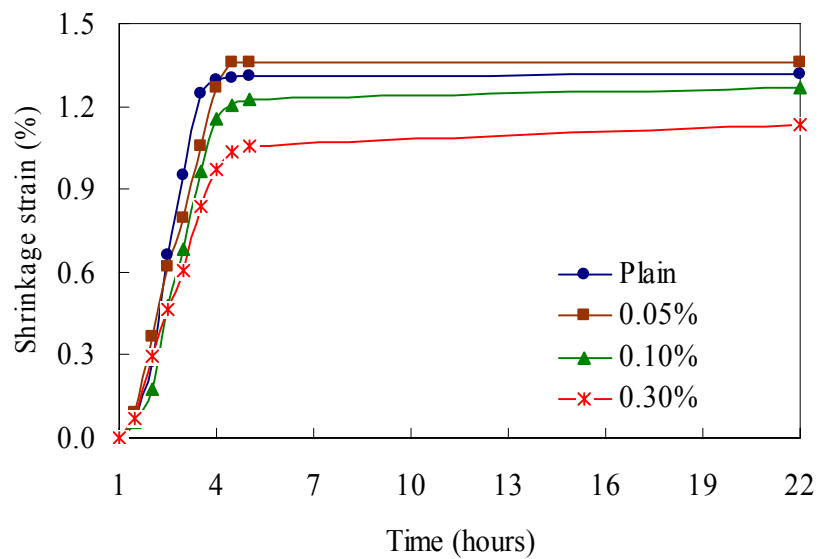


Figure D.5. Development of free shrinkage over time for 19 mm white baler twine.

T-test was carried out to assess whether the means of fibre reinforced specimens are statistically different from the plain control specimens. The calculate results are summarized in Table D. 97.

Table D.97. Unrestrained shrinkage strain, 95% confidence limit (one-sided), comparison to plain control.

FRC	Plain	C.O.V.	S ₁	FRC	C.O.V.	S ₂	n ₁	n ₂	v
FIB 1905	0.0125	0.109	0.0014	0.0128	0.024	0.0003	24	4	26
FIB 3805	0.0125	0.109	0.0014	0.0114	0.128	0.0015	24	4	26
FIB 1910	0.0125	0.109	0.0014	0.0121	0.035	0.0004	24	4	26
FIB 3810	0.0125	0.109	0.0014	0.0112	0.083	0.0009	24	4	26
FIB 1930	0.0125	0.109	0.0014	0.0103	0.071	0.0007	24	4	26
FIB 3830	0.0125	0.109	0.0014	0.0087	0.107	0.0009	24	4	26
RBT 1905	0.0125	0.109	0.0014	0.0132	0.033	0.0004	24	4	26
RBT 3805	0.0125	0.109	0.0014	0.0120	0.070	0.0008	24	4	26
RBT 1910	0.0125	0.109	0.0014	0.0119	0.027	0.0003	24	4	26
RBT 3810	0.0125	0.109	0.0014	0.0113	0.157	0.0018	24	4	26
RBT 1930	0.0125	0.109	0.0014	0.0120	0.064	0.0008	24	4	26
RBT 3830	0.0125	0.109	0.0014	0.0112	0.127	0.0014	24	4	26
WBT 1905	0.0125	0.109	0.0014	0.0124	0.067	0.0008	24	4	26
WBT 3805	0.0125	0.109	0.0014	0.0113	0.134	0.0015	24	4	26
WBT 1910	0.0125	0.109	0.0014	0.0118	0.043	0.0005	24	4	26
WBT 3810	0.0125	0.109	0.0014	0.0105	0.039	0.0004	24	4	26
WBT 1930	0.0125	0.109	0.0014	0.0109	0.042	0.0005	24	4	26
WBT 3830	0.0125	0.109	0.0014	0.0083	0.061	0.0005	24	4	26

Table D.97. (Cont'd) Unrestrained shrinkage strain, 95% confidence limit (one-sided), comparison to plain control.

FRC	S_c^2	S_d	t	t_{crit}	t/t_{crit}	Significant	Probability from same set
FIB 1905	1.667E-06	6.97E-04	0.379	1.706	0.222	NO	35.4%
FIB 3805	1.901E-06	7.45E-04	-1.466	1.706	0.860	NO	7.7%
FIB 1910	1.678E-06	7.00E-04	-0.554	1.706	0.325	NO	29.2%
FIB 3810	1.756E-06	7.16E-04	-1.875	1.706	1.099	YES	3.6%
FIB 1930	1.718E-06	7.08E-04	-3.121	1.706	1.830	YES	0.2%
FIB 3830	1.757E-06	7.16E-04	-5.279	1.706	3.094	YES	0.0%
RBT 1905	1.679E-06	7.00E-04	1.029	1.706	0.603	NO	15.6%
RBT 3805	1.738E-06	7.12E-04	-0.638	1.706	0.374	NO	26.5%
RBT 1910	1.669E-06	6.98E-04	-0.910	1.706	0.534	NO	18.5%
RBT 3810	2.021E-06	7.68E-04	-1.553	1.706	0.911	NO	6.6%
RBT 1930	1.725E-06	7.09E-04	-0.731	1.706	0.428	NO	23.6%
RBT 3830	1.889E-06	7.42E-04	-1.796	1.706	1.053	YES	4.2%
WBT 1905	1.736E-06	7.12E-04	-0.148	1.706	0.087	NO	44.2%
WBT 3805	1.921E-06	7.49E-04	-1.564	1.706	0.917	NO	6.5%
WBT 1910	1.686E-06	7.01E-04	-1.000	1.706	0.586	NO	16.3%
WBT 3810	1.676E-06	6.99E-04	-2.860	1.706	1.677	YES	0.4%
WBT 1930	1.681E-06	7.00E-04	-2.234	1.706	1.309	YES	1.7%
WBT 3830	1.686E-06	7.01E-04	-6.045	1.706	3.544	YES	0.0%